Department of Chemical Engineering

Development of Smart Bio-Polymeric Nanostructures for Stimuli-Response Based Applications

Bradley Hawkins

This thesis is presented for the Degree of
Doctor of Philosophy
of
Curtin University

May 2014

DECLARATION

To the best of my knowledge and belief this thesis contains no material previously published by any other person except where due acknowledgement has been made. This thesis contains no material which has been accepted for the award of any other degree or diploma in any university.

Signature: _____

Date: 16-07-2014

ABSTRACT

Biodegradable polymers have become more common in the plastics industry over the past decade, suiting the needs for both disposal and environmental concerns. This particular property coupled with biocompatibility has seen the use of these types of plastics in medical applications such as drug delivery and cell growth. This research delves into the synthesis of smart bio-polymeric nanostructures through the cost-efficient manufacturing process known as electrospinning. Poly-*N*-isopropylacrylamide (PNIPAM) and chitosan are two stimuli-responsive polymers that have been thoroughly investigated in this work, analysing their behaviour during electrospinning. Additionally, their interaction with embedded Fe_3O_4 nanoparticles has been researched. The behaviour of these types of nanostructures is not well understood, which reflects the significance of this work.

The electrospinning of thermo-responsive PNIPAM, both synthesised in the lab and commercially obtained, was undertaken. Nanofibres were produced in a coaxial arrangement with a poly(ε-caprolactone) (PCL) core and PNIPAM as the shell material. Furthermore, Fe_3O_4 nanoparticles with a size of 5 – 8 nm were embedded in the shell material to give the nanostructure a magnetic stimulus. The average nanofibre diameter for the coaxial nanofibres was 995 nm and 208 nm for synthesised and commercial PNIPAM/PCL, respectively. Thermal characterisation of the material concluded that the nanoparticles had little to no effect on the crystalline properties of the material, exhibiting one-dimensional crystal growth.

The pH-responsive biopolymer chitosan was relatively difficult to electrospin independently, so a polymer blend with PCL was produced. The effect of Fe_3O_4 nanoparticles on the nanofibre properties was observed using various characterisation techniques. The nanofibre diameter ranged from 36 – 262 nm, with superparamagnetism confirmed by magnetic analysis. The embedding of the nanoparticles produced a more uniform nanofibre diameter distribution, and had a noticeable effect on the crystalline properties. The nanoparticles acted as

nucleating sites within the material, promoting three-dimensional spherulitic growth throughout.

ACKNOWLEDGEMENTS

First and foremost, I would like to express my gratitude to my first supervisor Dr. Deeptangshu Chaudhary who accepted to undertake the supervision of my PhD study. His guidance was invaluable, and I am most thankful for his collaboration with the University of Hyogo which resulted in the opportunity to conduct my research on exchange in Japan in 2011. Unfortunately, Dr. Chaudhary moved to a new external appointment during early 2013, so I received Dr. Chi Phan and Dr. Gia Hung Pham as my new supervisor and co-supervisor, respectively. The transition for them into an unfamiliar research area did not take long, and I am thankful that they both have put in the effort to help me complete my last year as quickly and efficiently as possible.

I would like to thank the Curtin University scholarships program for offering the Curtin University Postgraduate Scholarship (CUPS) for the duration of 3.5 years, which made completion of my study a lot less stressful. I would also like to thank the Department of Chemical Engineer Laboratory staff and technicians for ensuring a safe and efficient work environment was available. This includes: Karen Haynes, Jason Wright, Ann Carroll, Xiao (Jimmy) Hua, and Roshanak Doroushi. Furthermore, I would like to thank Dr Shaomin Liu for organising regular seminars for the Department of Chemical Engineering over the past few years. The administration staffs have also been of great assistance, with special thanks to Jann Bolton and Tammy Atkins.

After receiving acceptance for the HUMAP scholarship to study at the University of Hyogo in Japan, there was a major shift in the work environment I am accustomed to. While working in Japan though, I received assistance from many great people who made my research smooth and enjoyable. I'd like to thank the follow people for the great experience: Prof. Mikio Ouchi, A/Prof. Shin-ichi Yusa, and Ms. Ryu Bun. Further thanks to my work colleagues: Mr. Ito, Mr. Inoue, Mr. Osawa, Mr. Enomoto, Mr. Nakai, Mr. Nagae, and Mr. Morihara.

BIOGRAPHY AND PUBLICATIONS

BIOGRAPHY

Bradley Hawkins graduated with a Bachelor of Engineering (Chemical Engineering) in 2009 from Curtin University, Australia. He commenced his PhD study shortly after on April 2010, receiving the Curtin University Postgraduate Scholarship (CUPS) award for the duration of his study. Additionally, he received the Hyogo University Mobility in Asia and the Pacific (HUMAP) scholarship in 2011 to undertake eight months exchange study at the University of Hyogo in Himeji, Japan.

Bradley's research interests and areas of expertise include: biodegradable polymers and nanostructures, electrospinning, microscopy analysis, and work with magnetic nanoparticles. Furthermore, he has proficiency in the common polymer synthesis technique RAFT (reversible addition-fragmentation chain-transfer polymerisation).

JOURNAL PAPERS

B. Hawkins, D. S. Chaudhary, C. Phan and G. H. Pham, "The effect of low concentration Fe_3O_4 nanoparticles in a chitosan-polycaprolactone electro-spun nano-fibre matrix.", Carbohydrate Polymers, **submitted 31st October 2013**.

CONFERENCE PROCEEDINGS

D. Chaudhary, R. K. Gupta, B. Hawkins and S. N. Bhattacharya, "Poly (lactic acid)/poly (butylene succinate) (PLA/PBS) Nanocomposites for thin film applications", Chemeca 2010: Engineering at the Edge; 26-29 September 2010, Hilton Adelaide, South Australia.

D. Chaudhary, B. Hawkins and Y. Dong**,** "Paramagnetic bionanocomposites from polyvinyl alcohol biopolymers", The Seventh Asian-Australasian Conference on Composite Materials (ACCM-7), Taipei, Taiwan, November 15-18, 2010.

H. Haroosh, D. S. Chaudhary, Y. Dong and B. Hawkins, "Electrospun PLA : PCL/ halloysite nanotube nanocomposites fibers for drug delivery", The Processing and Fabrication of Advanced Materials XIX conference (PFAM-19), Auckland, New Zealand, 14-17 January, 2011.

B. Hawkins and D. Chaudhary, “Analysis of the interaction an effect of magnetic nanoparticles in a bio-compatible polymeric electro-spun nano-fibre matrix”, Chemeca 2012: Quality of Life through Chemical Engineering; 23-26 September 2012, Wellington, New Zealand.

TABLE OF CONTENTS

LIST OF FIGURES

LIST OF TABLES

ABBREVIATIONS AND NOMENCLATURE

AIBN	Azobisisobutyronitrile
Avg	Average
Avrami Equation	Used to determine the dynamics of crystallisation
CAGR	Compound annual growth rate
$CDCl_3$	Deuterated chloroform
ChA-5	Cholesteryl 6-acryloyloxy hexanoate
CONH	Amide functional group in PNIPAM (*see PNIPAM)*
cP (units)	centi-Poise; dynamic viscosity unit
D_2O	Deuterated water
DCM	Dichloromethane
DSC	Differential scanning calorimetry
ECM	Extracellular matrix
EDS	Energy dispersive spectroscopy
emu	Electromagnetic units
f	Fraction of crystals; used in Avrami Equation
FC	Field-cooled
$FeCl_2$	Iron (II) chloride
$FeCl_3$	Iron (III) chloride
Fe_3O_4	Iron (II/III) oxide
GPC	Gel permeation chromatography
^1H NMR	Proton Nuclear Magnetic Resonance
ΔH	Heat of crystallisation
ΔH_m	Heat of melting
HA	Hyaluronic acid
K (units)	Kelvin; temperature unit
k	Rate constant; used in Avrami Equation
Kα peak	Representative of the K-alpha emission line (transition energy)
Kβ peak	Representative of the K-beta emission line (transition energy)
keV	Kilo-electronvolt
LCST	Lower critical solution temperature
mS (units)	milli-Siemens; electrical conductance unit
MTPA	(((methylthio)carbonothioyl)thio)-2-phenylacetic acid)

M_n	Number average molecular mass
M_w	Weight average molecular mass
n	Avrami exponent; used in Avrami Equation
NIPAM	*N*-isopropylacrylamide monomer
nm (units)	Nanometres
PCL	Poly(ε-caprolactone)
PEO	Polyethylene oxide polymer
PLGA	Poly(lactide-co-glycolide) polymer
PLLA	Poly(lactic acid) polymer
PNIPAM	Poly(*N*-isopropylacrylamide)
PVA	Poly(vinyl alcohol) polymer
RAFT	Reversible addition-fragmentation chain-transfer
SEM	Scanning electron microscopy
SQUID	Superconducting Quantum Interference Device
T_B	Blocking temperature
t_m	Experimental time
t	Time constant; used in Avrami Equation
T_C	Crystallisation temperature
TEM	Transmission electron microscropy
TFA	Trifluroroacetic acid
THF	Tetrahydrofuran
µm (units)	Micrometres
UV-vis	Ultraviolet-visible spectroscopy
V	Voltage (in kV)
wt%	Weight percentage
XRD	X-ray diffraction
XPS	X-ray photoelectron spectroscopy
ZFC	Zero-field cooled

CHAPTER 1

INTRODUCTION

1.1 Background

In the past decade, biopolymers and synthetic polymers have received an increasing amount of attention in the field of electrospinning. Electrospinning offers a simple, cost-effective process to produce a nanofibre material for a variety of applications ranging from bio-medicine to drug delivery. Biopolymers are useful for their biocompatibility and biodegradability, allowing for the use in tissue engineering and other *in vitro* studies. The drawback of these types of polymers is that they are often difficult to electro-spin due to their high viscosity in solution. Synthetic polymers on the other hand are much easier to electro-spin, and many are hydrophilic and biocompatible. The collaborative effect by blending these two polymers can produce nanostructures that possess the benefits of both constituents. This is particularly useful in electrospinning a polymer like chitosan, which is difficult to spin independently. These types of nanomaterials have also been combined with magnetic nanoparticles to introduce additional functionality to the material. These 'nanomagnetic' materials have had some success in cell growth proliferation and drug delivery applications (Wei et al., 2011; Lewkowitz-Shpuntoff et al., 2009; Wang et al., 2013a; Kannarkat, Battogtokh, Philip, Wilson & Mehl, 2010).

The global prospects for nanofibre technology and nanomagnetic materials have been reviewed by BCC Research. The global market for nanofibre-related products increased from $128.3 million in 2011 to $151.7 million in 2012. The forecast of the compound annual growth rate (CAGR) is 30.3% from 2012 to 2017, equating to $570.2 million global revenue by 2017 (BCC, 2013a). On the other hand, nanomagnetic materials have a much larger market with a value of $7.2 billion in 2011 and $7.3 billion in 2012. Global revenue of $9 billion is expected by 2017, with a five-year CAGR of 4.4% (BCC, 2013b).

1.1.1 Bio-polymeric and synthetic materials

Both biopolymers and synthetic polymers have been identified in the literature as viable constituents for biocompatible and biodegradable nanostructures. The collaborative effect of multiple types of polymers (and copolymers) has also been investigated. Polysaccharides (a type of bio-polymer) such as chitosan and hyaluronic acid have also been tested in electrospinning, but difficulty in their electrospinnability has limited their use (Lee, Jeong, Kang, Lee & Park, 2009). They are however biocompatible, biodegradable, and viable for cell transport suggesting they could be useful in blends (Ehrenfreund-Kleinman, Golenser & Domb, 2006). The range of synthetic polymers available are vast – some common materials used are: poly(ε-caprolactone), poly(L-lactic acid), and poly(lactic-co-glycolic acid) to name a few (Liao, Murugan, Chan & Ramakrishna, 2008). These materials are classified by the following polymer types: polyesters, polyfumarates, polyanhydrides, poly(ortho esters), poly(amino acids), polycarbonates, polyphosphazenes, and composites (Karande & Agrawal, 2008).

Functionalised polymers provide an alternative design approach for addressing the engineering problems of surface roughness and other nanoscale parameters. Possible functional agents include bioactive peptides and protein motifs, which can improve cell adhesion, growth, and functionality (Wieghaus & Botchwey, 2008). The mechanical, structural, and biodegradability of the functional groups are important design factors for using this approach. These physical factors, as well as cell transmission, can be incorporated into the design by using a coating approach or functionalising the entirety of the nanostructure material (Wieghaus & Botchwey, 2008). X-ray diffraction (XRD) can then be used to determine the distribution of the molecules throughout the polymer matrix (Uyar, Balan, Toppare & Besenbacher, 2009). In bone tissue engineering research, mineralisation has been used to produce mineralised nano-fibrous scaffolds. It has been found that functional groups can promote nucleation and crystal growth on the scaffold through the mineralisation process (Liao et al., 2008). Electrospinning further emphasises the surface chemistry of the nanofibres (increased atomic percentage and functional groups), which has been proven by X-ray photoelectron spectroscopy (XPS) (Deitzel et al., 2002). This innovative technique exploits the benefits of both the electrospinning and mineralisation process to imitate the extracellular matrix (ECM) of natural bone.

1.1.2 Superparamagnetic nanoparticles

The addition of nanoparticles can result in an improved performance of the electro-spun nanofibres. For example, the inclusion of clay particles such as montmorillonite can yield increased nanofibre strength and increased efficiency in drug delivery applications (Depan, Kumar & Singh, 2009). Factors affecting the quality of the reinforcement are: interfacial bonding, particle dispersion, and alignment with the nanofibres (Tan & Lim, 2008).

The superparamagnetic behaviour of nanoparticles is controlled by both heating and time. The magnetic moment of each particle 'flips' and the rate at which this occurs can change the apparent behaviour of the nanoparticles. If the flipping is faster than the experimental time (t_m), the particles are paramagnetic, whereas if they are slower they appear to have quasi-static properties. The blocking temperature, T_B, is the point at which t_m and the flipping time are equal. This concept is represented in Figure 1.1. This behaviour can be implemented into nanostructures to provide them with magnetic-response, via the application of an external magnetic field.

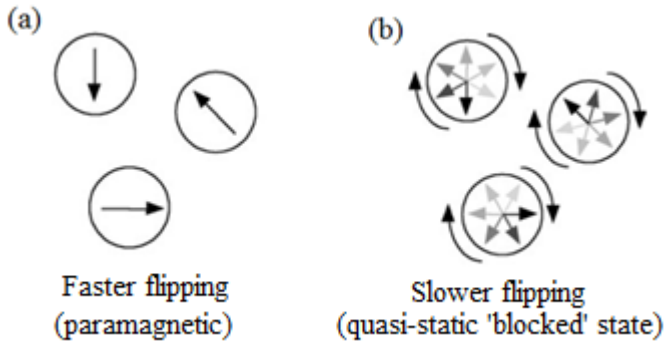

Figure 1.1: The concept of superparamagnetism, where the arrows are representative of the net magnetisation within a nanoparticle: (a) temperature is below the blocking temperature, T_B, and (b) temperature is above the blocking temperature, T_B (Pankhurst, Connolly, Jones & Dobson, 2003).

1.2 Motivation

1.2.1 Knowledge gaps

Electrospinning is a simple and cost effective process for producing nanofibres, and provides adequate control over the properties of the material. These properties include surface to volume ratio, porosity, and pore sizes. Desirable properties are

essential for biocompatibility, diffusivity (drug delivery), and cell growth within human tissue (scaffolding). In addition to these properties, stimuli-response has been identified in recent studies as a way to further the functionality of polymer nanofibres. The three primary stimuli are thermal, magnetic, and pH-response. These methods are often used individually to trigger a change within the material that causes release of a load, or even shearing with the nanostructure. A combination of two of these methods could lead to a more convenient release mechanism. This has not been researched specifically for nanofibres in the literature. This particular knowledge gap will be addressed by combining a thermo-responsive polymer (poly(*N*-isopropylacrylamide)) and magnetic Fe_3O_4 nanoparticles, as well as a pH-responsive (chitosan) with these particles. This dual functionality will provide a good understanding of how these nanoparticles affect the material properties of each polymer. Furthermore, these unique characteristics allow these nanostructures to be applicable to a wider range of applications that can utilise one or both stimuli.

Many nanofibre fabrication techniques have drawbacks, and these need to be minimised or eliminated in order to optimise the performance of the nanofibre-based products. In the case of the thermo-responsive polymer (PNIPAM), electrospinning optimisation has been poorly investigated in the literature with only a select few sources having researched this polymer. Therefore, rigorous optimisation methods will be required to provide a more concrete understanding of the behaviour of PNIPAM during electrospinning. This will include identification of the optimum operating parameters during the electrospinning process, as well as solution properties. Furthermore, the interactions between chitosan and magnetic nanoparticles in a polymer blend are poorly understood. Chitosan has been well researched in the field of electrospinning, but the difficulty of this procedure continues to be a problem (Geng, Kwon & Jang, 2005; Ohkawa, Cha, Kim, Nishida & Yamamoto, 2004). In order to address the knowledge gap surrounding magnetic nanoparticle interactions, the electrospinning of a consistent chitosan-based nanostructure will need to be achieved first. The development of these nanostructures will be crucial for future work completed in stimuli-responsive electrospinning and their applications.

This work will aim to close the aforementioned knowledge gaps, which are summarised below:

- Combination of two responsive stimuli within a nanofibre nanostructure,
- Rigorous optimisation methods in electrospinning PNIPAM, and
- The interaction between chitosan and Fe_3O_4 nanoparticles in a polymer blend.

1.2.2 Significance

Nanofibre research shows potential for various biomedical and drug delivery applications. As illustrated in past works, their importance in health-related research has been well recognised in the past decade. A common interest in hybrid material compositions has been the focal point of the more recent studies. The collaborative effect of a biological and synthetic polymer has been utilised to complement their properties – biopolymers provide biological signals and cell regulation, where synthetic polymers provide the necessary adhesion of cells (Mukherjee & Atala, 2006). This concept applies more specifically to tissue engineering, but can also be a common method for drug capsule manufacture.

Control over the behaviour of the release mechanism in any delivery system can be difficult to manage. By the introduction of stimuli-responsive materials into this field, external control of the material becomes more manageable and reliable. The preparation of nanostructures that follow this innovative design will provide the flexibility for a wider range of applications.

1.3 Methodology

The research plan for this thesis began with the selection of stimuli-responsive polymers for electrospinning and magnetic nanoparticles, followed by characterisation and analysis of the effect of embedding magnetic nanoparticles within the nanostructure. A brief statement of the steps taken is listed below:

- Selection of 2 – 3 stimuli-responsive polymers, a supporting polymer for blending, solvents, and magnetic nanoparticles.
- Planning of sample preparation tables for different concentrations, along with a matrix to record observations at different electrospinning parameters.

- Sample preparation and electrospinning.
- Selection of suitable characterisation methods to measure:
  - Average nanofibre diameter and distribution,
  - Average nanoparticle size,
  - Thermal and magnetic behaviour, and
  - Viscosity and conductivity properties.
- Assessment of the accuracy and reproducibility of the samples and results.

1.3.1 Material selection

In the selection of stimuli-responsive polymers for this study, many different properties were considered. The two main properties that are essential in polymer selection are solubility and electrospinnability. Initially, the three candidates under consideration were poly(*N*-isopropylacrylamide) (PNIPAM), chitosan, and hyaluronic acid (HA). After some preliminary trials of all three polymers, PNIPAM and chitosan were selected due to their higher electrospinnability and unique properties. The failure to electro-spin HA is outlined in Appendix F. Additionally, hydrophilic PNIPAM and chitosan both have stimuli-responsive properties: PNIPAM is thermo-responsive, and chitosan is pH-responsive. To further enhance the functionality of the nanostructures, iron (II,III) oxide (Fe_3O_4) nanoparticles were selected for their superparamagnetic properties. The addition of these nanoparticles allows magnetisation of the sample to induce localised heating as required. This can be used to trigger load release in applications such as drug delivery. A more exhaustive review of the selection criteria is shown in Appendix D.

1.3.2 Sample preparation and characterisation

All samples were prepared by mixing, followed by sonication for an appropriate length of time to ensure homogeneity. The synthesis of thermo-responsive poly(*N*-isopropylacrylamide) with a degree of polymerisation of 200 was completed using RAFT polymerisation. Measurement details and methods are specified in Chapter 3.

Characterisation was completed using various techniques to understand polymer chemistry, nanofibre size, magnetic properties, and thermal properties. The methods used are: Scanning Electron Microscopy (SEM), Transmission Electron Microscopy (TEM), Differential Scanning Calorimetry (DSC), and Superconducting Quantum Interference Device (SQUID). Polymer synthesis analysis was completed using:

Proton Nuclear Magnetic Resonance (^{1}H NMR), Gel Permeation Chromatography (GPC), and Ultraviolet-visible spectroscopy (UV-vis). Solution properties were also completed using a rheometer and conductivity meter.

1.4 Research contributions

The primary contributions made by this work are the understanding of the behaviour of biodegradable, biocompatible, stimuli-responsive polymers (PNIPAM and chitosan) in electro-spun nanostructures, and the effect that magnetic nanoparticles on the properties of these nanostructures. The key results and contributions are summarised below:

- The electrospinning of thermo-responsive PNIPAM was achieved through optimisation of electrospinning parameters. An average nanofibre diameter of 181 nm was measured. Furthermore, coaxial electrospinning was achieved with a PCL core and PNIPAM shell, with an average nanofibre diameter of 208 nm.
- It was found that magnetic Fe_3O_4 nanoparticles have an effect on the formation of the coaxial PNIPAM/PCL nanofibres. They result in an increased average nanofibre diameter (247 nm), and induce macromolecular folding of the shell via poor solvent interaction. Additionally, heating the nanostructure caused the exposure of the nanoparticles by the PNIPAM shell, which can be utilised for release-based studies.
- It was discovered that the complicated electrospinning of chitosan was trivialised by blending with PCL, with and without magnetic Fe_3O_4 nanoparticles. A variable nanofibre diameter of 36 – 262 nm was measured, and the nanoparticles resulted in a more consistent normal distribution of the nanofibre diameter. Furthermore, the nanoparticles were also proven to act as nucleation sites for spherulitic growth within the nanostructure.

1.5 Thesis outline

The primary research objectives for this study were: (1) To produce two stimuli-responsive nanostructures from ‘smart’ polymers; (2) To understand how electrospinning process parameters affect the outcome of nanofibre production; (3)

To determine how magnetic nanoparticles affect the characteristics of nanofibres during and after electrospinning; (4) To conclude how the results could be applied in the field of tissue engineering and/or drug delivery. The thesis is compiled into six chapters, which have been outlined as follows:

Chapter 1 makes a brief introduction to the background work, and identifies the problems that are being addressed by this thesis. The current knowledge gap is mentioned as the motivation and significance for this study, and the key research questions are stated. A brief methodology is also specified, and the contributions of this work are also addressed. ***Chapter 2*** is an in-depth literature review on the previous work completed in this area, using the current knowledge to identify knowledge gaps. ***Chapter 3*** discusses the experimental methodology, which details the materials used, solvent selection, sample preparation, experimental rig set-up, and characterisation methods (SEM, TEM, DSC, SQUID, ^{1}H NMR, GPC, UV-vis, viscosity and conductivity measurement). ***Chapter 4*** investigates the thermo-responsive polymer poly(*N*-isopropylacrylamide), and how different synthesis methods can affect the behaviour of the polymer in electrospinning. Additionally, the polymer is prepared via a coaxial configuration using the strong backbone polycaprolactone polymer. ***Chapter 5*** investigates the pH-responsive polymer chitosan, and explores the difficulties that arise when trying to electro-spin. The impact of polymer blending to benefit the electrospinning process is discussed, as well as the impact of embedding magnetic nanoparticles within the nanostructure. ***Chapter 6*** will present the conclusions from this work, and put forth recommendations for future work in this particular field.

CHAPTER 2

LITERATURE REVIEW

2.1 Electrospinning

Electrospinning is a simple, cost-effective technique for producing nano-scale biomaterials. It can be used to electro-spin a wide range of polymer materials into a matrix of randomly aligned nanofibres. The process involves the dispersion of polymer solution through a capillary such as a syringe, with a high voltage applied at the needle tip. The surface tension of the solution at the needle tip prevents the solution from discharging. This is where the high voltage comes into effect, by introducing an electrical potential that overcomes the surface tension (Palchesko et al., 2013). This phenomenon causes the solution to be drawn out in a whipping motion towards a grounded collector. As the solution is dispersed, the solvent rapidly evaporates causing the formation of a nanofibre mat on the collector. The typical setup for an electrospinning apparatus is shown in Figure 2.1.

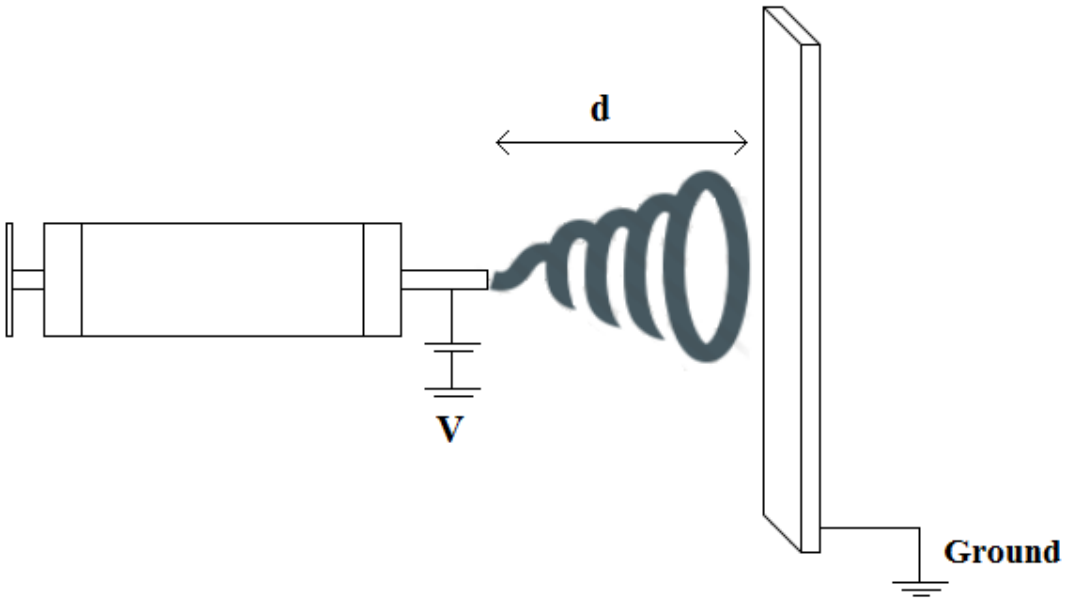

Figure 2.1: Standard electrospinning apparatus, where the voltage (V) is applied to the needle tip over the collector distance (d). Adapted from (Palchesko et al., 2013).

2.1.1 The Taylor cone

Once the critical potential is met to overcome the surface tension of the polymer solution, the droplet at the end of the capillary becomes elongated in the direction of the collector. This process forms a conical shape at the needle tip, referred to as the Taylor cone. The Taylor cone has a half angle of 49.3º and can usually be seen during the electrospinning process, indicating that the electrical threshold has been reached (Yarin, Koombhongse & Reneker, 2001). After the Taylor cone, elongation of the polymer solution is electrically-favoured. The Columbic interaction between the solution and the applied voltage causes the jet stream to exhibit a whipping 'spiral' motion (as illustrated in Figure 2.1) before reaching the collector (Nukavarapu, Kumbar, Merrell & Laurencin, 2008). It is imperative that this is allowed to occur over a sufficient distance for the solvent to evaporate and deposit uniform nanofibres. This is where optimisation and control over the process parameters are utilised.

2.1.2 Parameter control and optimisation

The electrospinning process operates using multiple control variables to manufacture specific product morphology. An understanding of how these parameters affect the nanofibre morphology is essential for successfully producing uniformly consistent nanofibres. The parameters may be classified by the following: solution, process, and ambient parameters (Li & Wang, 2013). The most important solution property is the concentration of the polymer in the solvent. The concentration is directly proportional to the viscosity of the solution, which is a key component for electrospinning. If the concentration is too high, the solution simply will not flow from the narrow needle tip. Generally, increasing the concentration with result in larger nanofibres (Chowdhury & Stylios, 2010). For process parameters, the applied voltage, collector distance, and flow rate must be optimised. Increasing the applied voltage will elongate the nanofibres, resulting in a reduced diameter. Increasing the distance to the collector allows a longer period of time for the solvent to evaporate from the jet, resulting in more uniform nanofibres. Similarly, control over the flow rate will promote uniformity although if the rate is too high, beading can occur throughout the product (Rodoplu & Mutlu, 2012; Nitanan et al., 2011; Chowdhury & Stylios, 2010). Ambient parameters basically refer to temperature control. This is maintained in more sophisticated systems, and may assist in solvent evaporation.

2.2 PNIPAM

Poly(*N*-isopropylacrylamide) is a synthetic, thermo-responsive polymer that can exhibit both hydrophilicity and hydrophobicity, dependent on the temperature. This unique behaviour has seen the use of this polymer in a wide range of research, from di-block copolymerisation to load-release applications (Pinol et al., 2007; Song, Wang & Wang, 2011).

2.2.1 Responsive behaviour

At a temperature of 32ºC and above, PNIPAM releases approximately 90% of its volume effectively shrinking itself. This reversible transition is referred to as the coil-to-globule transition, where the aqueous PNIPAM polymer coils convert to tightly aggregated globule formations. As the CONH functional groups become tightly collapsed, the water molecules hydrogen bonded to the CONH groups are released into the surrounding medium (Graziano, 2000). A basic representation of this transition is shown in Figure 2.2. The lower critical solution temperature (LCST) at 32ºC can be manipulated to lower or higher temperatures by modifying the polymer through functionalisation or similar methods. Typically, di-block or tri-block copolymerisation is undertaken using polymers such as cholesteryl and lactide-based groups (Chaw et al., 2004; Gan, Yuan, Liu, Pan & Gao, 2011; Kohori et al., 1998; Liu, Pramoda, Yang, Chow & He, 2004). In these particular investigations, the LCST was manipulated from 32 ºC to temperatures as high as 55 ºC. However, the most practical target temperature is 37 ºC – characteristic of the human body temperature, and associated applications.

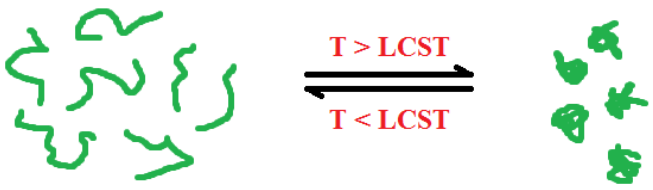

Figure 2.2: Coil-to-globule transition of PNIPAM.

2.2.2 Electrospinning of PNIPAM

The electrospinning of PNIPAM has been achieved in the past, with no complications for the linear, synthetic polymer. Typical solvents used for the

polymer are water, acetone, methanol, and tetrahydrofuran (THF) (Rockwood, Chase, Akins & Rabolt, 2008; Okuzaki, Kobayashi & Yan, 2009; Song et al., 2011). Although each of these solvents produces nanofibres to some degree, optimisation of the electrospinning methods in the literature is poor. The average diameter recorded by Rockwood and co-workers (Rockwood et al., 2008) was 5 – 17 μm (using water, acetone, and THF solvents), whereas Okuzaki and co-workers (Okuzaki et al., 2009) produced nanofibres with 165 nm using a methanol solvent. This comparison clearly indicates the impact of solvent selection, and how the polymer can behave differently. The optimal solvent for PNIPAM essentially comes down to how well the polymer interacts with the solvent. When the PNIPAM chain is allowed to extend and form intermolecular interactions, the solvent is good for the electrospinning process. In solvents where the PNIPAM macromolecule energetically favours collapsing on itself instead of interacting with the solvent, there will be difficulty when trying to electro-spin the solution (Rockwood, 2007).

The electrospinning parameters are dependent on the solvent used. Some solvents like acetone evaporate at a much faster rate, so electrospinning can occur over a shorter collector distance. Similarly, the conductivity and surface tension of the solution directly impact the applied voltage requirements to initiate the process. As detailed in Table 2.1, there is not a large difference between the electrical conductivity of the solvents mentioned. Therefore, the electrical conductivity is not crucial in the selection of a suitable solvent in this case. Methanol is likely the better solvent for nano-scale applications since it produced the smallest diameter in previous studies (Okuzaki et al., 2009).

Table 2.1: Electrical conductivity of common PNIPAM solvents.

Solvent	**Electrical conductivity (picosiemens/metre)**	**Reference**
Acetone	2×10^7	(Shell, 2010)
Methanol	7×10^6	(MI, 2014)
THF	1.5×10^6	(Invista, 2012)
Water	5×10^8	(MI, 2014)

2.2.3 Applications

Common applications for PNIPAM are: tissue engineering, drug delivery, and biosensors. It is used for its thermo-responsive stimulus in many nanofibre matrices

and gels. In tissue engineering, PNIPAM cannot independently support cell proliferation by the means of scaffolding. Another supporting polymer or material is required in order to provide the necessary mechanical strength and hydrophobicity for cell attachment (Chen et al., 2013). Studies have also found that the rate of cell de-adhesion increases with the polymerisation time for synthesising PNIPAM (Chen et al., 2008). In load-release applications such as drug delivery, PNIPAM excels by utilising the unique LCST transition. Studies have shown that the release rate can be controlled via temperature, observing slower release times above the LCST (Song et al., 2011). The permeability of the material has also been proven to be open-state, a necessity for the release mechanism (Lue et al., 2011). Biosensor studies are also common, using PNIPAM-based gels for glucose and protein adsorption (Sugiura, Imano, Takagi, Sakai & Kanamori, 2009; Suzuki & Kumagai, 2003).

2.3 Chitosan

Chitosan is a polysaccharide (a type of biopolymer) that is produced from crustacean shell or 'chitin'. Polycationic chitosan is pH-responsive due to the presence of the amine group of glucosamine in its molecular structure. When the surface charge of the molecule exhibits a neutral electrical charge, this is called the isoelectric point. The isoelectric point occurs at a pH of 7.4 for chitosan, which can be useful for applications where the isoelectric point can impact the system (Chen, Chung, Wang & Young, 2012).

2.3.1 Responsive behaviour

Similar to PNIPAM, chitosan has a threshold where it can reversibly alter how it behaves in a solution. The glucosamine within chitosan is protonated below the isoelectric point, allowing solubility in acidic solutions (Liu et al., 2012). Studies have shown that this property can be utilised in release applications, observing a high degree of molecular swelling in neutral media (Islam & Yasin, 2012). The degree of swelling is controllable by adding another hydrophilic polymer to the blend. Islam and co-workers (Islam & Yasin, 2012) added poly(vinyl alcohol) to increase thermal stability and reduce swelling in water-based media.

2.3.2 Electrospinning of chitosan

The electrospinning of chitosan is well-research in the literature, with complications arising due to the structure of this polymer. The backbone of the chitosan polymer is composed of the glucosamine groups, which are polycationic. This property results in high surface tension, which requires a high applied voltage to electro-spin (Lee et al., 2009). Furthermore, once this electrical threshold is achieved, the positively charged polymer causes repulsion between the ionic groups. This results in an unstable jet beyond the needle tip, causing solution to form droplets – separate from the stream (depicted in Figure 2.3).

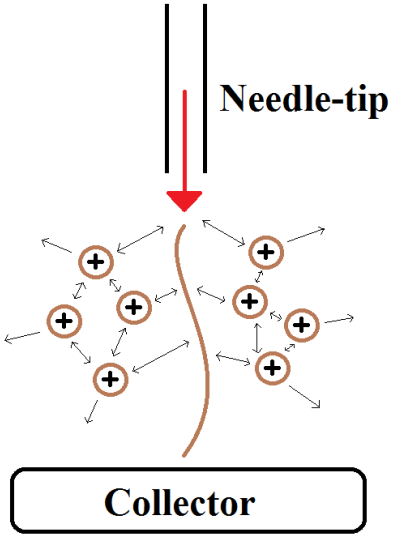

Figure 2.3: Repulsive forces from chitosan cationic groups resulting in droplets.

Electrospinning of chitosan has had some success in the literature, with a variety of different solvents and process parameters. The results of these works are shown in Table 2.2. A common solvent between all sources was acetic acid, usually at a concentration of 90%. The earlier works by Ohkawa and co-workers (Ohkawa et al., 2004) saw the use of other solvents such as dilute hydrochloric acid, neat formic acid, dichloromethane (DCM), and trifluoroacetic acid (TFA). The final average diameter of 330 nm was reached using a solvent mixture of DCM and TFA. As evident in Table 2.2, this was the largest average diameter measured from the literature. This suggests that the concentrated acetic acid has a better interaction with the chitosan molecule than the previously mentioned solvents. The concentration was consistent between each study, using less than 10%. This is attributed to the high degree of viscosity as more chitosan is added to the solution.

Table 2.2: Electrospinning parameters for pure chitosan.

Reference	Chitosan conc. (%)	Applied voltage	Degree of acetylation (%)	Average diameter
(Ohkawa et al., 2004)	8	15 kV	77	330 nm
(Geng et al., 2005)	7	4 kV/cm	56, 54, 65	100 – 290 nm
(Vrieze, Westbroek, Camp & Langenhove, 2007)	3	2 kV/cm	75 – 85	70 ± 45 nm
(Homayoni, Ravandi & Valizadeh, 2009)	7 – 7.5	17 kV	75 – 85	140 nm

2.3.3 Applications

Due to the biocompatibility and non-toxic nature of chitosan, this material has seen extensive use in applications involving biosensor, novel gels, enzymes, medicines, drug and gene delivery stems, plastic surgery, dermo-cosmetics, and therapy (Liu et al., 2012; Islam & Yasin, 2012; Kumbar, Nukavarapu, James, Hogan & Laurencin, 2008). The pH-responsive nature of chitosan assists in medical delivery systems that require sustained release over a period of time. Chitosan nanofibres alone are mechanically weak, so cell proliferation is difficult to maintain. For this reason, chitosan is often blended with reinforcing polymers such as PVA and PCL (Duan, Dong, Yuan & Yao, 2004; Sarasam & Madihally, 2005).

2.4 Magnetic nanocomposites

Magnetic nanoparticles draw their functionality through their ability to be controlled by an external magnetic field. Iron-based nanoparticles are the most common type used in electrospinning, such as iron(II,III) oxide (Fe_3O_4) (Wang, Singh, Hatton & Rutledge, 2004; Kannarkat et al., 2010). These nanoparticles are superparamagnetic in nature, which allows the magnetic field to manipulate them in polymer nanostructures. This is useful in applications such as cellular proliferation.

2.4.1 Iron-based nanoparticles and nanocomposites

When nanofibres are being produced with nanoparticles embedded within them, the size of the nanoparticles is very important. If their size is too close to the average nanofibre diameter, structural failure of the material is likely to occur. For this reason, nanoparticles less than 10 nm in diameter such as Fe_3O_4 nanoparticles have seen use in fibre-based nanocomposites. Other iron-based nanoparticles that have

seen use in larger scale applications are: polyisobutylene-coated Fe_3N (Burke & Stöver, 2002), $NiFe_2O_4$ from ball milling (Nathani, Gubbala & Misra, 2004), $CoFe_2O_4$ nanopowder (Chao & Cheng, 2006; Provenzano et al., 2006), γ-Fe_2O_3 (Mack, Cox, Lee, Dunn & Wu, 2007), and $Fe(CO)_5$ (Lewkowitz-Shpuntoff et al., 2009). During the synthesis of Fe_3O_4 nanoparticles, or before they are processed, they are often coated with a material to increase cyto-compatibility and cellular uptake (Pradhan, Giri, Banerjee, Bellare & Bahadur, 2007). This material is usually a polymer or some other biocompatible substance, such as lauric acid.

2.4.2 Applications

Magnetically-loaded nanostructures can provide a non-invasive method for actuation *in vivo* by an external field. As the superparamagnetic nanoparticles become magnetised, they put shear stress on the nanostructure (typically a scaffold) causing cells to become stimulated and nutrients to flow (Mack et al., 2007). The polymer scaffold mimics the role of the extracellular matrix, as a temple for cell growth. The biocompatibility of the nanostructure is improved by coatings that promote cellular adhesion, with lauric acid and dextran proven to be viable in past work (Pradhan et al., 2007). Other applications that have seen the use of coated Fe_3O_4 nanoparticles are targeted drug delivery, magnetic resonance imaging(Wang, Liu & Zhang, 2013b), bone healing and regeneration (Kannarkat et al., 2010), magnetic filters, sensors (Wang et al., 2004), and as a nano-adsorbent for Cu(II) ions (Chang, Chang & Chen, 2006).

2.5 PNIPAM-based nanocomposites

Thermo-responsive materials consisting of PNIPAM have had great success in the past in tissue engineering, drug delivery, and biosensors. The LCST of unmodified PNIPAM occurs at 32ºC, which can cause some difficulties when controlling drug release in an environment at body temperature (around 37 ºC). Therefore, researchers have investigated the modification of this ‘smart’ polymer by introducing new polymer materials through co-polymerisation and polymer blending. These actions result in an increase in the LCST, allowing controlled release at desirable temperatures.

2.5.1 PNIPAM nanocomposites via co-polymerisation

Modification of PNIPAM through organic chemistry (usually by reversible addition-fragmentation chain transfer – RAFT), is a common method for controlling the LCST for various nanocomposites. A hydrophobic component can be added to the PNIPAM polymer such as cholesterol-based groups, which result in the formation of micelles in solution. Polymer micelles such as these are useful for solubilising drugs that are normally hydrophobic (Chaw et al., 2004; Liu et al., 2004). Similarly, hydrophobic poly(DL-lactide) has been successful in micelle formation intended for active targeting as drug carriers (Kohori et al., 1998). Upon reaching the LCST, the micelles aggregate and then can dissociate again upon cooling. This behaviour is similar to that of pure PNIPAM molecules. Therefore, applications for these types of nanocomposites are similar to those mentioned in Section 2.2.3: temperature sensing, drug release, and other biomedical applications (Lue et al., 2011; Chuang & Chiu, 2012).

2.5.2 PNIPAM nanocomposites via polymer blending

The collaborative effect of blending two polymers is invaluable when you want to utilise multiple polymer properties. PNIPAM-based blends in electrospinning for controlled-release applications is relatively new, only mentioned by a select few sources (Chen et al., 2010; Tateishi, Chen & Ushida, 2002). The addition of a second polymer can not only alter the LCST and mechanical properties of the nanocomposites, but can also provide control of release rates in applications such as drug delivery. The main issue with manufacturing these blends is the selection of a solvent that is both suitable for electrospinning (meeting conductivity and viscosity requirements), and adequately solubilises both polymers. In some cases this is not possible due to toxicity concerns, so a core-and-sheath nanofibre design is an acceptable alternative. By using a mechanically strong polymer as the core (preferably hydrophobic), the responsive polymer can then be used as the shell material to release the drug (Chen et al., 2010). The core-and-sheath approach can also have complications with nanofibre uniformity and stability during the electrospinning process. Electrospinning should be undertaken vertically so the shell can maintain a uniform thickness for the whole circumference of the nanofibre product.

2.6 Chitosan-based nanocomposites

Pure chitosan nanofibres have low process-ability, a fast dissolution rate, average biological affinity, and are mechanically weak and brittle. These issues are solved through polymer blending, which has received a lot of attention in the past. A wide range of polymers/materials have been used in blends with chitosan, including: PLGA (Perugini, Genta, Conti, Modena & Pavanetto, 2003), PEO (Duan et al., 2004), PLLA (Duarte, Mano & Reis, 2010), PCL (Sarasam & Madihally, 2005), montmorillonite clay (Depan et al., 2009), PVA (Islam & Yasin, 2012) and collagen (Wang et al., 2013a). Although the properties of each of these materials vary, they all serve the same function in chitosan-based nanocomposites – to improve the mechanical strength. Furthermore, biological properties are enhanced such as cellular affinity and tissue compatibility (Shalumon et al., 2010; Van der Schueren, Steyaert, De Schoenmaker & De Clerck, 2012)

The electrospinning of chitosan is also drastically improved by a more linear and stable polymer. The hydrophobic polymer PCL is a great candidate for blending with chitosan, assisting with mechanical strength, reducing the biodegradation rate (improves sustained release applications), and increases the overall bio-functionality of the nanostructure (Sarasam, Samli, Hess, Ihnat & Madihally, 2007).

Summary

In summary, there is a general understanding of the behaviour of both PNIPAM and chitosan during the electrospinning process. The literature relevant to electrospinning PNIPAM however is very narrow, and does not investigate more rigorous methods of nanocomposites functionality. This research aims to address this knowledge gap via the manufacture of a 'smart' PNIPAM-based composite that has the additional benefit of magnetic nanoparticles. A faster drug release at the LCST is expected for the core-and-sheath system (Chaw et al., 2004).

Chitosan and PCL blends are well investigated in the literature, having success with many different solvent combinations. This particular blend can form a mechanically sound scaffold for applications that include cell growth. To further the functionality of this blend, magnetic nanoparticles have been added in the work conducted in this thesis to introduce directional control over cellular growth within the scaffold. The final product aims to exhibit:

- Mechanical strength,
- A prolonged release profile,
- Improved process-ability,
- A uniform distribution of the nanofibre diameter, and
- Enhanced cellular affinity.

CHAPTER 3

EXPERIMENTAL METHODOLOGY

3.1 Materials

3.1.1 Linear polymers

The two linear-structured polymers selected for the focus of this research were poly(*N*-isopropylacrylamide) (PNIPAM) and polycaprolactone (PCL). The molecular structure for these polymers and their base monomers (NIPAM and caprolactone) is shown in Figure 3.1.

	Polymer structure	***Monomer model***
P(NIPAM)$_m$	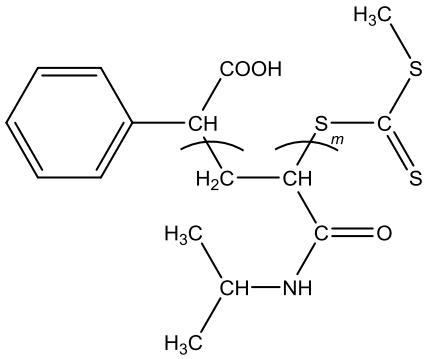	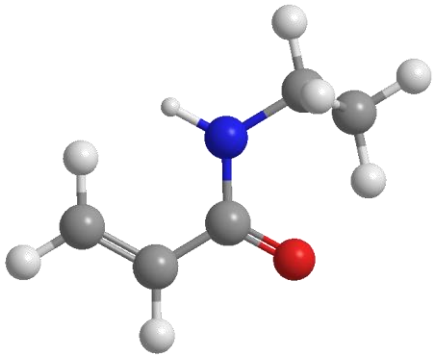
PCL	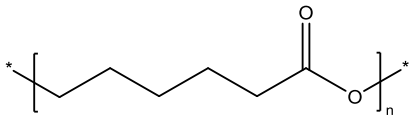	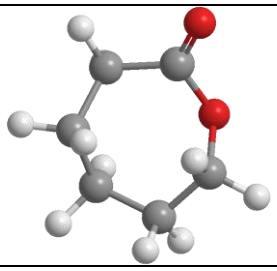

Figure 3.1: Molecular structure of PNIPAM and PCL and their respective base monomer (molecular structures obtained via Chem3D Pro 13.0).

PNIPAM with a molecular weight of 19,000 – 30,000 was purchased from Sigma-Aldrich Co. LLC, Australia. PNIPAM was also prepared by RAFT polymerisation, with a degree of polymerisation of 50 and 200. PCL with a molecular weight of 80,000 was also purchased from Sigma-Aldrich Co. LLC, Australia. The properties of these polymers are shown in Table 3.1.

Table 3.1: Properties of PNIPAM and PCL.

	Source	M_{wt}	Melting point
PNIPAM	Sigma (as received)	19,000 – 30,000	96°C
$PNIPAM_{200}$	Synthesised in lab	21,862	–
PCL	Sigma (as received)	80,000	60°C

3.1.1.1 PNIPAM synthesis using RAFT

PNIPAM was synthesised from the precursor monomer *N*-isopropylacrylamide (NIPAM) through reversible addition-fragmentation transfer polymerisation (RAFT). The solvent used was tetrahydrofuran (THF), with MTPA (2-(((methylthio)carbonothioyl)thio)-2-phenylacetic acid) as the chain transfer agent and azobisisobutyronitrile (AIBN) as the initiator. The NIPAM (99.3%) monomer was purchased from Kohjin Co. Ltd., and AIBN (>98%) was purchased from Wako Pure Chemical Industries, Ltd. The molecular structure and properties for NIPAM and MTPA are shown below in Figure 3.2.

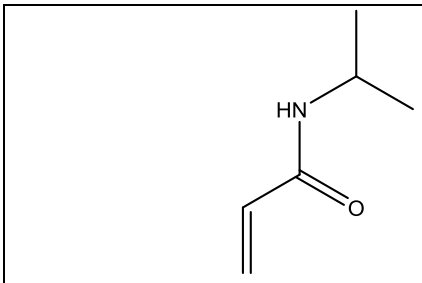

N-isopropylacrylamide
Chemical Formula: $C_6H_{11}NO$
Molecular Weight: 113.16
Elemental Analysis: C, 63.69; H, 9.80; N, 12.38; O, 14.14

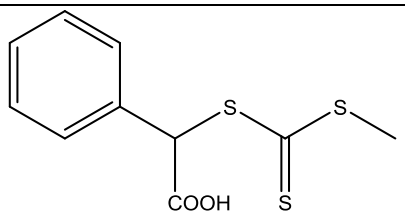

2-(((methylthio)carbonothioyl)thio)-2-phenylacetic acid
Chemical Formula: $C_{10}H_{10}O_2S_3$
Molecular Weight: 258.37
Elemental Analysis: C, 46.49; H, 3.90; O, 12.38; S, 37.23

Figure 3.2: Molecular structure and properties of NIPAM and MTPA (molecular structures obtained via Chem3D Pro 13.0).

3.1.1.2 Solvent selection

In preparation for electrospinning, PNIPAM was dissolved using methanol. The THF solvent was only used for the RAFT polymerisation step. For PCL, glacial acetic acid was used at a concentration of 90% (from Chem-Supply Pty Ltd, Australia).

3.1.2 Networked polymers

Networked polymers that have been tested in this research include chitosan and hyaluronic acid. Hyaluronic acid was trialled with multiple solvent compositions, but

consistently was unable to produce uniform fibres. There was much better success with chitosan, which was then selected to make a stimuli-responsive nanocomposite with magnetite nanoparticles (Fe_3O_4). The complete chitosan polymer structure is linear, however in this study it is referred to as 'networked' due to the structure of the D-glucosamine repeating unit. This monomer unit creates intermolecular chain entanglement, resulting in a high solution viscosity at low polymer concentrations. Chitosan with 85% deacetylation was purchased from Sigma-Aldrich Co. LLC, Australia. The chitosan was dissolved using glacial acetic acid at a concentration of 90%. The molecular structure of chitosan and the base monomer (D-glucosamine) is shown in Figure 3.3, and the properties of chitosan are shown in Table 3.2.

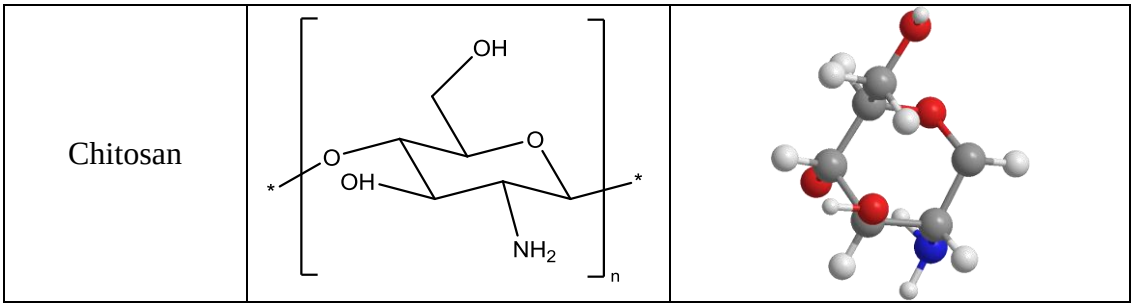

Figure 3.3: Molecular structure of chitosan and its respective base monomer (molecular structure obtained via Chem3D Pro 13.0).

Table 3.2: Properties of chitosan, from crab shells.

	Source	% Deacetylation	Viscosity (cps)	M_{wt}
Chitosan, from crab shells	Sigma (as received)	≥ 85	> 200	~ 150,000

3.1.3 Synthesised nanoparticles

Magnetite nanoparticles (Fe_3O_4) were prepared by a precipitation reaction using iron (II) chloride ($FeCl_2$) and iron (III) chloride ($FeCl_3$), with lauric acid to control particle agglomeration. $FeCl_2$, $FeCl_3$, and lauric acid were purchased from Sigma-Aldrich Co. LLC, Australia.

3.2 Methodology

The process of electrospinning is affected by not only the process parameters, but also the methods used during sample preparation. This includes the concentration of each sample, and the method of mixing used to ensure the homogeneity of the

solution prior to electrospinning. The concentration of each polymer has been determined using trial and error to determine the appropriate solution composition that yields satisfactory nanofibres formation. This ultimately comes down to the physical properties of the solution: molecular weight, concentration, viscosity, conductivity, and surface tension (Li & Wang, 2013).

The primary process parameters that affect electrospinning are the voltage, flow rate, collector specification, and the ambient conditions. By controlling these process parameters in conjunction with the solution preparation, direct control of the nanofibre properties can be achieved.

3.2.1 Sample preparation

3.2.1.1 Preparation of PNIPAM using RAFT

PNIPAM was prepared using RAFT polymerisation with the aim of 200 for the degree of polymerisation. The ratios of the reactants were calculated according to this target, shown in Table 3.3. The mole ratios were selected based on the recommendation of Dr. Shin-ichi Yusa and his past experience with this polymerisation technique (Iwasaki, Sakiyama, Fujii & Yusa, 2013). After combining the reactants in a 50 mL pear-shaped flask, a magnetic stirring chip is added and the solution is swirled until all reactants are dissolved. Then argon gas is bubbled through for 30 minutes to purge oxygen, while also on a magnetic stirrer. The solution is then placed in an oil bath at 60ºC for 16 hours, which is also equipped with a magnetic stirrer at the base.

Table 3.3: Measurements of the reactants (to produce $PNIPAM_{200}$).

	M_{wt}	Moles (mmol)	Weight	Mole ratio
NIPAM	113.16	44.19	5.0 g	200
MTPA	258.38	0.221	57.1 mg	1
AIBN	164.21	0.0884	14.5 mg	0.4
THF	0.88 g/mL		22.1 mL (17.7 g)	

3.2.1.2 Preparation of the PNIPAM-based solutions for electrospinning

PNIPAM was prepared in methanol and acetone at a concentration of 10% and 15% w/v. PCL was prepared separately from the PNIPAM solution; using a PCL concentration of 10% w/v in 90% concentrated acetic acid. These solutions were

mixed via sonication for 10 minutes. Magnetite nanoparticles were also added as a concentration of 1% w/v. This concentration was selected since a higher concentration of nanoparticles could weaken the nanofibre mechanically. The nanoparticles were added to form a combined solution with PNIPAM that was used in a core-and-shell electrospinning setup with the PCL solution (detailed in Section 3.2.3). The solution constituents for these solutions are detailed in Table 3.4.

Table 3.4: Measurements of the reactants for PNIPAM and PCL nanocomposites.

	PNIPAM samples		
	PNIPAM	Methanol	Acetone
PNIPAM-M1	1.0 g	10 mL	–
PNIPAM-M2	1.5 g	10 mL	–
PNIPAM-A1	1.0 g	–	10 mL
PNIPAM-A2	1.5 g	–	10 mL
	PCL sample		
	PCL		Acetic acid (90%)
PCL-10	2.0 g		20 mL
	PNIPAM nanocomposite sample		
	PNIPAM-M2 solution		Magnetite solution (Fe_3O_4)
PNIPAM-M2-1	10 mL		1%

3.2.1.3 Preparation of the chitosan-based solutions for electrospinning

Chitosan was dissolved in 90% concentrated acetic acid to give two solutions at a concentration of 0.5% and 1% w/v. PCL was dissolved in chloroform and was added to the chitosan solutions at 6% and 8% w/v to make a total of four compositions. All four solutions were then sonicated for two hours and their viscosity was measured. Each sample was divided into two separate solutions, and magnetic nanoparticles were added to one of them at a concentration of 1% w/v for the solid Fe_3O_4 (outlined in Table 3.5). Sonication was performed once more to ensure homogeneity throughout the solution. This was done using a Vibra-Cell™ ultrasonicator, shown in Figure 3.4. The required amount of Fe_3O_4 solution to be added was calculated using the stoichiometric relationship between the Fe^{+2} ions and Fe_3O_4 product during the nanoparticle synthesis (detailed in Appendix E), expressed by:

$$\boldsymbol{Fe^{+2}_{(aq)} + 2\ Fe^{+3}_{(aq)} + 4\ H_2O_{(l)} \rightarrow Fe_3O_{4(s)} + 8H^{+}_{(aq)}}$$

Table 3.5: Measurements of the reactants for chitosan and PCL nanocomposites.

Sample	A	B	C	D	E	F	G	H
Chitosan (wt%)	0.5	0.5	0.5	0.5	1	1	1	1
PCL (wt%)	6	6	8	8	6	6	8	8
Fe_3O_4 (wt%)	0	1	0	1	0	1	0	1

Figure 3.4: Ultrasonicator used for sample mixing.

3.2.1.4 Preparation of the magnetite nanoparticles

Magnetite was formed by combining 60 mL of 0.2 M iron (III) chloride and 30 mL of 0.2 M iron (II) chloride. Each solution was prepared in distilled water, and then sodium hydroxide was added to precipitate the magnetic nanoparticles. The solutions were stirred, and then 1 mL of lauric acid was added to control particle agglomeration (Pradhan et al., 2007; Kurtoğlu et al., 2012). The solution was then sonicated, and allowed to cool to room temperature afterward.

3.2.2 Experimental setup for RAFT polymerisation

After the sample has been prepared as per Section 3.2.1.1, polymerisation was carried out in the oil bath using the setup shown in Figure 3.5. The glass valve seals the flask, which was closed after flushing it with argon gas. After 16 hours, 1-2 drops

of the solution was placed into an NMR tube with deuterated chloroform ($CDCl_3$) to calculate the conversion before purification.

Figure 3.5: Polymerisation in the oil bath at 60ºC in the airtight flask.

The purification step was carried out using a poor solvent to precipitate the PNIPAM product from the solution. A 400 mL solution of 1:1 di-ethyl ether/*n*-hexane was prepared, and the solution was added drop-wise to the poor solvent while undergoing magnetic stirring. Once all the solution had been dropped into the poor solvent, the solid precipitate was then separated by vacuum filtration. The filter paper was wetted down by *n*-hexane prior to filtration, and took approximately 10 minutes.

The precipitate was collected into a beaker from the filter paper, and dissolved in a minimum amount (to fully dissolve the precipitate) of THF. This was performed while heating in a water bath. The precipitation in the 1:1 di-ethyl ether/*n*-hexane poor solvent step was then repeated. Once the precipitate was collected after the second purification step, it was put in a dry vacuum oven at 60ºC equipped with a cold trap apparatus (using liquid nitrogen). After approximately 90 minutes, the cold trap apparatus was removed and the vacuum oven was left to heat the sample for 24 hours. The summary of this methodology is shown in Figure 3.6 below.

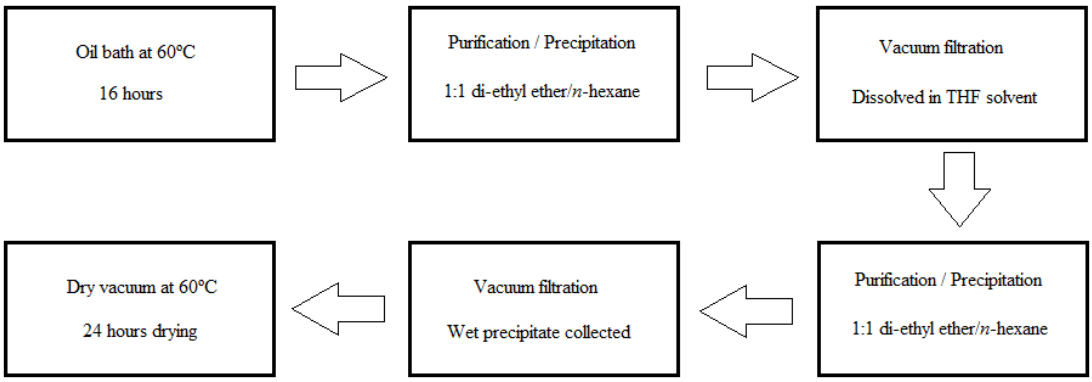

Figure 3.6: RAFT polymerisation methodology.

3.2.3 Experimental setup for electrospinning

An electrospinning and spray unit from NaBond Technologies Co., Limited was used to produce the nanofibres. The machine is equipped with a dual-channel syringe pump, background light, x-axial slider, motorised rotating collector, linear actuator, fan, heater, and a voltage supply (0 – 50 kV). The front panel provides direct control over important process parameters during electrospinning, including the voltage, collector distance, and temperature conditions. The SN-50 dual-channel syringe pump is equipped to use 10, 20, 30, and 50 mL syringes, and provides accurate control for the flow rate of the discharging solution. A simplified representation of the experimental setup is shown in Figure 3.7.

A minimum solution volume of 5 mL is required for this setup in order to fill the feed tube to the needle. The needle size selected had an inner diameter of 0.7 mm, which could be changed to a wider needle if there was congestion at the needle tip.

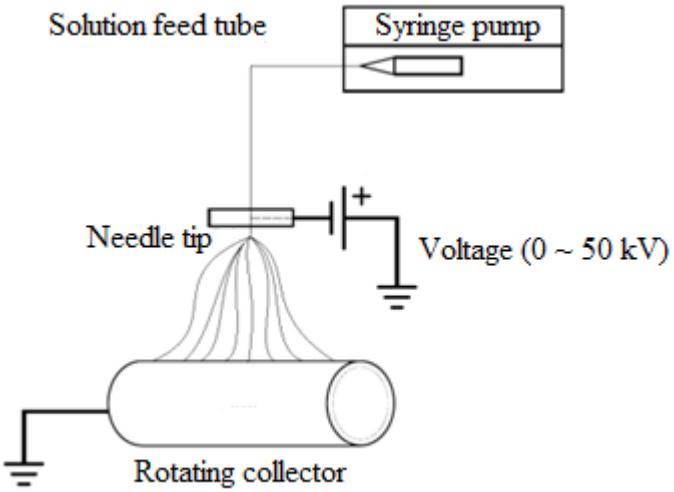

Figure 3.7: NaBond Electrospinning Unit setup.

3.2.3.1 Core-and-shell electrospinning setup

A coaxial spinneret, provided by NaBond, was used to produce the core-and-shell nanofibres. The aim of this setup is to produce a single nanofibre that exhibits the advantages of two different polymers. The core is typically the polymer with good electrospinnability (relative to the shell polymer), and can be used to improve the mechanical strength of the fibre. The needle size of the spinneret is shown in Figure 3.8.

The difference in the area between the core and shell spinneret is to be taken into account when setting the flow rate of each solution. To ensure that the core and shell thickness are adequately distributed, the velocity at which they are both ejected from the spinneret should be similar. This is shown in the example calculation below, where the core flow rate (F_{core}) is specified as 1.5 mL/h.

$$V_{core} = \frac{4F_{core}}{\pi D_{core}^2} = \frac{4 \times 1.5}{\pi \times 0.07^2} = 389.77\ cm\ /\ h$$

$$Assume\ V_{core} = V_{shell} = 389.77\ cm\ /\ h$$

$$F_{shell} = \frac{1}{4}\pi D_{shell}^2 V_{shell} - \left(1.5\frac{mL}{h}\right) = 6.34\ mL\ /\ h$$

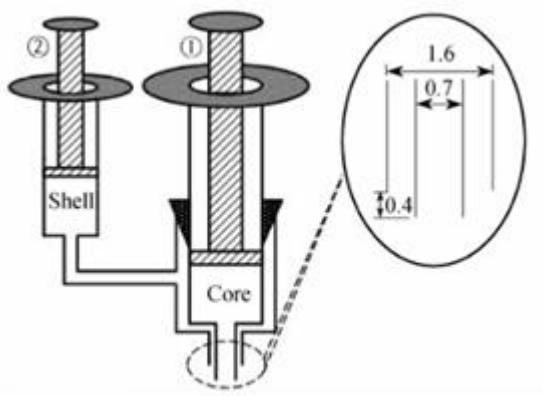

Figure 3.8: Core-and-shell needle size, measured in mm (provided by NaBond Technologies Co., Limited).

3.2.4 Process parameter optimisation

3.2.4.1 Voltage

When electrospinning, there exists a threshold voltage at which point the surface tension of the solution is overcome at the needle tip and forms the Taylor cone. This value ranges differently for each solvent system, so it is necessary to slowly increase the voltage during the initial electrospinning trials to see when the Taylor cone begins to form. In the literature, it is inconclusive to whether the voltage has a significant impact on nanofibre properties such as the diameter (Li & Wang, 2013). However, the voltage still is an important parameter during electrospinning optimisation since it can assist in determining whether the conductivity and surface tension of the solution are suitable.

3.2.4.2 Flow rate

The flow rate of the solution directly affects the morphology of the nanofibres as they are formed. Generally, a low flow rate of 1.0 mL/h or lower is preferable do allow enough time for the solvent to evaporate and form the nanofibres. If the nanofibres are beaded, or the solution jet is sporadic, this can indicate that the flow rate is too high.

3.2.4.3 Collector and distance

Common collectors used for electrospinning are a static or rotation drum substrate, covered with aluminium foil. The substrate used must be conductive for nanofibre

deposition, and is grounded. In this study, a rotating collector is used to distribute the nanofibres over a larger area. The distance between the collector and the needle tip is controlled by the linear actuator in the NaBond Electrospinning Unit. The linear actuator is connected directly to the insulated attachment that houses the needle tip, as shown in Figure 3.9. This distance also is included in the optimisation process, since there must be sufficient time for the solvent to completely evaporate before reaching the collector. Large distances have also been found to be unsuitable, causing beaded nanofibres and resulting in nanofibres to ground to other surfaces inside the machine.

3.2.4.4 Process environment control

The temperature and air flow in the machine are controlled by the heating and fan system provided. A temperature sensor is located in front of the heating bar (see Figure 3.8), which relays the system temperature to the front panel of the machine. The temperature can be increased to slightly increase solvent evaporation if the nanofibres produced appear to be wet. The fan system is located at the back side of the machine, but has no control over the speed. Therefore, it was not used in the experiments completed in this study since it had a noticeable effect on the direction of the electrospinning jet.

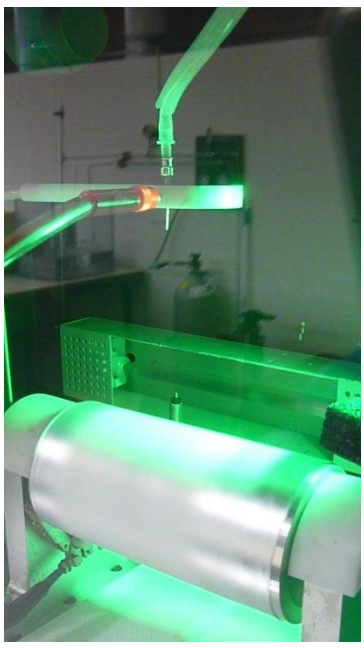

Figure 3.9: Rotating collector in the NaBond Electrospinning Unit.

3.3 Characterisation

Multiple characterisation techniques were exercised to understand how the polymer solution behaves prior to electrospinning, and to assess the uniformity and distribution of the nanofibres after the process. The polymer solutions were characterised using a rheometer and conductivity meter. The apparatus used for analysis of the nanofibres and nanoparticles included: Scanning Electron Microscopy (SEM), Transmission Electron Microscopy (TEM), Differential Scanning Calorimetry (DSC), and a Superconducting Quantum Interference Device (SQUID). Furthermore, Proton Nuclear Magnetic Resonance (^{1}H NMR), Gel Permeation Chromatography (GPC), Ultraviolet-visible Spectroscopy (UV-vis), and Lower Critical Solution Temperature (LCST) were utilised for the analysis of the synthesised PNIPAM.

3.3.1 Viscosity and conductivity measurement

The viscosity of the polymer solution is critical to successfully producing continuous fibres. The viscosity is directly controlled by the molecular weight and concentration of the polymer used, and thus can be easily tuned to meet electrospinning requirements. At low viscosities, surface tension causes significant beading in the fibres, whereas high viscosities can cause blockages in the feeding tube or needle tip (Li & Wang, 2013). The viscosity of each polymer solution was measured using a HAAKE MARS rotational rheometer platform (Thermo Scientific) fitted with a C35/4º Ti L cone. This state of the art platform has a temperature range of –150ºC to 600ºC, with a torque range from 0.01 µNm to 200 mNm. The automatic temperature module recognition and automated software routines made use of this rheometer trivial for analysing polymer solutions. The HAKKE RheoWin software graphically produces the data for the viscosity (η) and shear stress (τ) as a function of the shear rate ($1/\gamma$). Each measurement was performed at 20ºC, and was completed after the 180 second programmed routine.

It has been proven in past works that the conductivity of the solution can impact fibre diameter and bead formation. Common methods of increasing the conductivity are solvent selection and the addition of salt ions (Angammana & Jayaram, 2011). In this study, magnetic nanoparticles were utilised to increase the conductivity to reduce

bead formation and to see if thinner fibres were produced. The conductivity of the solutions was measured with a digital handheld conductivity meter.

3.3.2 Scanning electron microscopy (SEM)

Scanning electron microscopy (SEM) was used to analyse the formation, consistency, and dispersion of the nanofibres. After imaging, the average nanofibre diameter and distribution was measured by taking approximately 50 diameter measurements. The consistency of the nanofibres was assessed by the degree of bead formation or diameter variation for one unique nanofibre. Additionally, energy dispersive spectroscopy (EDS) was completed using the SEM equipment for elemental analysis of the samples.

The samples were prepared for imaging by cutting a 1 x 1 cm square from the aluminium foil with the nanofibres. They were then placed on stubs with carbon tape and sputtered with a platinum coating 2 nm thick. A Zeiss Evo 40XVP scanning electron microscope was used to capture high resolution images of the nanofibres. In most cases, an accelerating voltage of 15 kV and spot size of 400 was used. For EDS, the settings used were: accelerating voltage of 20 kV, working distance of 8.5 cm, and spot size of 450.

3.3.3 Transmission electron microscopy (TEM)

Transmission electron microscopy (TEM) was used to measure the size of the nanoparticles, which require a high resolution than that supplied by SEM (Angammana & Jayaram, 2011). The JEOL 2000FX TEM (University of Western Australia) with a tungsten filament was used to measure the diameter of the nanoparticles, operating at a voltage of 80 kV. The samples were prepared by depositing the solution onto the grids, then allowing the solvent to evaporate.

3.3.4 Differential Scanning Calorimetry (DSC)

Thermal and crystalline properties are commonly analysed using differential scanning calorimetry (DSC). The crystallisation, melting point, and heat flow through the sample can be determined from the data, using a pre-determined heating and cooling sequence (Vasanthan, Ly & Ghosh, 2011).

A Perkin Elmer DSC 6000 unit was used with an autosampler to complete the analysis. An aluminium pan was loaded with 10 – 20 mg of each sample, and then sealed. The samples were heated from 35°C to 150°C at 5°C/min with an isothermal reading held at 150°C for two minutes, followed by cooling down to 35°C at 5°C/min. The heat of melting, ΔH_m, was measured using the provided software, and the data was exported for use in Microsoft Excel.

3.3.5 Superconducting Quantum Interference Device (SQUID)

To determine if the nanoparticles are stimuli-responsive in the nanostructure, a superconducting quantum interference device (SQUID) magnetometer is used (Wang et al., 2004). This method will confirm the superparamagnetism of the nanoparticles, and provides information about the saturated magnetisation, remanence, and coercivity.

Magnetic testing was performed using a SQUID Quantum Design MPMS-7 (University of Western Australia). Zero-field cooled (ZFC), field cooled (FC), and hysteresis testing were used to determine the magnetic nature of the nanoparticles in the polymer matrix. The samples were cooled to 10 K at 0 and 200 oersteds for ZFC and FC, respectively. To better observe the behaviour before the blocking temperature, T_B, was reached, 5 K increments were used when heating from 10 to 50 K. Increments of 10 K were then used for 50 to 100 K, and 20 K increments for the remainder of the experiment. The sequences for these trials are detailed in Appendix B.

3.3.6 Nuclear Magnetic Resonance (NMR)

Nuclear magnetic resonance (NMR) is used to calculate the conversion of NIPAM after RAFT polymerisation (You et al., 2007). ^{1}H NMR is completed before and after polymerisation, and a reference peak is selected. This reference peak is the value of a functional group(s) that will remain unchanged after the polymerisation process. Once the conversion is calculated, this value is confirmed by GPC (Section 3.3.7).

The ^{1}H NMR analyses was completed using the Bruker DRX500 spectrometer (University of Hyogo, Japan) operating at 500 MHz. Solvent peaks for deuterated chloroform ($CDCl_3$) and deuterated water (D_2O) were set at 7.25 and 4.8 ppm,

respectively. These deuterated solvents allow the use of frequency-field lock to compensate for any natural drift from the magnetic field, B_0. The data range was set from –0.1 to 9.9 ppm and the number of scans was 16.

3.3.7 Gel Permeation Chromatography (GPC)

To complement the results from NMR analysis, GPC is used to calculate the number average molecular weight (M_n), weight average molecular weight (M_w), and dispersity (M_w/M_n) (Park, Yoon & Kim, 2010). GPC was performed using a refractive index (RI) detector equipped with a Shodex GF-7M HQ column (University of Hyogo, Japan), operating at 40°C with a flow rate of 0.5 mL/min.

3.3.8 Ultraviolet-visible Spectroscopy (UV-vis)

Ultraviolet-visible spectroscopy (UV-vis) is used to determine the absorbance peak of different concentrations of the polymer at a set wavelength. The relationship between the concentration and absorbance can be used to determine the absorption coefficient by the Beer-Lambert law (temperature sensitivityHermann et al., 2013). This can then be used to calculate the degree of polymerisation, and then the molecular weight (M_n) of the synthesised polymer. In the case of analysing PNIPAM, it is also possible to calculate the lower critical solution temperature (LCST) using the UV-vis equipment.

The absorption spectra were measured using a JASCO V-630 UV/VIS spectrophotometer (University of Hyogo, Japan) with a 1 cm path length quartz cell. The LCST samples were prepared at a concentration of 1 g /L and were heated at 0.5°C/min with JASCO ETC-505T thermostat system. The software “Spectra Manager” was used to export the absorbance data and heating and cooling curves for use in the calculations.

CHAPTER 4

PNIPAM-BASED NANOSTRUCTURES

4.1 Introduction

4.1.1 Outline

A wide range of linear polymers have been process to form nanostructures, including the widely investigated temperature-responsive polymer, PNIPAM. This chapter will investigate the synthesis of PNIPAM to study its unique properties, and then will be electro-spun into a stimuli-responsive nanofibre structure. Furthermore, coaxial electrospinning was performed with another linear polymer (PCL), and with magnetite nanoparticles to create a dual-responsive system. The impact of using of using PNIPAM with a variation in molecular weight was studied by synthesising a long chain PNIPAM in the laboratory. There was a distinct difference in the electrospinning results between this polymer and the other which was commercially purchased.

The effect of the nanoparticles also resulted in substantial changes in the electrospinnability of the solutions, and also the crystallinity of the samples. Analysis of the nanostructure properties was completed using: SEM (including EDS), TEM, SQUID, DSC, rheometer measurements, and conductivity measurements. Finally, a short discussion will complete the chapter by relating the experimental results to potential applications.

4.1.2 Material selection

PNIPAM is a biocompatible, temperature-responsive polymer that exhibits different behaviour below and above its lower critical solution temperature at 32ºC. Above this temperature, the polymer becomes hydrophobic as hydrogen bonding with the aqueous solution is replaced by intramolecular hydrogen bonding between the polymer functional groups (Chen et al., 2010; Song et al., 2011). These unique properties have resulted in a broad range of research for this polymer; however there is a significant knowledge gap in the electrospinning of PNIPAM. The successful

preparation of a PNIPAM-based nanostructure can lead to applications in cell culturing, drug delivery, and sensors (Okuzaki et al., 2009). Polycaprolactone (PCL) was selected to be used in a coaxial electro-spun nanostructure with PNIPAM. PCL is biodegradable, and will provide mechanical strength and hydrophobicity to the nanofibre. This coaxial (or core-sheath) method provides a simple manufacturing process that does not require any complex functionalisation or copolymerisation to the PNIPAM molecule (Chen et al., 2010). Copolymerisation was attempted between the PNIPAM molecule and a cholesterol-based polymer, but was unsuccessful (outlined in Appendix G). In order to extend the application and stimuli-responsive nature of this nanostructure, magnetic nanoparticles of iron (II,III) oxide (Fe_3O_4) will be introduced to the PNIPAM shell.

Although there is limited knowledge on the electrospinning of PNIPAM, common solvents such as methanol, acetone, DMF, THF, and water have been used in past studies for the dissolution of PNIPAM (Rockwood et al., 2008; Wang, Sutti, Wang & Lin, 2011). For this study, methanol and acetone were used to compare the solvent effect on electrospinning PNIPAM. Chloroform was selected as a suitable solvent for the electrospinning of PCL (Chen et al., 2010). Through the addition of the nanoparticles to the PNIPAM solution, this study will aim to produce a dual-responsive system to thermal and externally applied magnetic stimuli. Potential applications for these smart nanofibres are outlined in Section 4.5.

4.2 Sample preparation

4.2.1 Synthesis of the PNIPAM polymer

PNIPAM was synthesised using the RAFT polymerisation method with the precursor NIPAM and THF (22.1 mL) for the solvent. MTPA was used as the chain transfer agent with AIBN as the initiator. A mole ratio of 200:1:0.4 was used for measuring NIPAM (5.0 g), MTPA (57.1 mg), and AIBN (14.5 mg) respectively to achieve a degree of polymerisation of 200. The solution was de-gassed with argon gas for 30 minutes, and then placed into an oil bath at 60°C for 16 hours to complete polymerisation. NMR measurements were performed using a deuterated chloroform ($CDCl_3$) solvent before and after the polymerisation to estimate the conversion of NIPAM. The polymerisation reaction is shown in Figure 4.1.

After polymerisation, the sample was purified using a 'poor solvent' of di-ethyl ether and *n*-hexane (1:1, 400 mL solution). The precipitate was collected using vacuum filtration, dissolved in a minimal amount of THF, and was then purified again using the same 'poor solvent' procedure. After vacuum filtration, the precipitate was put into a dry vacuum oven at 60°C where the solvent is removed using a cold trap apparatus. After 24 hours, the final PNIPAM product was collected and weighed (4.5044 g). Characterisation of the PNIPAM polymer was carried out using NMR (D_2O solvent), GPC (THF solvent), UV-Vis (ethanol solvent), and LCST (purified water solvent). For UV-vis, concentrations of 0.5, 1, 2, and 3 g/L were performed in an ethanol solvent. For the LCST measurement, a concentration of 1 g/L was used in purified water.

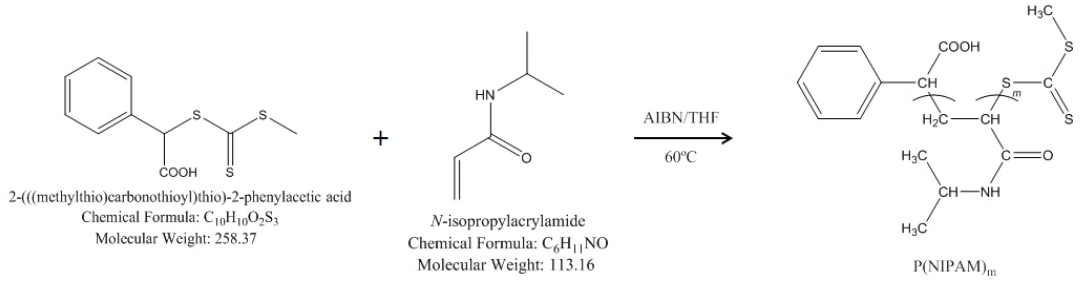

Figure 4.1: RAFT polymerisation of the NIPAM monomer.

4.2.2 Analysis of synthesised PNIPAM

4.2.2.1 ^1H NMR

The NIPAM monomer was characterised with ^1H NMR in deuterated chloroform ($CDCl_3$), and the peaks were assigned in accordance to the SDBS database (Yamaji, Saito, Hayamizu, Yanagisawa & Yamamoto, 2013). By identifying these peaks, the monomer conversion can be estimated from measuring the peaks of PNIPAM (before and after purification). The NMR spectrum of NIPAM is shown in Figure 4.2. Each proton peak was assigned, with the chloroform solvent peak at 7.26 ppm. The two large unassigned peaks are the THF solvent.

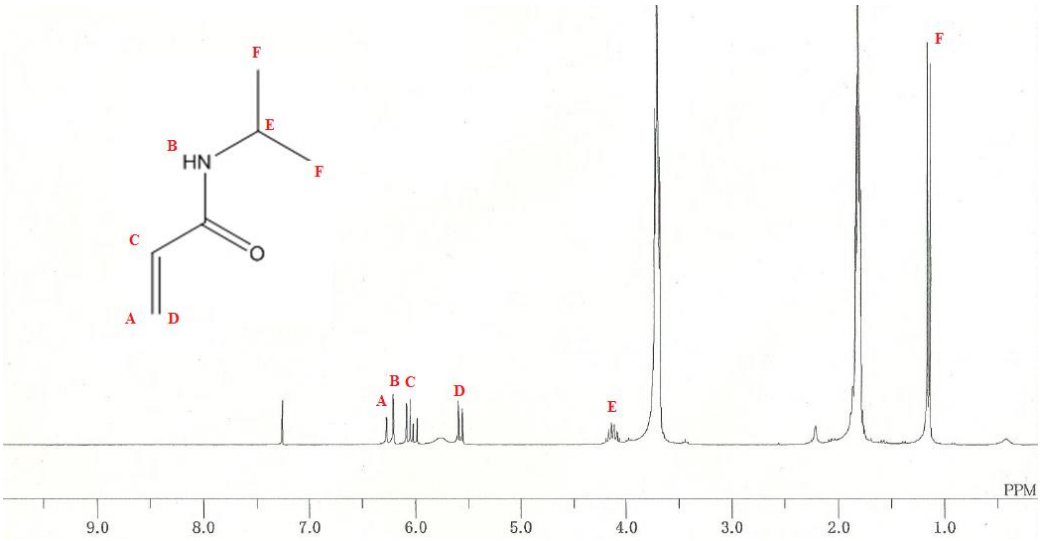

Figure 4.2: NMR spectrum peak assignments for the NIPAM monomer in $CDCl_3$.

After the purification and precipitation of the final PNIPAM product, ^1H NMR was performed in a deuterium oxide (D_2O) solvent. The characteristic peak of D_2O can be observed at 4.8 ppm in Figure 4.3. This solvent was selected because $CDCl_3$ would overlap the peak designated as 'E', which is representative of the phenyl group of the synthesised polymer. The peaks of A – E were assigned based on the work done previously with this synthesis technique (Iwasaki et al., 2013). The conversion of the polymer was calculated by taking an NMR measurement after polymerisation in $CDCl_3$ (see Appendix A). By using the THF peak at 3.65 ppm as a reference, the vinyl peak 'D' in Figure 4.2 decreased by 94.7%. This is the approximate conversion of the monomer to the impure polymer.

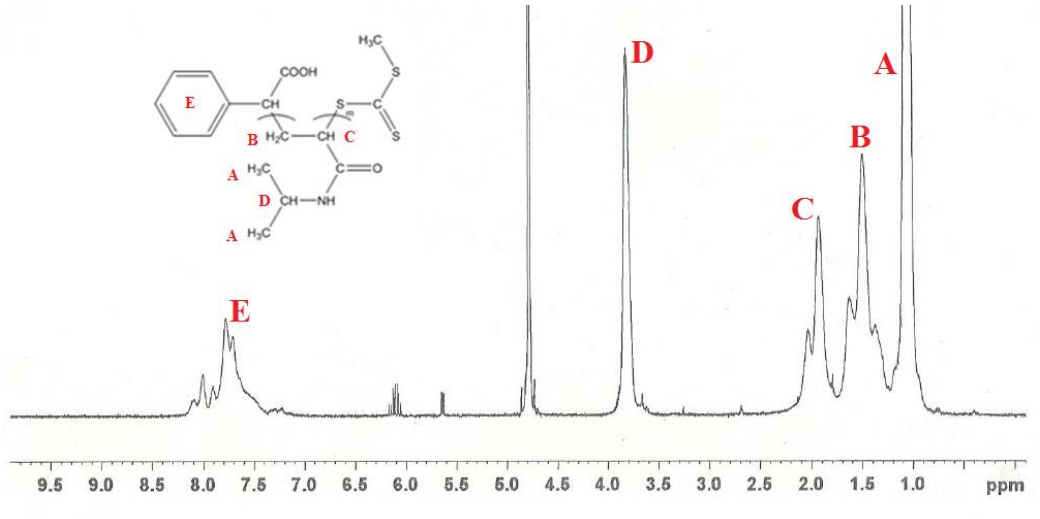

Figure 4.3: NMR spectrum peak assignment for purified PNIPAM in D_2O.

4.2.2.2 GPC

The purified PNIPAM produced was analysed using GPC to get an estimate of the molecular weight distribution of the synthesised polymer. A small portion of the dried polymer was dissolved in 5 mL of THF and placed into a filtered syringe for the GPC measurement. The analysis was completed after 60 minutes, and the peak characteristic of PNIPAM was measured after 32 minutes (Figure 4.4). The GPC results measured the number average molecular mass (M_n) as 10359 g/mol, with a polydispersity (M_w/M_n) of 1.342. To confirm this value, UV-vis spectroscopy was completed to get a better sense of the degree of polymerisation.

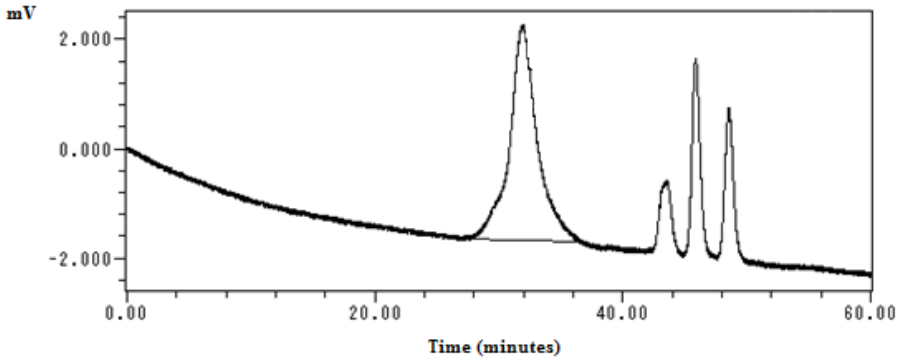

Figure 4.4: Chromatogram of purified PNIPAM in THF.

4.2.2.3 UV-vis and LCST

In order to use UV-vis spectroscopy to calculate the degree of polymerisation, four different concentrations of PNIPAM were dissolved in ethanol. The spectrophotometer then measured the absorbance peak (in Absorbance Units, A.U) at each concentration, with a constant wavelength of 305 nm. The results are shown in Table 4.1.

Table 4.1: UV-vis results for PNIPAM at different concentrations.

Concentration (g/L)	Absorbance peak	Wavelength (nm)
0.5	0.130394	305
1	0.261080	305
2	0.522574	305
3	0.800494	305

To determine the molar absorptivity, ε, of PNIPAM, the concentration of PNIPAM is plotted against the absorbance. From the slope of the data, the value of ε for PNIPAM can be calculated (0.2676 L/g.cm from Figure 4.5). This value is then compared to the molar absorptivity of MTPA (ca. 1.546×10^4 L/mol.cm from a previous experiment) to determine the value of the number average molecular weight, M_n. A value of 25,312 g/mol was obtained based on the Beer-Lambert Law (calculation shown in Appendix A).

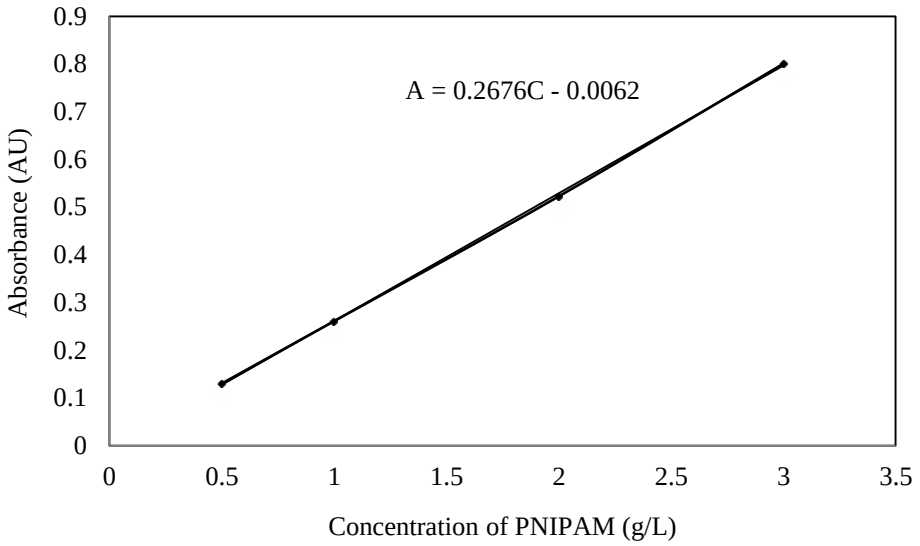

Figure 4.5: UV-vis measurement of the molar absorptivity of PNIPAM.

The UV-vis spectrophotometer was also used to measure the lower critical solution temperature (LCST) of PNIPAM. The polymer was dissolved at a concentration of 1 g/L in purified water. The temperature was increased from 20ºC to 50ºC, while the transmittance was measured. The result is shown in Figure 4.6, with the LCST measured to be approximately 34.5ºC. This value is consistent with expected value, which usually is around 32ºC ± 3ºC (Tauer, Gau, Schulze, Völkel & Dimova, 2009). The variance in the LCST from commercial PNIPAM is likely attributed to the unique chain transfer agent (MTPA) used to end-cap the polymer.

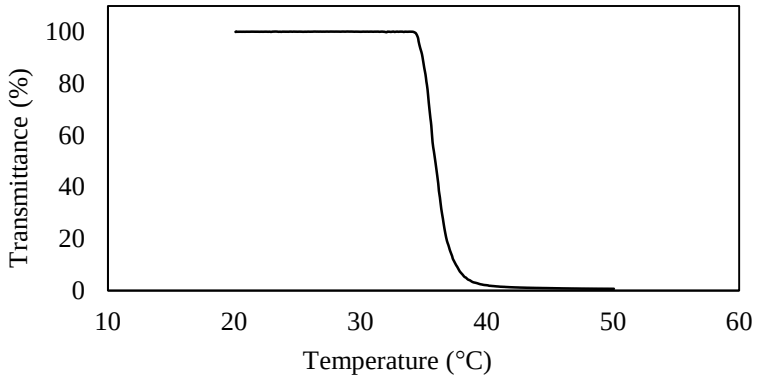

Figure 4.6: Representation of the LCST of PNIPAM (during heating).

4.2.3 PNIPAM and PCL solutions

The synthesised PNIPAM and commercial PNIPAM from Sigma were both dissolved in methanol for electrospinning. PNIPAM was also prepared in acetone, but the solvent was too evaporative for electrospinning. PCL was dissolved in 90% acetic acid, and 1% Fe_3O_4 nanoparticles were added to test with the commercial PNIPAM. Each of the solution was sonicated for two hours. The samples prepared are summarised in Table 4.2.

Table 4.2: Sample composition for the PNIPAM and PCL trials.

	Polymer composition	Fe_3O_4 nanoparticles
Sample A1	10% commercial PNIPAM	–
Sample A2	15% commercial PNIPAM	–
Sample B	15% synthesised PNIPAM	–
Sample C	10% PCL	–
Sample D	15% commercial PNIPAM	1%

The required amount of Fe_3O_4 solution to be added was calculated using the stoichiometric relationship between the Fe^{+2} ions and Fe_3O_4 product during the nanoparticle synthesis, expressed by:

$$Fe^{+2}_{(aq)} + 2\ Fe^{+3}_{(aq)} + 4\ H_2O_{(l)} \rightarrow Fe_3O_{4(s)} + 8H^{+}_{(aq)}$$

4.2.3 Polymer solution properties

To determine how the nanoparticles impact the viscosity, measurements of the viscosity were taken for Sample A2 and Sample D. Before measuring the viscosity with the rheometer, both solutions appeared to have a low viscosity. This was

confirmed in the viscosity profile measurement in Figure 4.7, with a representation of non-Newtonian thinning behaviour. The nanoparticles had little effect on this particular solution parameter, which is due to the low concentration of the particles. For the shear stress profile, there was an increased amount of shear stress at rates above 200 1/s. This is representative of small increased resistances to the directional rotation on the fluid by the nanoparticles during the rheometer test.

The nanoparticles did however have an effect on the conductivity of the solutions, exhibiting a higher conductivity in Sample D than Sample A. A conductivity value of 0.02 mS and 0.28 mS was measured for the solution without nanoparticles and 1% nanoparticles, respectively.

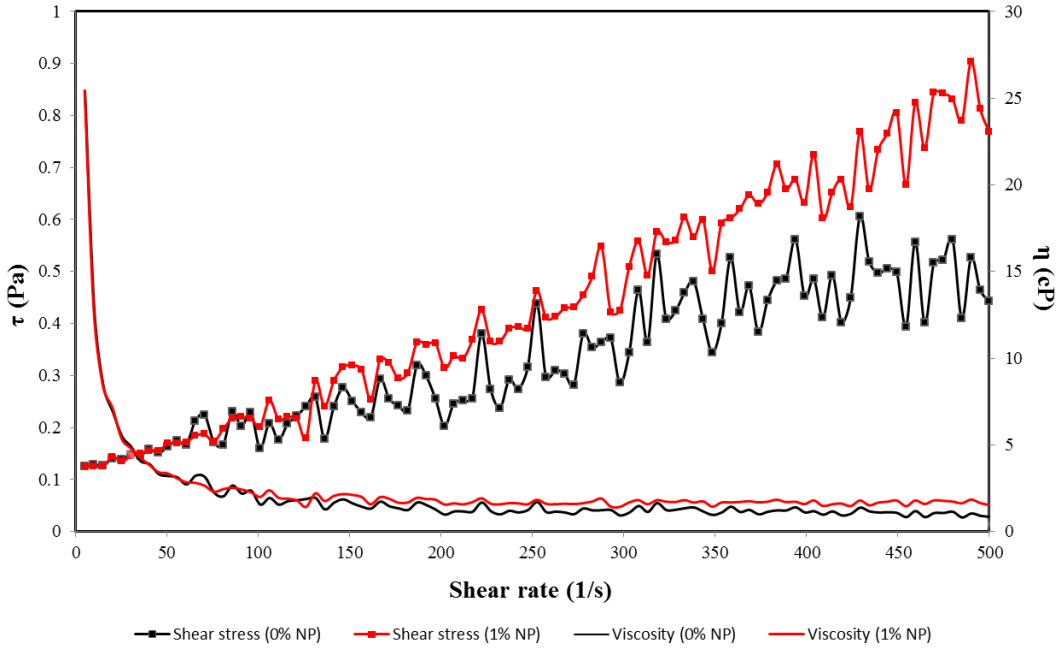

Figure 4.7: Viscosity profiles at variable shear rates for PNIPAM with 0% and 1% Fe_3O_4.

4.3 Electrospinning PNIPAM

4.3.1 Parameter optimisation

The behaviour of PNIPAM during electrospinning is not well known, and can be influenced by various factors such as the concentration, voltage, and collector distance. These parameters were manipulated in order to determine the optimal electrospinning conditions for PNIPAM. The voltage was varied from 10 – 30 kV, in

increments on 5 kV, and the distance was measured at 8, 12, and 16 cm. As mentioned in Section 4.2.3, concentrations of 10% and 15% PNIPAM were trialled. The flow rate and system temperature were kept constant at 1 mL/h and 25ºC, respectively. Electrospinning of the pure PNIPAM samples was completed for the commercial PNIPAM only, with the synthesised PNIPAM to be tested in Section 4.4 with PCL. The observations and optimisation of electrospinning the commercial PNIPAM is summarised in Table 4.3. The electrospinning of Sample A2 presented the best results; at distances of 8 and 12 cm. Sample A1 was too low in concentration to avoid the formation of large droplets from the jet stream. Voltages of 20 – 25 kV produced the most stable jet, and visibly there was a lot less 'spitting' of the solution from the needle. These findings are consistent with similar studies, which also successfully produced PNIPAM nanofibres at 15 – 20 kV and distances of 10 – 20 cm (Okuzaki et al., 2009; Song et al., 2011).

Table 4.3: Optimisation of the electrospinning parameters for PNIPAM.

	Sample A1 (10% PNIPAM)				
	Voltage (kV)				
Distance (cm)	**10**	**15**	**20**	**25**	**30**
8	Fine fibres being formed at needle tip. Spots deposited.	White mist-like deposit.	White mist spray.	White mist spray.	White mist spray.
12	Fine spray.	White mist spray.	White mist spray.	Fine white mist spray.	Fine white mist spray.
16	Droplets only.	Spray; liquid droplets visible.	White mist; liquid droplets still present.	White mist spray.	White mist spray.
	Sample A2 (15% PNIPAM)				
	Voltage (kV)				
Distance (cm)	**10**	**15**	**20**	**25**	**30**
8	Spraying.	White spray deposit.	Consistent white layer has formed.	Consistent white layer.	Consistent white layer.
12	Fine, short fibres deposited.	Drops mostly; had bad needle flow.	White spray.	Fine spray. Consistent white layer.	Fine spray. Consistent white layer.
16	Numerous short fibres.	Short fibres and drops.	A lot of fibres grounding to side of the machine (due to distance).	Spray/mist starting again.	Voltage too high; bad flow (sporadic).

4.3.2 Nanofibre size and distribution analysis

The consistency and distribution of the electro-spun nanofibres was measured using SEM, complemented with the ImageJ software. The images shown in Figure 4.8 show the effect of concentration and collector distance. For Sample A1, SEM was completed for the sample that was electro-spun at 20 kV over a distance of 8 cm. In comparison to Sample A2 under the same conditions, thinner nanofibres were observed. This is illustrated in the diameter distributions shown in Figure 4.9. Typically an increase in concentration will produce thicker nanofibres, however in this case there was a wide distribution and inconsistency (Okuzaki et al., 2009). This is attributed to the large spherical objects that can be seen on the images of the first two samples. These spheres are representative of the PNIPAM polymer chain 'folding' and interacting with other polymer molecules instead of the solvent. The presence of these spheres causes the nanofibre mat to be inconsistent and mechanically unstable (Rockwood et al., 2008). From the SEM analysis of Sample A2 at longer distances, there was a substantial decrease in the presence and size of the PNIPAM spherical formations. This is suspected to be a result of increased solvent evaporation, which leads to less mobility for the PNIPAM molecules to combine together. A narrow distribution was recorded in Figure 4.9 for these two samples, with the average nanofibre diameter decreasing as the distance to the collector increased. The narrow distribution is characteristic of a greater consistency throughout the nanofibre mat, which can be explained by the reduced amount of 'folded' PNIPAM objects. Complementary images of these samples are recorded in Appendix C.

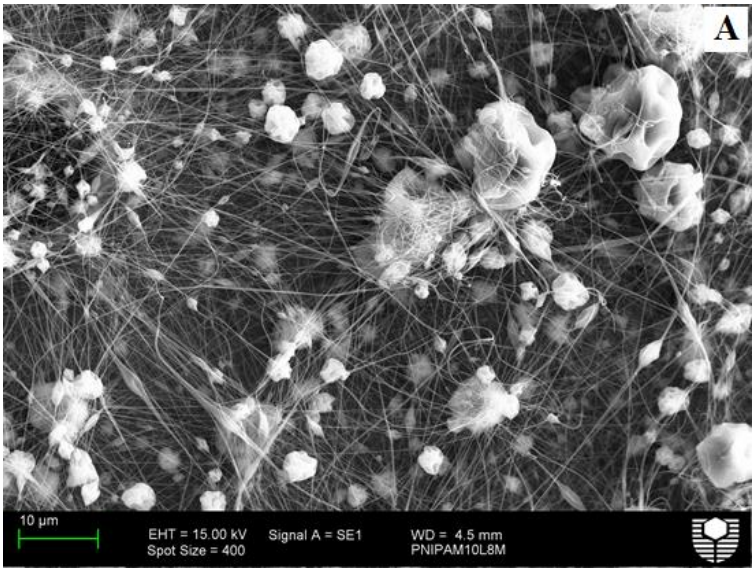

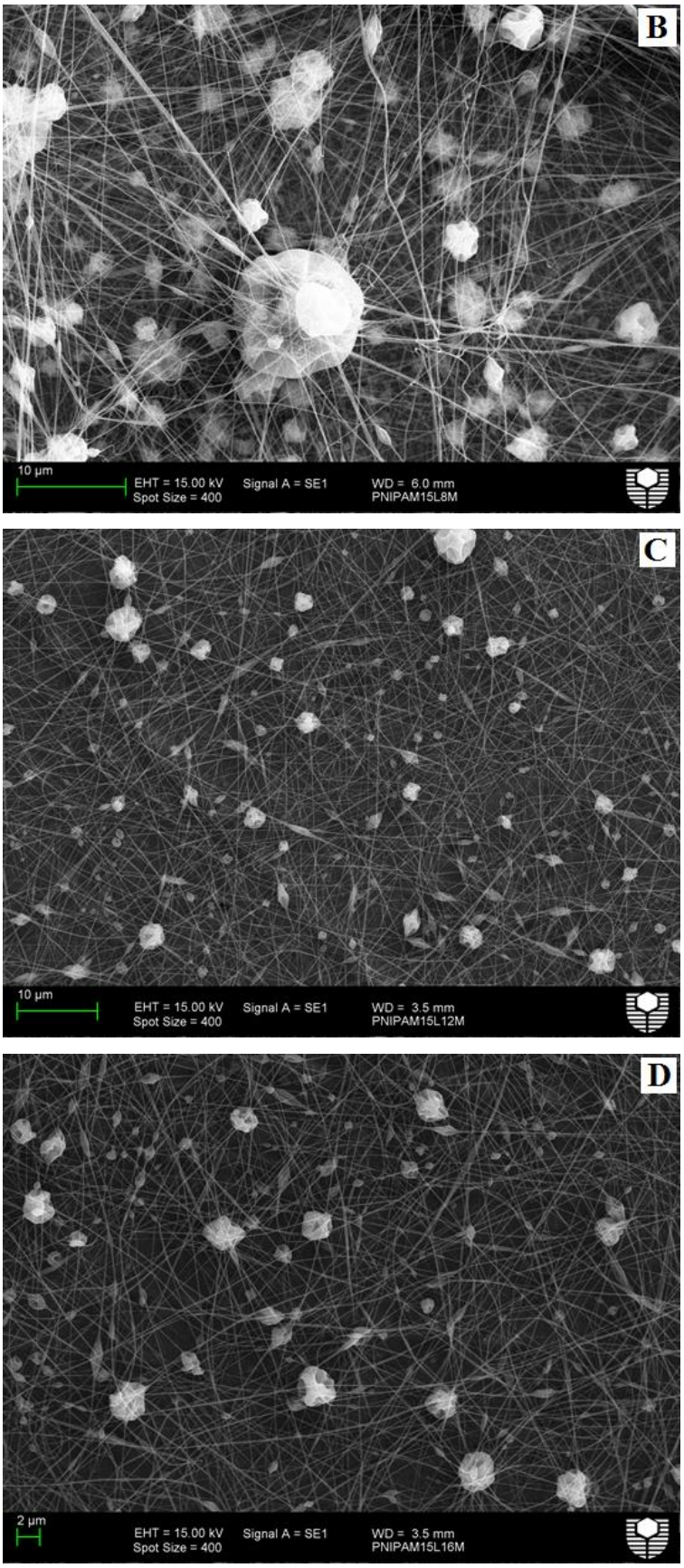

Figure 4.8: SEM of electro-spun PNIPAM nanofibres at variable distances; (A) 10% PNIPAM at 8 cm, (B) 15% PNIPAM at 8 cm, (C) 15% PNIPAM at 12 cm, (D) 15% PNIPAM at 16 cm.

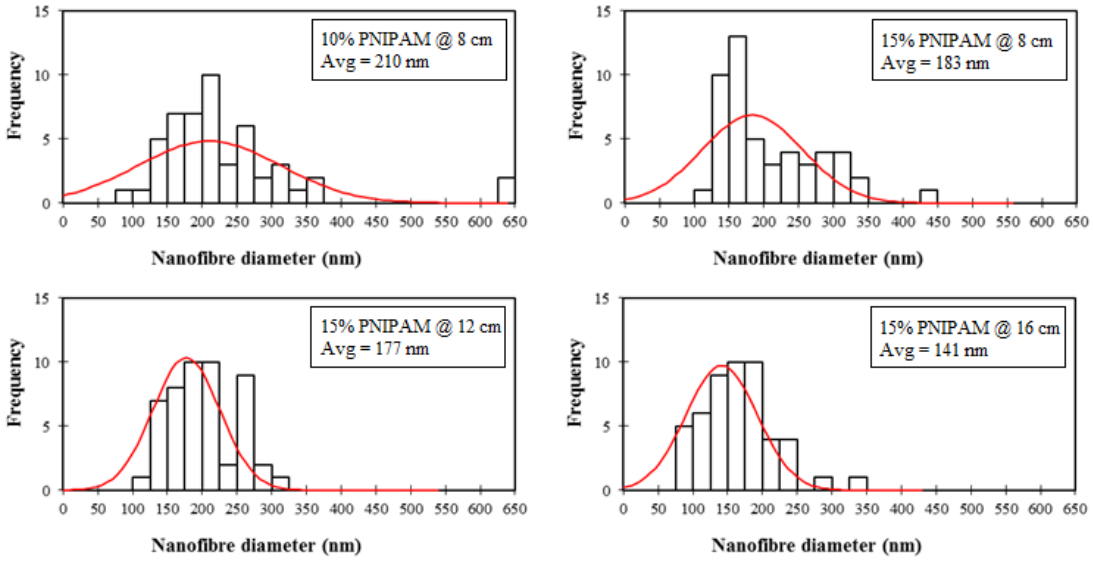

Figure 4.9: Nanofibre diameter distribution plots for variable electrospinning distances.

As a result of this previous analysis, the optimum concentration and collector distance were determined to be 15% and 12 cm, respectively. Implementing these optimised parameters, the effect of the electrospinning voltage was then analysed using SEM on Sample B as voltages of 10, 15, 20, and 25 kV. From Figure 4.10, the images show successful nanofibre formation at all voltages, with PNIPAM sphere formation becoming more prominent at 25 kV. The average nanofibre diameter and distribution for each sample is shown in Figure 4.11. At 10 kV there was a wide distribution in the nanofibre diameter, which is indicative of an insufficient applied voltage to maintain a consistent flow of the solution. There was a decrease in the nanofibre diameter as voltage increased, however the diameter increased once 25 kV was reached. This is likely attributed to the increased electrostatic activity within the solution, leading to increased polymer chain mobility and the formation of collapsed PNIPAM spheres. As it was seen earlier in Figure 4.9, the presence of these spheres creates a wider nanofibre distribution. The optimum voltage was determined to be 20 kV, giving a consistent, narrow nanofibre distribution and an average diameter of 181 nm.

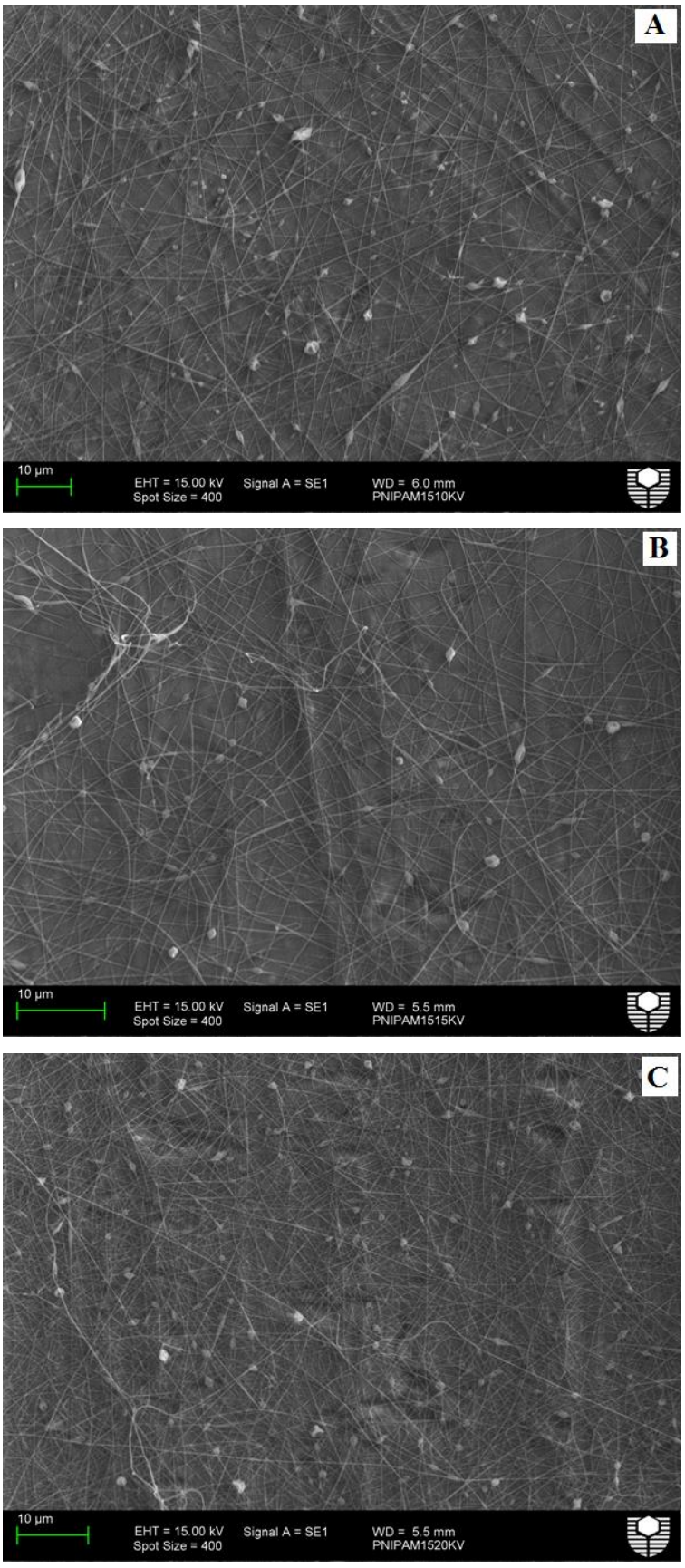
A
10 µm
EHT = 15.00 kV
Spot Size = 400
Signal A = SE1
WD = 6.0 mm
PNIPAM1510KV
B
10 µm
EHT = 15.00 kV
Spot Size = 400
Signal A = SE1
WD = 5.5 mm
PNIPAM1515KV
C
10 µm
EHT = 15.00 kV
Spot Size = 400
Signal A = SE1
WD = 5.5 mm
PNIPAM1520KV

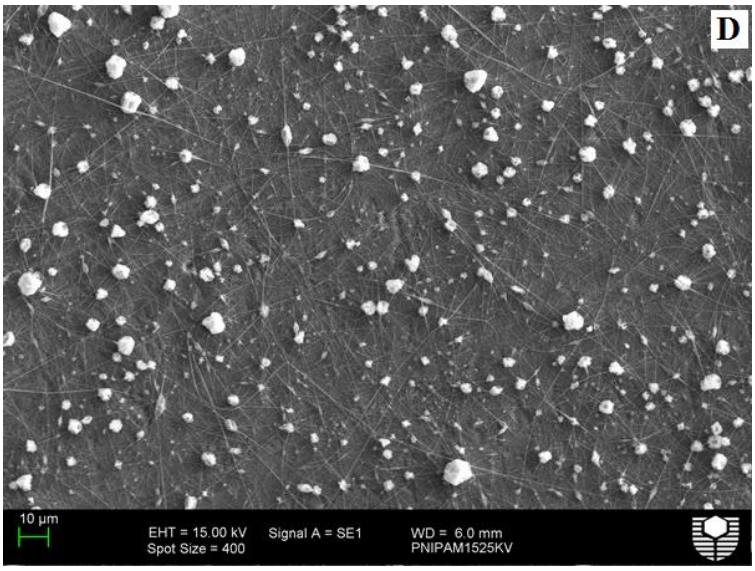

Figure 4.10: SEM of electro-spun nanofibres with 15% PNIPAM at variable voltages; (A) 10 kV, (B) 15 kV, (C) 20 kV, (D) 25 kV.

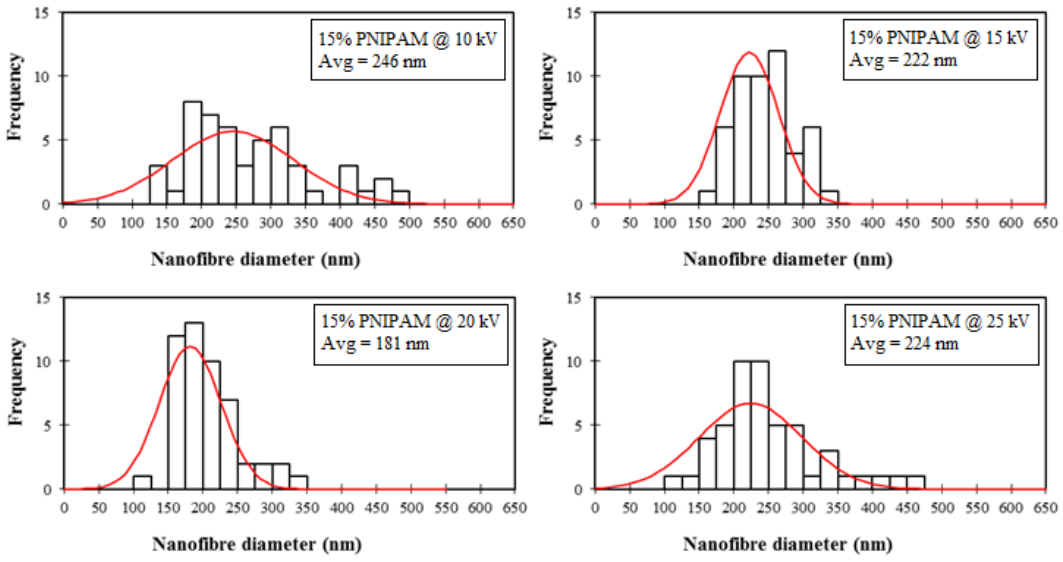

Figure 4.11: Nanofibre diameter distribution plots for variable electrospinning voltages.

4.4 Coaxial electrospinning PNIPAM with PCL

4.4.1 Parameter optimisation

Coaxial electrospinning was performed using the coaxial needle setup mentioned in Chapter 3, Figure 3.8. Due to the difference in cross-sectional area between the core and sheath needle tip, different flow rates were calculated to ensure the same solution velocity from the needle tip. This allows the nanofibre core-and-shell structure to form with a consistent shell width. A core flow of 1.5 mL/h and shell flow of 6.3

mL/h was set for the first trials. This proved to be too excessive for the flow of the shell, so they were scaled down to 0.5 mL/h and 2.1 mL/h for the core and shell, respectively. The system temperature was kept at 25ºC ± 0.2ºC, and the rotating collector was operated at 400 rpm. Optimisation of the PNIPAM shell and PCL core was completed for both the synthesised and commercial PNIPAM samples. From the optimisation of PNIPAM in the previous section, a distance of 12 cm was set to limit PNIPAM spherical formations. A similar applied voltage study was completed to analyse how the electrospinning process changes from 10 to 30 kV. The results for the two samples are shown in Table 4.4.

Table 4.4: Optimisation of the electrospinning parameters for PNIPAM/PCL.

	Sample A (Synthesised PNIPAM shell and PCL core)				
	Voltage (kV)				
Distance (cm)	**10**	**15**	**20**	**25**	**30**
12	Spinning starts, breaking the surface tension of the solution at the needle	Very fine spinning of the solution	Variations in polymer jet, possibly wide diameter distribution	Stream is still constant, but inconsistent motion	Stream is still constant, but inconsistent motion
	Sample B (Commercial PNIPAM shell and PCL core)				
	Voltage (kV)				
Distance (cm)	**10**	**15**	**20**	**25**	**30**
12	Spinning starts, breaking the surface tension of the solution at the needle	Stable stream with minimal spitting.	Stable polymer jet.	Stable polymer jet.	Stable polymer jet, with increased whipping motion
	Sample C (Commercial PNIPAM shell and PCL core, with 1% Fe_3O_4)				
	Voltage (kV)				
Distance (cm)	**10**	**15**	**20**	**25**	**30**
12	Spinning starts, breaking the surface tension of the solution at the needle	Appears that the core is spinning, but shell is spitting solution separately	Polymer jet consistency much better; appears the core-shell are spinning together	Consistent polymer jet, some spitting.	Polymer jet starts to become unstable at this voltage, large whipping motion

A stable polymer jet was seen for Sample A and B, with a higher stability in Sample B at 20 – 25 kV. Due to the more favourable nanofibre formation in Sample B, the commercial PNIPAM was used for preparation of a core-and-shell structure with magnetic Fe_3O_4 nanoparticles. This is represented in Table 4.3 as Sample C, and was tested using the same process variables. There was some droplets visible from 10 – 30 kV, however this was minimised at approximately 25 kV with a consistent polymer jet.

4.4.2 Nanofibre size and distribution analysis

In order to clarify the optimal electrospinning parameters, SEM of each sample was completed to examine the nanofibre formation behaviour. Two images of the synthesised PNIPAM/PCL core-and-shell samples (Sample A) are shown in Figure 4.12. Immediately, a substantial difference in the nanofibre diameters can be seen with an abundance of both thick and thin nanofibres. The distribution of these diameters is shown in Figure 4.13, which suggests there is a somewhat bi-modal distribution for this particular sample. There was a narrow distribution of thin fibres over the range of 250 – 750 nm and a wider distribution of thick fibres over the range of 1.5 – 2.5 µm. The resulting average nanofibre diameter was approximately 1 µm. This kind of behaviour suggests phase separation has occurred during electrospinning at the needle tip. Phase separation is thermodynamically favoured in this case because of the difference in the solvent boiling points: 118ºC and 64.7ºC for acetic acid and methanol, respectively. Further factors that impact this separation are relative permittivity (ε) of the solvents, and also the degree of solubility for each polymer (Chen et al., 2010). It is unclear if there was any compatibility between the two polymer solutions to form the core-and-shell nanostructure.

The commercial PNIPAM/PCL core-and-shell sample (Sample B) seen in image 'C' of Figure 4.12 had more consistent nanofibre formation than Sample A. The formation of folded PNIPAM was once again observed, having similar morphology to the formations observed in the electrospinning of pure PNIPAM. There was also beading evident in the sample, which is suspected to be characteristic of the PCL. The nanofibre distribution was excellent, as shown in Figure 4.13, measuring an average nanofibre diameter of 208 nm.

After the addition of Fe_3O_4 nanoparticles, the occurrence and size of the PNIPAM formations increased (image 'D' of Figure 4.12). The presence of these formations is related to the interaction between PNIPAM and the solvent. It appears that the nanoparticles reduce the solubility between the methanol solvent and PNIPAM, resulting in energetically-favourable PNIPAM macromolecules (Rockwood et al., 2008). This leads to mechanically fragile nanofibres, but in this case PCL acts as the mechanical 'backbone' strength of the nanofibre so there is little hindrance to the

nanofibre integrity. The nanofibre diameter distribution shown in Figure 4.13 shows a wide distribution, with an average diameter of 247 nm. The increase in diameter from Sample B is attributed to the presence of the folded PNIPAM spheres. A similar result to this was mentioned earlier for pure PNIPAM electrospinning (Figure 4.10).

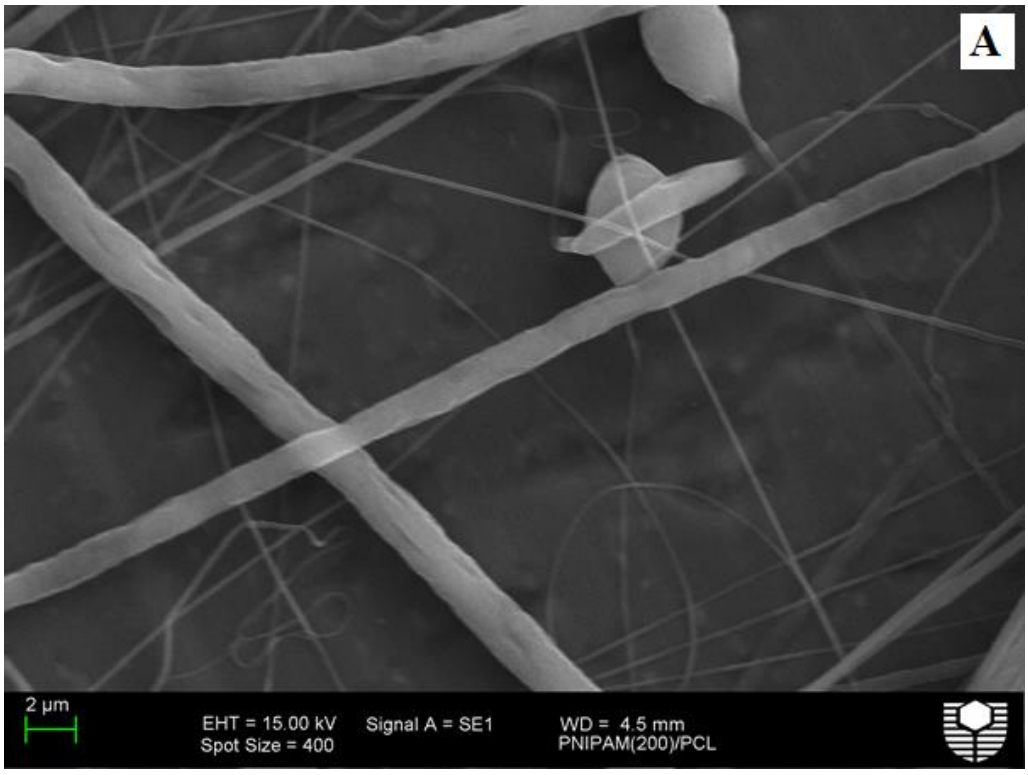

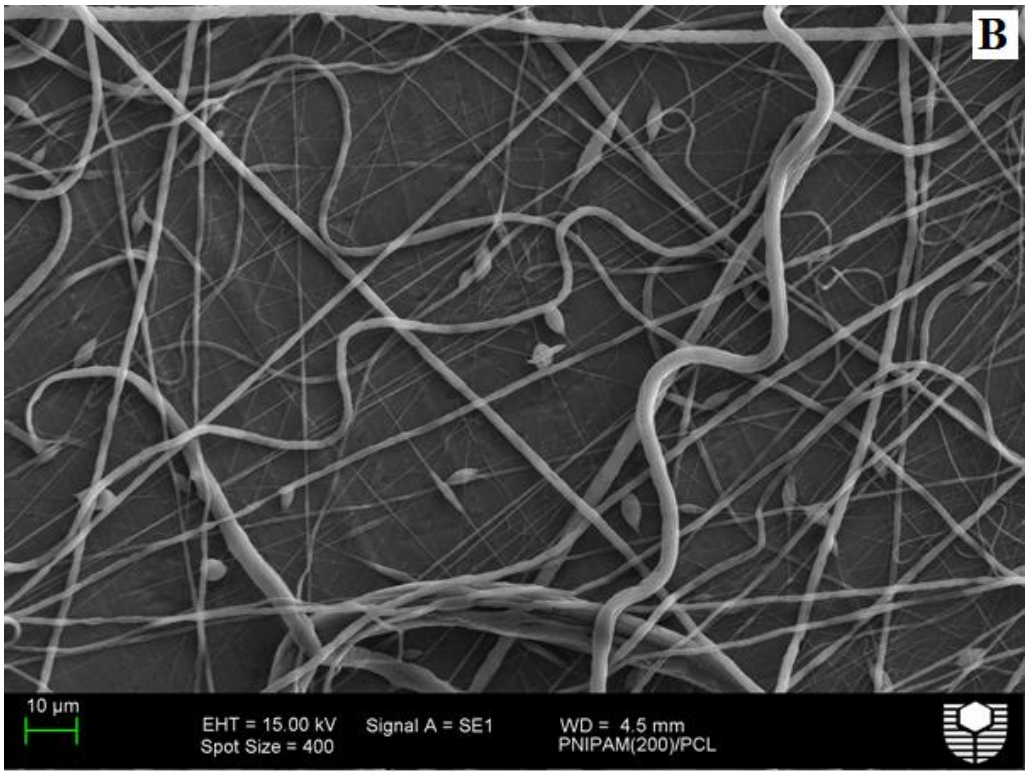

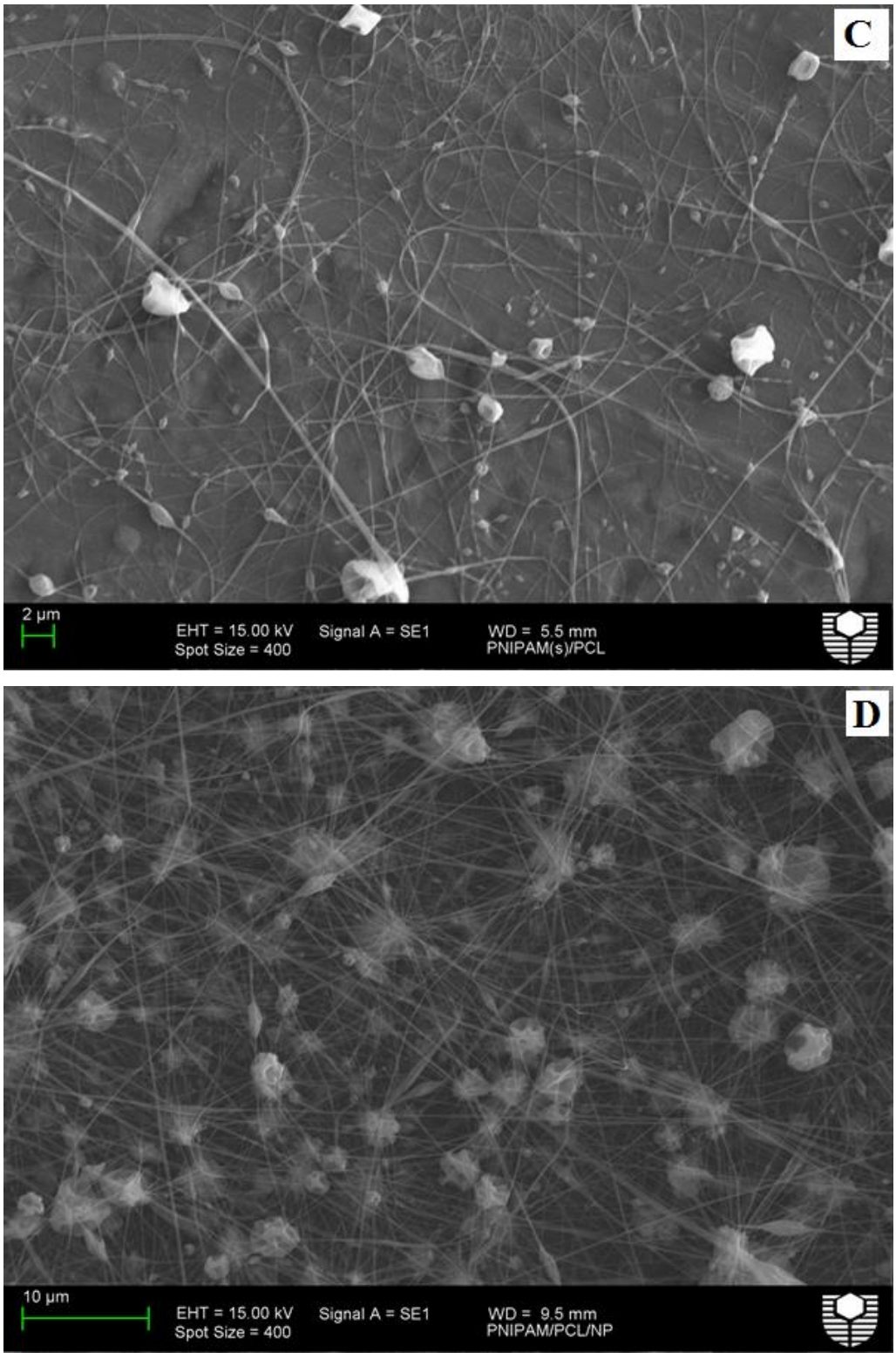

Figure 4.12: SEM of electro-spun nanofibres for each sample; (A) Sample A at high magnification, (B) Sample A at low magnification, (C) Sample B, thin layer, (D) Sample C.

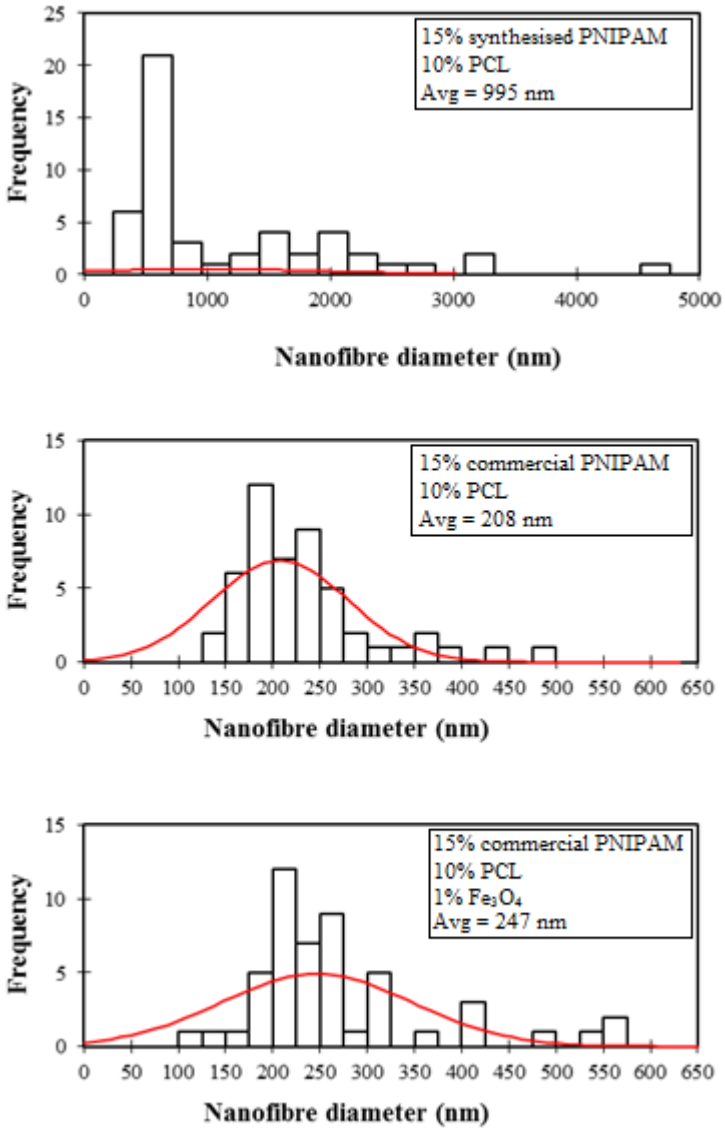

Figure 4.13: Nanofibre diameter distribution plots for coaxial electrospinning.

Energy dispersive spectroscopy (EDS) was performed using the additional functionality of the Zeiss Evo 40XVP scanning electron microscope. This analysis was used to determine the elemental composition of the nanofibres in Sample C, which will confirm the presence of Fe_3O_4 nanoparticles with the sample. The EDS spectrum for this sample is shown in Figure 4.14, displaying characteristic peaks for carbon, oxygen, iron, and aluminium. The aluminium peak is representative of the foil substrate used to collect the nanofibres. The carbon and oxygen peaks were measured at 0.277 and 0.523 keV, respectively. They are representative of the long polymer chains for both PCL and PNIPAM. The Kα peak of iron was measured at 6.403 keV, and the Kβ peak at 7.057 keV. A third peak for iron at 0.705 keV

represents the L-series peak (Satcher, 2006). The amplitude of these iron peaks is quite low, which is to be expected since the nanoparticles are only 1% concentration. Additionally, they are only contained within the shell of the nanofibre, so this suggests that the PNIPAM shell is quite thin.

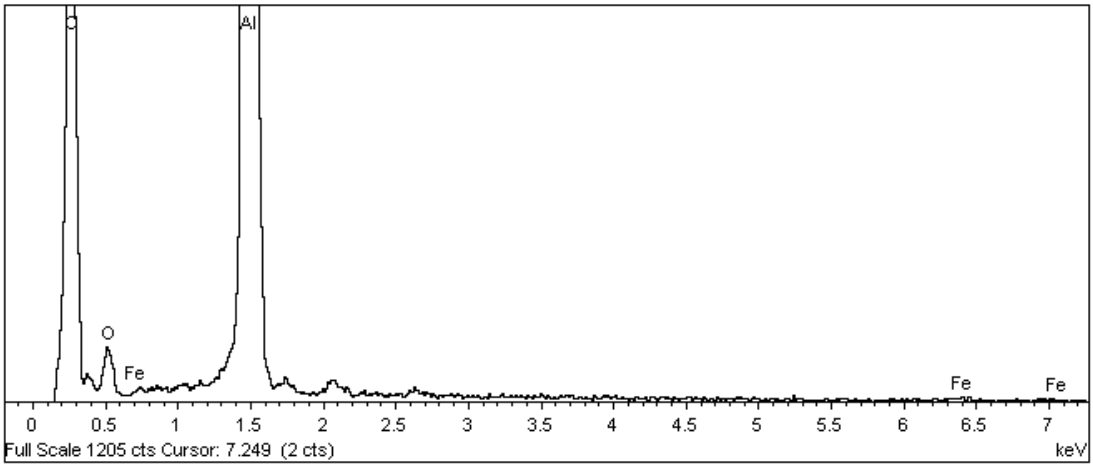

Figure 4.14: EDS spectrum of Sample C.

4.4.3 Thermal characterisation

A thermal profile of Sample C was completed using DSC to observe the crystallisation effect of the magnetic nanoparticles in the PNIPAM shell. DSC was completed using a range of 30 – 150ºC, shown in Figure 4.15. A heating rate of 10ºC/min was used, and was held for 2 minutes at 150ºC for an isothermal step. A minor peak at 60.2ºC was recorded, indicative of the melting point of PCL. The melting point of PNIPAM was expected to be observed at 96ºC (according to the MSDS), however there was no peak. This suggest that the PNIPAM weight in the sample is quite low, which is supportive of the low shell thickness predicted from EDS. The crystallisation temperature of the sample was measured at 32.6ºC, with a total crystallisation time of 2.5 minutes (see Figure 4.16). This is a result of the first-order phase transition of PNIPAM, indicating that the polymer retains its LCST quality in an electro-spun nanostructure (Rockwood, 2007; Sousa, Magalhaes & Freitas, 1998). As the PNIPAM shrinks to its dehydrated state above the LCST, the nanoparticles become exposed which likely leads to the initiation of crystallisation (represented in Figure 4.17).

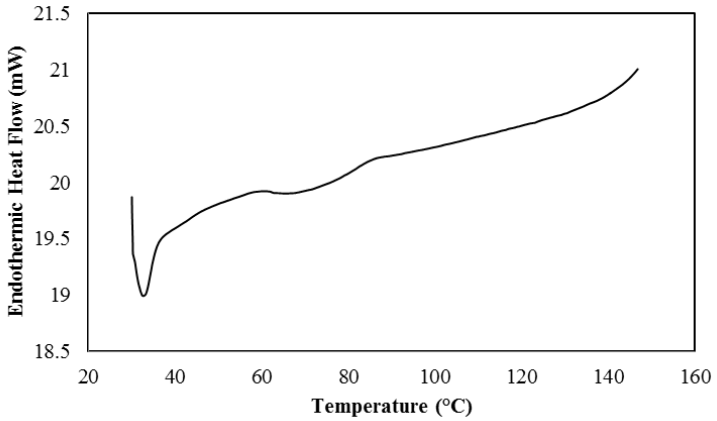

Figure 4.15: DSC curve of Sample C (1% Fe_3O_4).

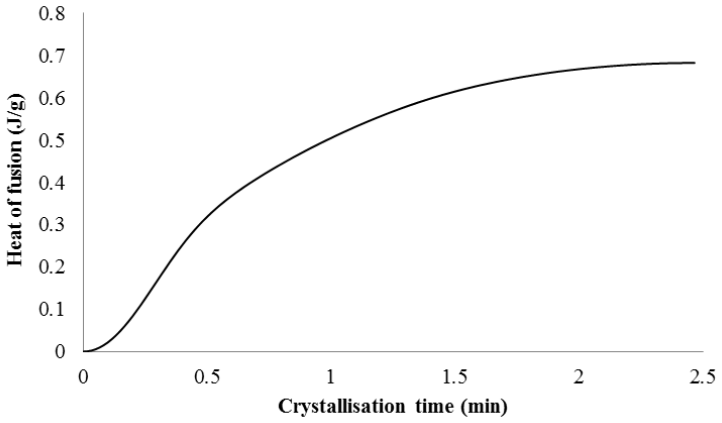

Figure 4.16: Crystallisation time of Sample C (1% Fe_3O_4).

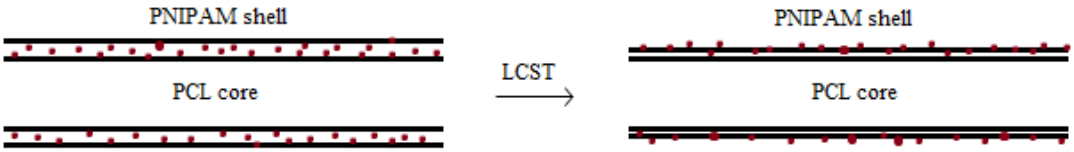

Figure 4.17: Schematic representation of the PNIPAM shell shrinking above its LCST, and exposing the nanoparticles.

In order to explain the crystallisation phenomena at the LCST of PNIPAM, the Avrami Equation can be used to determine the nature of the transition. From the relationship between the heat of crystallisation and crystallisation time, it can be determined whether the nanoparticles act as nucleating sites for the crystallisation. The Avrami Equation is expressed as:

$$\ln[-ln(1-f)] = n\ln t + \ln k$$

Where *f* is the fraction of crystals at any time *t* during the crystallisation process, *k* is the rate constant and *n* is the Avrami exponent (Chong, 2001). The exponent is determined by plotting $\ln[-ln(1-f)]$ against ln *t*, giving a linear relationship such that *n* can be measured as the gradient. For every time measurement during the crystallisation process, the value of *f* must be determined using:

$$f = \frac{[\int_{t=0}^{t} \frac{d\Delta H(t)}{dt} . dt]}{\Delta H}$$

Where ΔH is the heat of crystallisation (Chong, 2001). The Avrami relationship for Sample C is shown in Figure 4.18, with the equation of the relationship to extract the Avrami constants. The dimensionless values of 'n' and 'k' are expressed in Table 4.5. The value of 'n' is typically between 1 and 4, where a value of 1 represents one-dimensional or planar growth, and higher values represent three-dimensional spherulitic growth. For Sample C, the value of 'n' indicates that there is rod-like growth from sporadic nuclei (Chong, 2001). This means that instantaneous nucleating sites are not available upon the phase transition of PNIPAM, which suggests the nanoparticles do not become fully exposed as sites for spherulitic nucleation.

Table 4.5: Avrami exponent and rate constant values.

Sample	Avrami exponent, *n*	Avrami constant, *k*
1% Fe_3O_4 (Sample H)	1.9	2.7

An important note for generating the Avrami plot is to ensure linearity is maintained when plotting the data. It is common to limit the data when plotting the data to account for deviations caused by voids in the crystal mass (Chong, 2001; Vasanthan et al., 2011). For Sample C, the value of 'f' (the fraction of crystals) was limited to represent from 0 – 50%.

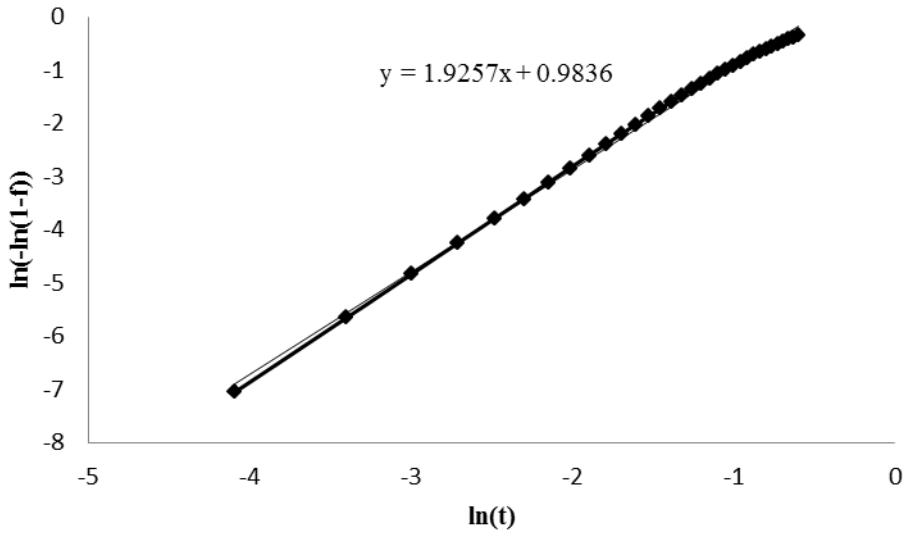

Figure 4.18: Avrami plot of ln[–ln(1–f)] vs. ln(t) for Sample C (1% Fe_3O_4).

4.5 Discussion

The thermo-responsive property of PNIPAM is the primary stimulus that was targeted for the preparation of the electro-spun nanostructures. As it was seen from the synthesised PNIPAM analysis, the LCST is quite close to that of body temperature. This has resulted in a wide range of studies for PNIPAM release-based applications. However, before potential applications can be addressed, the behaviour of PNIPAM during electrospinning should be discussed in more detail. The difference between the synthesised and commercial PNIPAM in electrospinning came down to the morphology of the nanofibres produced. There appeared to be enough phase separation between the two solutions to have them spin independently. Since the same solvents are used, this behaviour can only be attributed to the solubility difference between the two different PNIPAM polymers (Chen et al., 2010). This is caused by the difference in the end-cap functional groups: methyl groups for commercial PNIPAM and MTPA-based groups (phenyl, carboxyl and sulphide-based) for synthesised PNIPAM. For this reason, the commercial polymer was used in the coaxial study with nanoparticles.

Due to the expulsion of its liquid contents above the LCST, PNIPAM has been used extensively for release mechanisms that occur at these temperatures (such as body temperature). The release of the drug is often controlled by the polymer and drug concentration. Release is very rapid below the LCST due to the hydrophilicity of the

PNIPAM polymer. In order to sustain the release over a longer time period (24 hours for example), high polymer concentration is needed and the temperature must be above the LCST (Song et al., 2011). The presence of the superparamagnetic nanoparticles in the shell is invaluable for controlling this release profile. By applying an external magnetic field, the nanoparticles become magnetised and generate localised heat. This localised heating may be used to trigger slower release in a media that is below the LCST, or even ‘burst’ release by alternating the temperature (Wei, Cheng, Zhang & Zhuo, 2009).

4.6 Summary

The electrospinning of a PNIPAM-based, stimuli-responsive nanofibre was successfully completed and characterised using relevant characterisation techniques. The difference between the behaviour of synthesised and commercial PNIPAM was investigated in a coaxial electrospinning arrangement with PCL, and the effect of the presence of Fe_3O_4 nanoparticles was studied. The key design parameters and characteristics are summarised below.

- The electrospinning of commercial PNIPAM was optimised in a methanol solvent, concluding that a concentration of 15% provided the most consistent nanofibres. The ideal parameters were determined to be 20 kV with a collector distance of 12 cm. It was discovered that increasing voltage and the collector distance both results in a reduced average nanofibre diameter. The average nanofibre diameter for PNIPAM was 181 nm at optimal conditions

- Coaxial electrospinning of PNIPAM (shell material) and PCL (core material) was completed using optimised parameters of 25 kV and a collector distance of 12 cm. A bi-modal distribution was measured for synthesised PNIPAM, with a higher phase separation tendency than commercial PNIPAM. Synthesised PNIPAM/PCL had an average nanofibre diameter of 995 nm, whereas commercial PNIPAM/PCL was 208 nm.

- The addition of nanoparticles to the PNIPAM shell resulted in an increased average nanofibre diameter of 247 nm, which was attributed to macromolecular folding of PNIPAM due to poor solvent interaction in the presence of Fe_3O_4 nanoparticles.

- DSC analysis displayed a crystallisation temperature of 32.6ºC that was consistent with the LCST of PNIPAM. Since the polymer shrinks at this temperature, it is logical that some of the nanoparticles become partially exposed during the contraction of the polymer. The nanoparticles did not fully incur nucleation, as only one-dimensional (and possibly planar) crystal growth occurred, which was determined from the Avrami relationship.

CHAPTER 5

CHITOSAN-BASED NANOSTRUCTURES

5.1 Introduction

5.1.1 Outline

Chitosan, a linear polysaccharide produced from naturally occurring chitin, was selected as the next material to be assimilated into this study. From Chapter 4, the base polymer PNIPAM was easily optimised for the electrospinning process. In this chapter, optimisation of chitosan as the base polymer is a lot more problematic. Due to the intermolecular entanglement of chitosan, which is less prominent in linear polymers like PNIPAM, the solution viscosity and surface tension are very high. This issue has been addressed by blending chitosan with another polymer that has more favourable electrospinnability. Similarly to Chapter 4, PCL is once again being used; however a blended nanostructure was formed instead of using a coaxial arrangement.

This chapter will explain the polycationic and pH-responsive nature of the chitosan molecule, and will investigate the electrospinning procedures for nanofibre formation with and without blending. The electrospinning behaviour and final product will be analysed using the similar procedures to Chapter 4. Additionally, potential applications will be discussed and conclusions will be summarised at the end of this chapter.

5.1.2 Material selection

As mentioned in Chapter 3, chitosan was selected to be used in a blend with PCL. Chitosan was chosen over hyaluronic acid because it creates a more consistent solution with PCL, and has relatively better electrospinnability. The electrospinning parameters and solvent concentration are important variables when spinning chitosan. Complications usually arise because of its polycationic nature, high molecular weight, and a highly variable molecular weight distribution (Homayoni et

al., 2009). The most efficient solvent for chitosan has been found to be concentrated acetic acid, which has also been utilised in the preparation of blended polymer solutions (Duarte et al., 2010; Sarasam et al., 2007). Notably, decreasing the concentration of the acetic acid will increase the average diameter of the electro-spun nanofibres, allowing control over the process. Thus, these parameters offer the best control for the electrospinning of chitosan (Homayoni et al., 2009).

A limiting factor for chitosan is its weak mechanical strength, which can be addressed by blending with a mechanically sound polymer, such as PCL. PCL is a hydrophobic polymer with a high molecular weight, which is quite different from the slightly hydrophilic chitosan. Chloroform offers great solubility for PCL, and has been used to successfully produce nanofibres in the past (Kenawy, Abdel-Hay, El-Newehy & Wnek, 2009). In the literature, research has been performed using chitosan and PCL in formic acid and acetone solvents for electrospinning. The polymers were blended together using different concentrations of chitosan, while keeping PCL concentration constant. It was discovered that a lower concentration of PCL resulted in beaded nanofibres, while only small amounts of beads were observed at concentration of 8 – 10 wt% PCL (Shalumon et al., 2010).

This study aims to extend the knowledge in this area through a different solvent system, and introducing nanoparticles into the fibres themselves. A novel application of magnetic nanoparticles to control the conductivity of the polymer matrix is tested. The effect of magnetic nanoparticles with the structure of an electro-spun nanofibre matrix is not well known. However, it is known that the conductivity of the sample will be increased, resulting in greater electrospinnability. These nanoparticles have been very effective in the field of tissue engineering by increasing bone cell growth, proliferation, and differentiation (Kannarkat et al., 2010). Potential applications such as these are outlined in Section 5.5.

5.2 Sample preparation

5.2.1 Chitosan solution

Before the preparation of the blended solution, chitosan was electro-spun with 1% Fe_3O_4 nanoparticles to determine favourable operating parameters. The optimum

solvent for chitosan was determined to be 90% concentrated acetic acid, and was prepared accordingly at a concentration of 0.5% and 1% w/v (outlined in Table 5.1). The solutions were sonicated for two hours, and the polymer was allowed to dissolve overnight. The viscosity was measured for Sample A and Sample C to compare the effect of chitosan concentration. A viscosity of 46.1 cP and 113 mP was measured for Sample A and Sample C, respectively.

Table 5.1: Sample composition for chitosan with nanoparticles.

Sample	A	B	C	D
Chitosan (wt%)	0.5	0.5	1	1
Fe_3O_4 (wt%)	0	1	0	1

5.2.2 Chitosan/PCL blended solution

Chitosan was dissolved in 90% v/v aqueous acetic acid to give two solutions at a concentration of 0.5% and 1% w/v. PCL was dissolved in chloroform and was added to the chitosan solutions at 6% and 8% w/v to make a total of four compositions. All four solutions were then sonicated for two hours and their viscosity was measured. Each sample was divided into two separate solutions, and magnetic nanoparticles were added to one of them at a concentration of 1% w/v for the solid Fe_3O_4 (outlined in Table 5.2).

Table 5.2: Sample composition for the chitosan/PCL blends.

Sample	A	B	C	D	E	F	G	H
Chitosan (wt%)	0.5	0.5	0.5	0.5	1	1	1	1
PCL (wt%)	6	6	8	8	6	6	8	8
Fe_3O_4 (wt%)	0	1	0	1	0	1	0	1

Sonication was performed once more to ensure homogeneity throughout the solution. The required amount of Fe_3O_4 solution to be added was calculated using the stoichiometric relationship between the Fe^{+2} ions and Fe_3O_4 product during the nanoparticle synthesis, expressed by:

$$Fe^{+2}_{(aq)} + 2\ Fe^{+3}_{(aq)} + 4\ H_2O_{(l)} \rightarrow Fe_3O_{4(s)} + 8H^{+}_{(aq)}$$

5.2.3 Blended solution properties

Within the solvent, the two polymers were miscible, which is likely from the formation of hydrogen bonds between the carbonyl group of PCL and the chitosan functional groups (Sarasam & Madihally, 2005). The effect of the magnetic nanoparticles on the conductivity of the solution was measured for the two optimal solutions (designated Sample G and Sample H), which was determined after completion of electrospinning and nanofibre analysis.

A conductivity value of 0.06 mS and 0.4 mS was measured for the solution without nanoparticles and 1% nanoparticles, respectively. The viscosity of the solution was measured using a rheometer at variable shear rates, shown in Figure 5.1. The nanoparticles evidently caused a decrease in the viscosity of the solution, but this appears to have been superseded by the increased conductivity of the solution as there was no hindrance to electrospinnability. However, bead formation seems to have been a direct result, which is discussed further in the SEM analysis (Section 5.4).

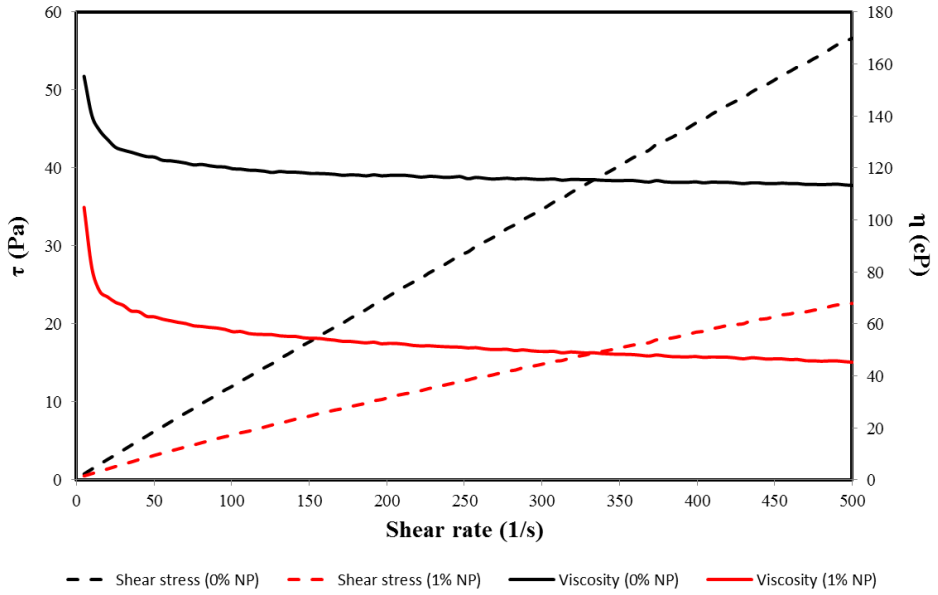

Figure 5.1: Viscosity profiles at variable shear rates for 0% and 1% Fe_3O_4.

5.3 Electrospinning chitosan

5.3.1 Parameter optimisation

To determine the optimal parameters for electrospinning chitosan, a series of trials were completed at different voltages and collector distances. For these trials, the flow rate and system temperature were kept constant at 1 mL/h and 25ºC, respectively. The voltage was incremented by +5 kV, up to a maximum of 30 kV at distances of 10 and 15 cm (see Table 5.3). From the results in Table 5.3, a common trend was failed fibre formation below 20 kV. This is attributed to the high surface tension of the solutions, a result of the high molecular weight and larger molecular weight distribution of chitosan (Homayoni et al., 2009). Between 20 and 25 kV saw the most consistent jet of solution from the needle tip, however the Taylor cone was quite unique. Unlike typical Taylor cone shapes, the chitosan solutions formed a wide dispersive jet at the needle tip, which made it appear to be 'spraying' the solution. The repulsive forces between the protonated amine groups of chitosan are likely responsible for this behaviour (Klossner, Queen, Coughlin & Krause, 2008; Lee et al., 2009). For chitosan, a collector distance of 15 cm provided more stability in the jet stream. Voltages in excess of 25 kV resulted in an inconsistent Taylor cone, and the spraying of the solution was very sporadic. The presence of the Fe_3O_4 nanoparticles in the solution increased the electrospinning stability slightly; however it is difficult to assess their physical impact before looking at microscopy analysis.

5.3.2 Nanofibre size and distribution analysis

After electrospinning, a fine white layer was formed on the aluminium foil and was analysed using SEM. Before imaging, it was expected that the film would be mostly droplets after the solution appeared to only spray during the electrospinning process. From Figure 5.2, it can be seen that some fibre formation did take place for Sample C and D. There were no fibres formed for the 0.5% chitosan samples. The first two images (A & B) show a wide range of fibre diameters, and most of them appear to not have fully evaporated their solvent. The fibre surface morphology is also quite diverse, with some fibre becoming split down the centre, suggesting that they are mechanically weak. From the latter two images (C & D), a lot of droplets are present and the fibres appear to have been squashed upon deposition on the foil. This is likely caused by the poor solvent evaporation during the electrospinning process. The

agglomeration of crystallite structures in image ‘C’ is likely composed of a large amount of Fe_3O_4 nanoparticles.

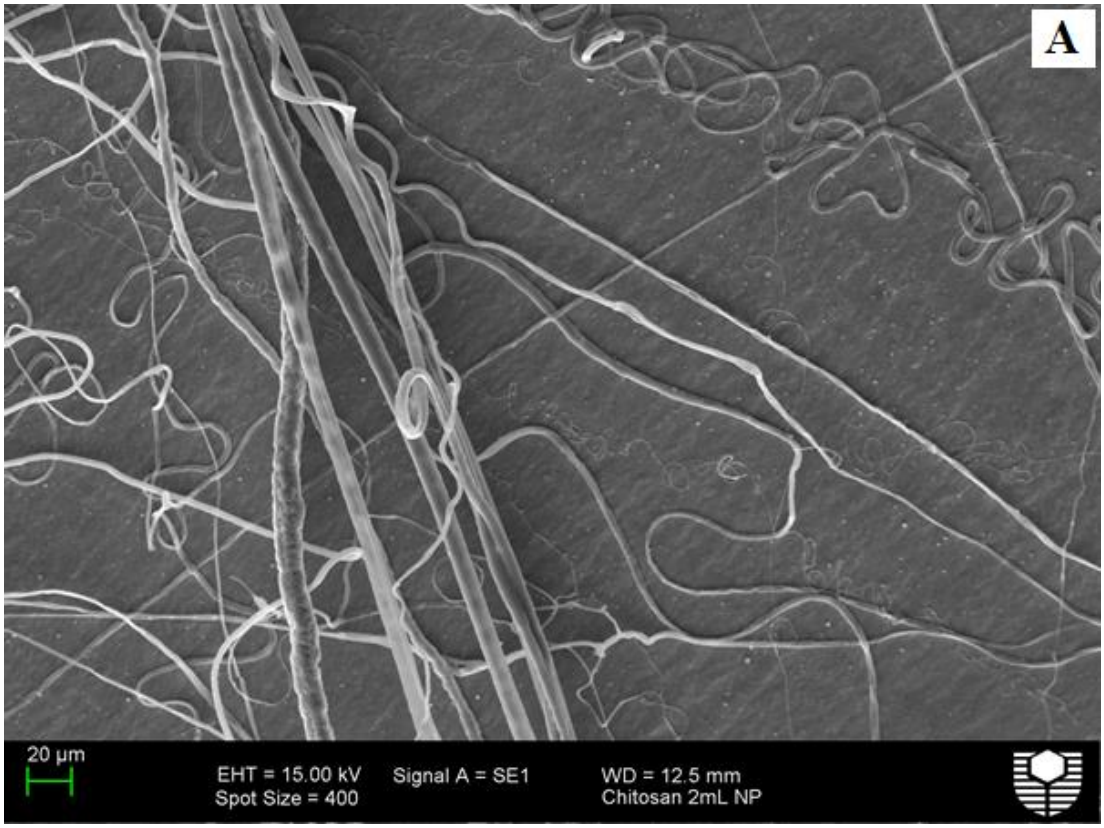

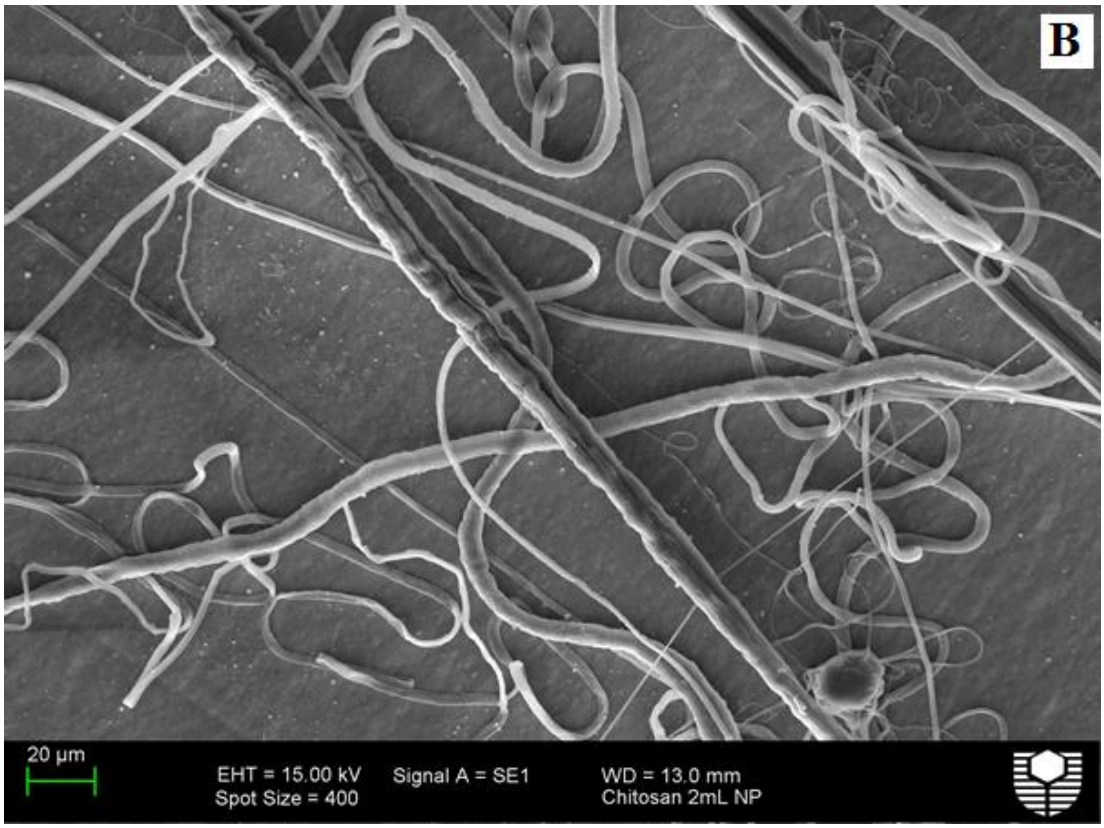

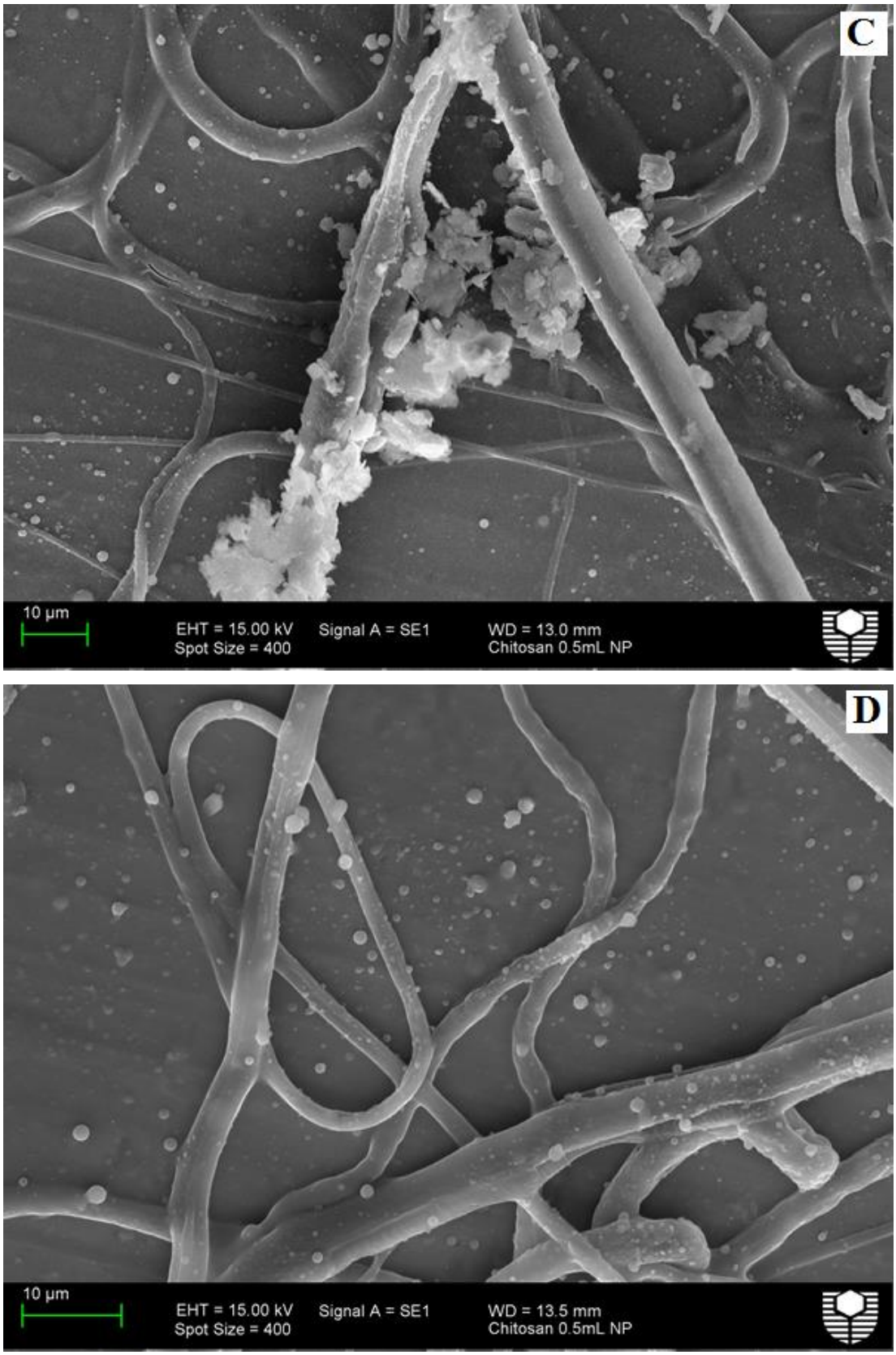

Figure 5.2: SEM images of the chitosan nanofibres: Sample C (image A & B), Sample D (image C & D). Scale: 10 – 20 µm.

Table 5.3: Optimisation of the electrospinning parameters for chitosan.

	Sample A (0.5% chitosan)					
	Voltage (kV)					
Distance (cm)	**5**	**10**	**15**	**20**	**25**	**30**
10	No jet formed	No jet formed	Droplets on collector; wet.	Droplets on collector; wet.	Spraying	Spraying
15	No jet formed	No jet formed	Droplets on collector; wet.	Droplets on collector; wet.	Spraying	Spraying
	Sample B (0.5% chitosan, 1% Fe_3O_4)					
	Voltage (kV)					
Distance (cm)	**5**	**10**	**15**	**20**	**25**	**30**
10	No jet formed	No jet formed	Droplets on collector; wet.	Spraying	Spraying	Sprays more sporadically
15	No jet formed	No jet formed	Droplets on collector; wet.	Spraying	Spraying	Sprays more sporadically
	Sample C (1% chitosan)					
	Voltage (kV)					
Distance (cm)	**5**	**10**	**15**	**20**	**25**	**30**
10	No jet formed	Polymer jet is spitting solution	Can see a more consistent jet forming	Taylor cone formed, however appears to be spraying	Still seems to spray, similar to 0.5wt%	Sprays more sporadically
15	No jet formed	Polymer jet is spitting solution	Polymer jet is spitting solution	Taylor cone formed, however appears to be spraying	Spraying	Sprays more sporadically
	Sample D (1% chitosan, 1% Fe_3O_4)					
	Voltage (kV)					
Distance (cm)	**5**	**10**	**15**	**20**	**25**	**30**
10	No jet formed	Polymer jet is spitting solution	Polymer jet is spitting solution	Spraying consistently	Spraying becoming more inconsistent	Sprays more sporadically
15	No jet formed	Polymer jet is spitting solution	Polymer jet is spitting solution	Spraying and spitting	Spraying	Sprays more sporadically

Analysis of the fibre diameter of Sample C and Sample D was completed using the ImageJ software. The average fibre diameter and diameter range is summarised in Table 5.4. The average diameter of the samples were in excess of 4 microns, which is very large in comparison to the electrospinning of chitosan in similar studies (Geng et al., 2005; Ohkawa et al., 2004; Homayoni et al., 2009). Due to the low concentration of chitosan, a likely explanation for the thick fibres is a combination of the high molecular weight being used and poor solvent evaporation. Additionally, chitosan is known to undergo swelling in aqueous solution when it is not cross-linked with another polymer (Lee et al., 2009). The presence of the Fe_3O_4 nanoparticles resulted in an increase in the size of the produced fibres; however the electrospinnability was reduced (as it was shown by SEM in Figure 5.2). It was concluded from these results that polymer blending is essential in order to provide sufficient mechanical strength via cross-linking for chitosan-based nanofibre formation.

Table 5.4: Summary of the chitosan nanofibre diameter distribution.

Sample	C	D
Chitosan (wt%)	1	1
Fe_3O_4 (wt%)	0	1
Average fibre diameter (μm)	4.3	5.9
Fibre diameter range (μm)	0.5 – 14.4	2.4 – 13.0

5.4 Blended electrospinning of chitosan with PCL

5.4.1 Parameter optimisation

Similarly to the optimisation of chitosan, the voltage and collector distance were the two key variables for the electrospinning of chitosan blended with PCL. The flow rate and system temperature were kept constant at 1 mL/h and 25ºC, respectively. The same voltage and collector distance variable range was used so the results are comparable to chitosan. The results shown in Table 5.6 detail how the behaviour of the solutions changed with voltage, collector distance, and also polymer concentration. For samples A – D, consistent fibre formation was very difficult to achieve, whereas consistency was significantly improved for samples E – H. This difference comes from the concentration of chitosan, which drastically changes the viscosity of the solution at even low concentrations. As it was seen for chitosan, no fibre formation was observed for voltages less than 10 kV. The most optimal

conditions for electrospinning this blend was 20 – 25 kV, and a distance of 10 cm. These conditions are similar to those found in the literature for electrospinning PCL/Fe_3O_4 in glacial acetic acid (Kannarkat et al., 2010). Although there was no discernable difference between 10 and 15 cm, a shorter distance will allow more fibres to be collected on the rotating drum (some fibres missed the collector at longer distances). The optimum polymer concentration was determined to be 1% chitosan, and 6 – 8% PCL (with and without nanoparticles). SEM analysis was then used to determine which concentration of PCL formed the more uniform nanofibre distribution.

5.4.2 Nanofibre characterisation

The nanofibres were characterised by SEM to assess the formation, consistency, and dispersion of the nanofibres. The nanofibres produced were found to be dry, long and continuous, and beaded in some areas. An increased amount of beading was evident for the samples containing lower polymer concentrations (0.5% chitosan and 6% PCL). Based on the consistency of the nanofibre diameter, the most optimal composition was determined to be 1% chitosan and 8% PCL, with similar results presented in the literature (Shalumon et al., 2010). The embedded Fe_3O_4 nanoparticles aim to further the knowledge in this area by analysing nanofibre diameter stability, which is assessed through SEM. At this ratio, the polymer solution was successfully electro-spun to form nanofibres with an average diameter of 99.8 nm and 109.7 nm for Sample G and H, respectively. The diameter range was more extensive for Sample G, as seen in Figure 5.3. Also, Sample H followed a more normalised distribution of the diameter size. A total of 50 measurements of unique nanofibres were made for each sample to get an estimate of the distribution. A summary of the SEM analysis for all eight samples is shown in Table 5.5.

Table 5.5: Summary of the chitosan/PCL nanofibre diameter distribution (NF represents no fibres produced, BF represents beaded fibres produced).

Sample	A	B	C	D	E	F	G	H
Chitosan (wt%)	0.5	0.5	0.5	0.5	1	1	1	1
PCL (wt%)	6	6	8	8	6	6	8	8
Fe_3O_4 (wt%)	0	1	0	1	0	1	0	1
Average diameter (nm)	NF	NF	BF	BF	95.4	97.6	99.8	109.7
Diameter range (nm)	NF	NF	BF	BF	36 - 219	41 - 228	44 - 262	34 - 245

Table 5.6: Optimisation of the electrospinning parameters for chitosan/PCL.

	Sample A (0.5% chitosan, 6% PCL)					
	Voltage (kV)					
Distance (cm)	**5**	**10**	**15**	**20**	**25**	**30**
10	No jet formed	No jet formed	Intermittent spinning/drops	Intermittent spinning/drops	Intermittent spinning/drops	Intermittent spinning/drops
15	No jet formed	No jet formed	No jet formed	Intermittent spinning/drops	Intermittent spinning/drops	Intermittent spinning/drops
	Sample B (0.5% chitosan, 6% PCL, 1% Fe_3O_4)					
	Voltage (kV)					
Distance (cm)	**5**	**10**	**15**	**20**	**25**	**30**
10	No jet formed	No jet formed	Intermittent spinning/drops	Intermittent spinning/drops	Intermittent spinning/drops	Intermittent spinning/drops
15	No jet formed	No jet formed	Intermittent spinning/drops	Intermittent spinning/drops	Intermittent spinning/drops	Intermittent spinning/drops
	Sample C (0.5% chitosan, 8% PCL)					
	Voltage (kV)					
Distance (cm)	**5**	**10**	**15**	**20**	**25**	**30**
10	No jet formed	Spinning partially	Fibres visibly being formed	Fibres formed, some drops	Fibres formed, some drops	Fibres formed, some drops
15	No jet formed	No jet formed	Fibres visibly being formed	Fibres formed, some drops	Fibres formed, some drops	Fibres formed, some drops
	Sample D (0.5% chitosan, 8% PCL, 1% Fe_3O_4)					
	Voltage (kV)					
Distance (cm)	**5**	**10**	**15**	**20**	**25**	**30**
10	No jet formed	Spinning partially	Intermittent spinning/drops	Intermittent spinning/drops	Intermittent spinning/drops	Intermittent spinning/drops
15	No jet formed	No jet formed	Intermittent spinning/drops	Intermittent spinning/drops	Intermittent spinning/drops	Intermittent spinning/drops
	Sample E (1% chitosan, 6% PCL)					
	Voltage (kV)					
Distance (cm)	**5**	**10**	**15**	**20**	**25**	**30**
10	No jet formed	No jet formed	Starting to spin	Spinning, few drops	Spinning more consistently	Thin, white layer formed
15	No jet formed	No jet formed	Starting to spin	Spinning, few drops	Spinning more consistently	Thin, white layer formed
	Sample F (1% chitosan, 6% PCL, 1% Fe_3O_4)					
	Voltage (kV)					
Distance (cm)	**5**	**10**	**15**	**20**	**25**	**30**
10	No jet formed	No jet formed	Intermittent spinning/drops	Spinning stabilised	Thin, white layer formed	Thin, white layer formed
15	No jet formed	No jet formed	Intermittent spinning/drops	Spinning stabilised	Thin, white layer formed	Thin, white layer formed
	Sample G (1% chitosan, 8% PCL)					
	Voltage (kV)					
Distance (cm)	**5**	**10**	**15**	**20**	**25**	**30**
10	No jet formed	Spinning partially	Visibly spinning	Consistently spinning	White layer formed	White layer formed
15	No jet formed	Spinning partially	Visibly spinning	Consistently spinning	White layer formed	White layer formed
	Sample H (1% chitosan, 8% PCL, 1% Fe_3O_4)					
	Voltage (kV)					
Distance (cm)	**5**	**10**	**15**	**20**	**25**	**30**
10	No jet formed	Spinning partially	Visibly spinning	Consistently spinning	White layer formed	White layer formed
15	No jet formed	Spinning partially	Visibly spinning	Consistently spinning	White layer formed	White layer formed

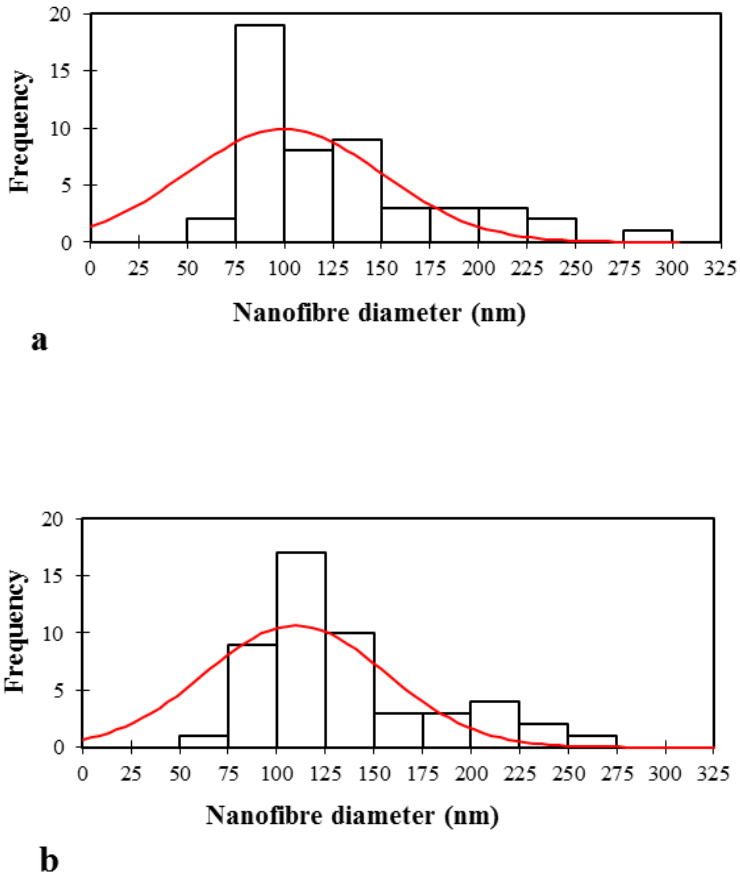

Figure 5.3: Nanofibre diameter uniformity distribution: (a) Sample G, (b) Sample H.

The SEM images in Figure 5.4 show the progress of the nanofibre structure as the polymer concentration was increased between samples. Successful nano-fibre formation was observed for Sample G, with limited beading in the sample. There was however still beading present for the solution containing the nanoparticles (Sample H), where a larger average nanofibre diameter was measured. The beading in these samples is attributed to an insufficient voltage supply and steady flow rate, which is necessary for overcoming the surface tension of a chitosan-based solution. The presence of the nanoparticles should theoretically reduce the surface tension of the solution, improving the electrospinnability (Wang et al., 2004). This was not observed during the process, requiring high voltages to achieve electrospinnability for Sample H. This was likely due to the relatively low concentration of the nanoparticles, which had a negligible effect of the surface morphology of the

nanofibres. However, the concentration of the nanoparticles had to be limited to 1% to maintain an acceptable viscosity for electrospinning to occur.

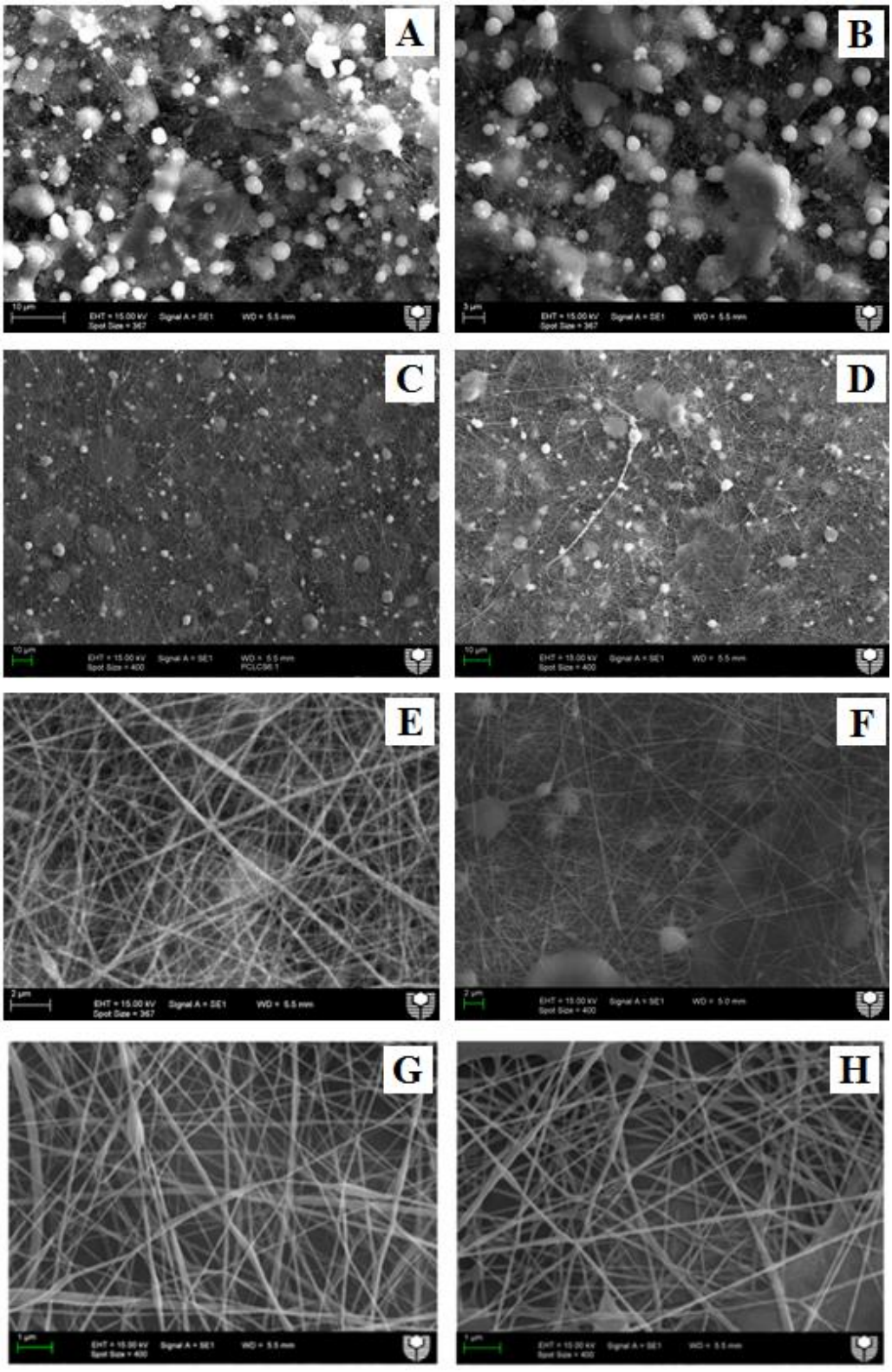

Figure 5.4: SEM images of the nanofibres (image letter represents sample name from Table 5.5). Scale: 1 µm.

Energy dispersive spectroscopy (EDS) was also performed by the Zeiss Evo 40XVP scanning electron microscope. EDS was used to identify the elemental composition of the nanofibres in Sample H, to confirm the presence of the Fe_3O_4 nanoparticles. The spectrum shown in Figure 5.5 identifies the presence of carbon, oxygen, and iron within the sample. The characteristic peak for aluminium is from the foil substrate, and can be omitted. The Kα peak for iron was confirmed at 6.403 keV, and the Kβ peak at 7.057 keV. The iron peak shown at 0.705 keV is representative of the L-series peaks, which overlap each other in the spectrum (Satcher, 2006). The Kα peak for carbon and oxygen were measured at 0.277 and 0.523 keV, respectively. The long polymer chains of chitosan and PCL are represented by the carbon peak, whereas the oxygen is peak is characteristic of the ester groups of PCL, hydroxyl and ether groups of chitosan, and the Fe_3O_4 nanoparticles themselves.

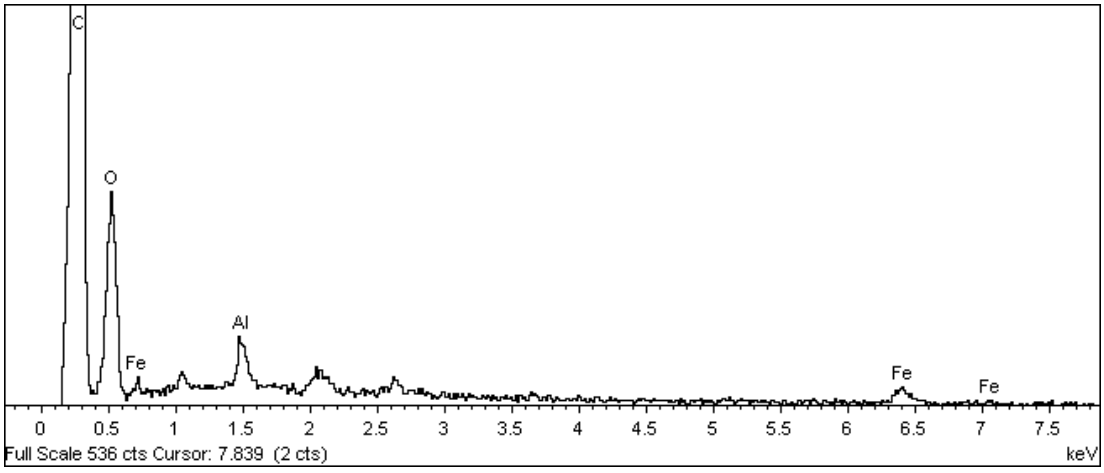

Figure 5.5: EDS spectrum of Sample H (1% chitosan, 8% PCL, 1% Fe_3O_4).

5.4.3 Magnetic characterisation

The characterisation of the nanoparticles was carried out using SQUID to determine the magnetisation of the nanoparticles, and to prove their superparamagnetic nature. This study was carried out by using zero-field-cooled (ZFC), field-cooled (FC), and hysteresis testing. The samples were cooled to 10 K at 0 and 200 oersteds for ZFC and FC, respectively. As it was stated in Section 3.3, 5 K increments were used when heating from 10 to 50 K, 10 K increments were then used for 50 to 100 K, and 20 K increments for the remainder of the experiment. The resulting data for the ZFC/FC testing is shown in Figure 5.6.

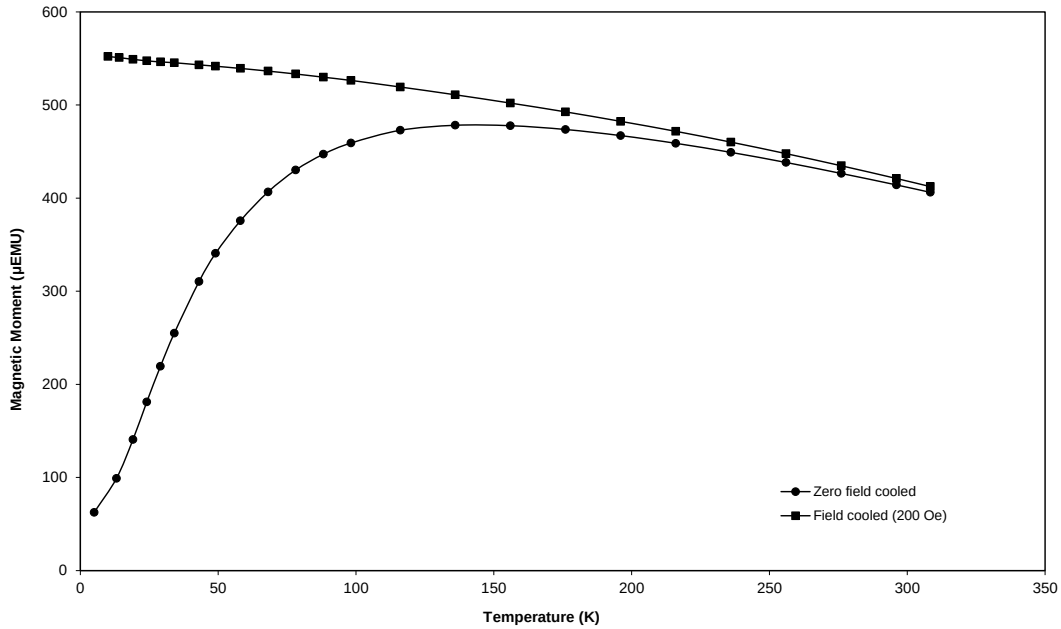

Figure 5.6: ZFC and FC characterisation of the Fe_3O_4 nanoparticles in the polymer matrix.

A similar trend at high temperatures is observed between the two data sets, with a significant difference at lower temperatures. This behaviour is typical for nano-structures with single domains, and is representative of magnetic moment inhibition below the blocking temperature at 150 K (Nathani et al., 2004). Once the temperature exceeds this point, the nanoparticles are free to align under the effect of the external magnetic field. The hysteresis loop shown in Figure 5.7 displays the superparamagnetic nature of the Fe_3O_4 nanoparticles clearly. A saturated magnetisation, M_S, value of 972 µemu is observed. This was calculated to be approximately 10 emu/g Fe_3O_4, which is lower compared to other studies using chitosan (Chang et al., 2006; Huang, Shieh, Shih & Twu, 2010). Chang and co-workers recorded a saturated magnetisation of 62 emu/g (coated particle size was 13.5 nm), whereas Huang and co-workers recorded a value of 27.91 emu/g (200 – 500 nm coated particle size). The lower magnetisation is attributed to the small size of the magnetic nanoparticles relative to the sample matrix that they are contained within. This effectively represents a lower concentration of nanoparticles, or iron atoms per gram of polymer. Therefore, since the concentration of Fe_3O_4 nanoparticles in this study is lower, the magnetisation can be expected to be lower. This relatively low concentration is confirmed by the EDS spectrum that was shown

in Figure 5.5. The remanence and coercivity are also measured as zero, defining the superparamagnetic nature of the nanoparticles (Huang et al., 2010). As mentioned in the literature, the sizes of the iron-based particles also impact the magnetisation, with lower values for smaller sized particles. The surface morphology of magnetic nanoparticles often have crystalline disorder, and this is more prominent in smaller particles due to the higher mass of atoms near the surface compared to the bulk of the particles (Burke & Stöver, 2002). However, due to the low concentration used in this experiment, no definite changes were seen for the nanofibre surface morphology. TEM was used to measure the particle size of the nanoparticles, with an approximate diameter of 5 – 8 nm (Figure 5.8).

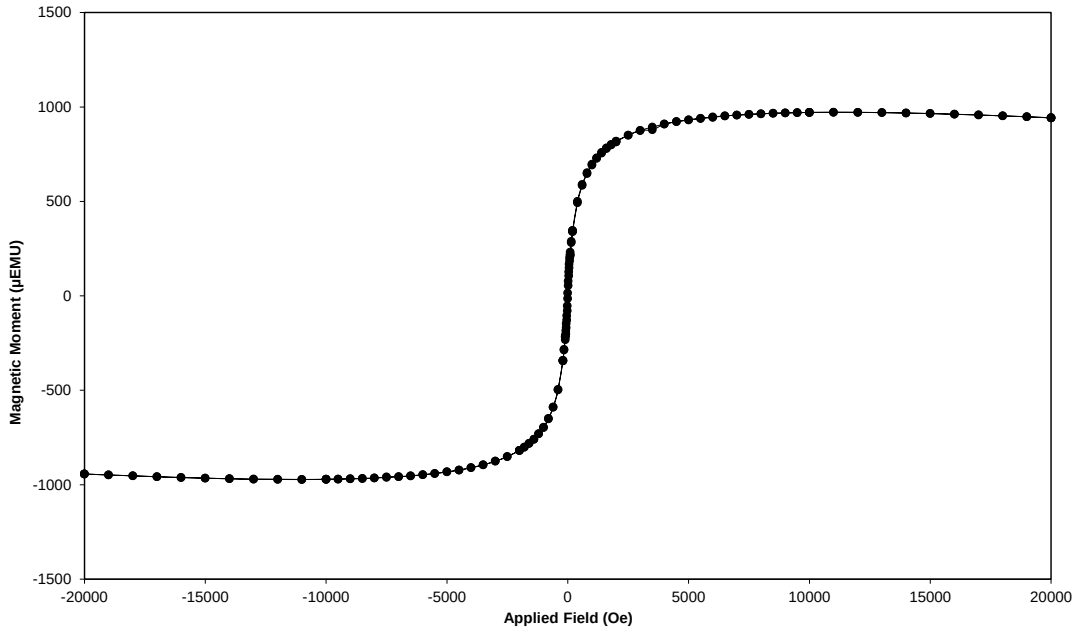

Figure 5.7: Hysteresis curve of the Fe_3O_4 nanoparticles in the polymer matrix.

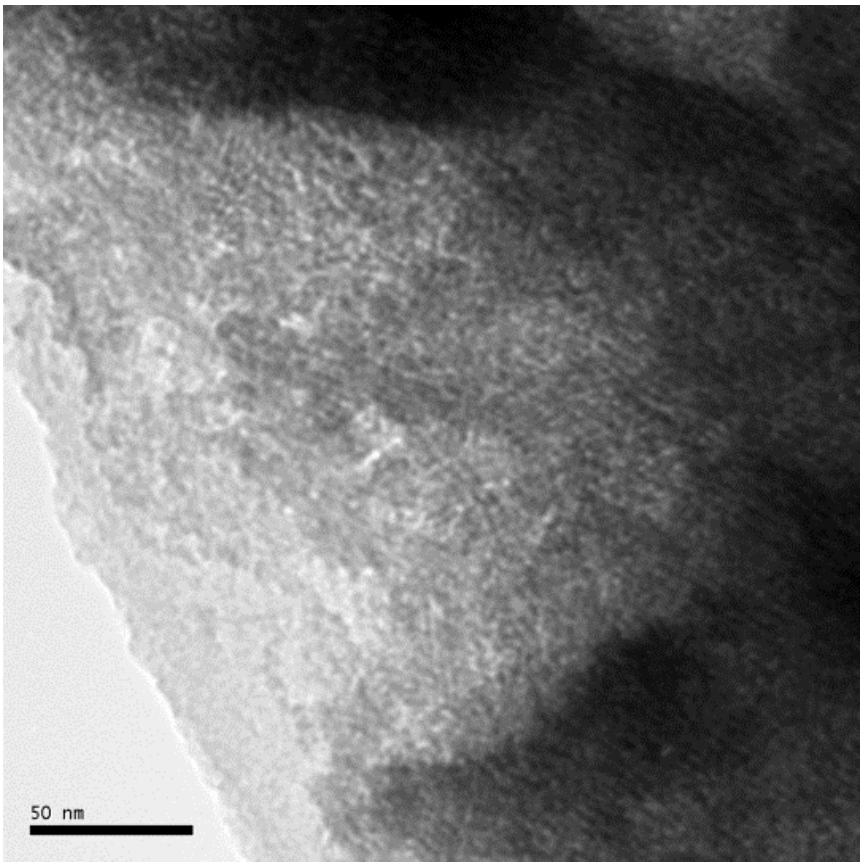

Figure 5.8: TEM of the Fe_3O_4 nanoparticles. Scale: 50 nm.

5.4.4 Thermal characterisation

Thermal profiles were measured for the two samples containing 1% chitosan and 8% PCL (Sample G & H) to observe the effect of the nanoparticles in the nanofibre matrix. DSC was completed using a range of 35 – 150ºC, shown in Figure 5.9. A heating and cooling rate of 5ºC/min was used, with an isothermal reading held at 150ºC for two minutes. For Sample H (with Fe_3O_4), the polymer matrix exhibited a higher degree of endothermic heat flow during the melting transition at 57ºC. The melting point was similar for both samples, whereas the crystallisation temperature was at 45ºC for 0% Fe_3O_4 (6°C above 1% Fe_3O_4). The heat of melting, ΔH_m, was 21.85 and 40.08 J/g for 0% Fe_3O_4 and 1% Fe_3O_4, respectively. The increased amount of heat flow for the sample containing the nanoparticles was expected due to the higher heat capacity of Fe_3O_4. As soon as the polymer material surrounding the nanoparticles undergoes melting, the nanoparticles are exposed and the endothermic heat flow increased, as shown by the DSC curve.

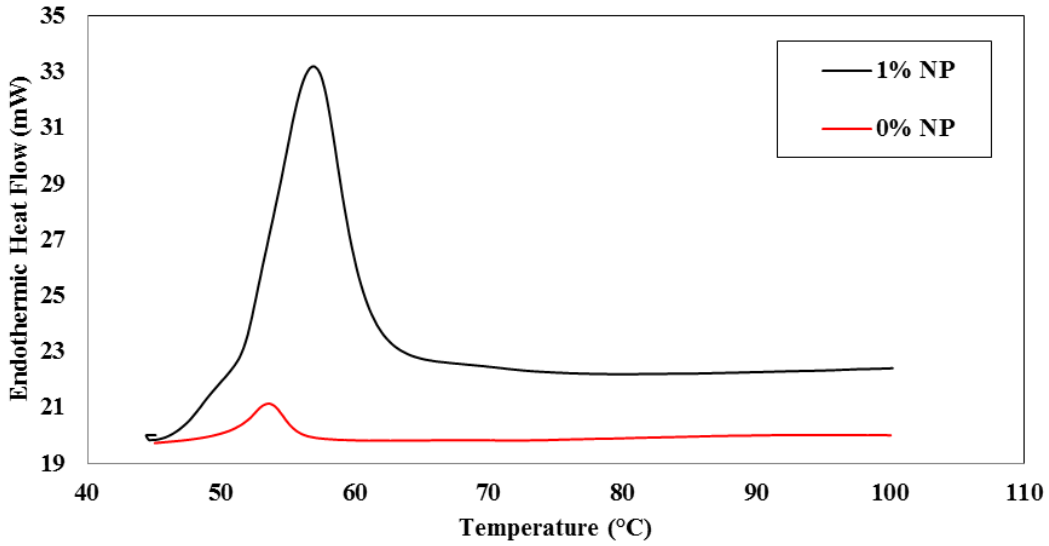

Figure 5.9: DSC curves of the samples containing 0% and 1% Fe_3O_4 nanoparticles.

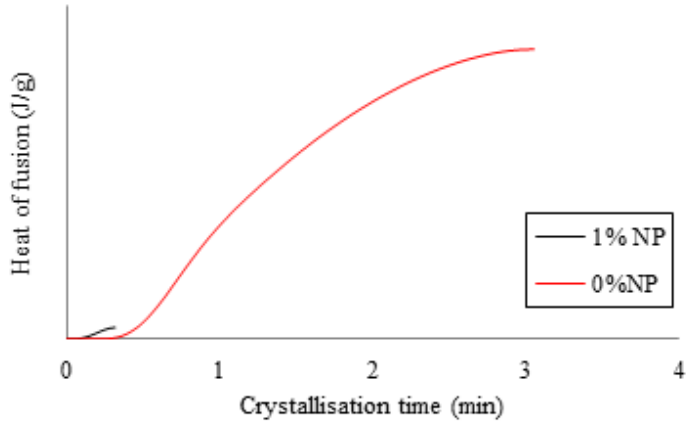

Figure 5.10: Crystallisation times for both samples.

It is suspected that the nanoparticles have a heterogeneous nucleating effect, resulting in an increased amount of crystallinity within the sample and considerably shorter crystallisation time (Wang et al., 2013a). This assumption is based on the crystallisation temperature, T_C, which increased from 36.8ºC to 44.7ºC from the presence of the nanoparticles. The rate of crystallisation for both samples is shown in Figure 5.10. To better understand the effect of the nanoparticles, the Avrami equation was used to determine if nucleation was occurring as expected. The crystallisation behaviour can be determined graphically from the data presented by DSC, utilising the heat of crystallisation and crystallisation time period. For this purpose, the Avrami Equation is expressed as:

$$\ln[-ln(1-f)] = n\ln t + \ln k$$

Where *f* is the fraction of crystals at any time *t* during the crystallisation process, *k* is the rate constant and *n* is the Avrami exponent (Chong, 2001). The exponent is determined by plotting $\ln[-ln(1-f)]$ against ln *t*, giving a linear relationship such that *n* can be measured as the gradient. For every time measurement during the crystallisation process, the value of *f* must be determined using:

$$f = \frac{[\int_{t=0}^{t} \frac{d\Delta H(t)}{dt} . dt]}{\Delta H}$$

Where ΔH is the heat of crystallisation (Chong, 2001). From the Avrami plots in Figure 5.12, the dimensionless value of *n* and *k* for each sample can be determined, which are summarised in Table 5.7. The higher value of *n* represents spherulitic growth in three dimensions, with a higher rate constant. This suggests that the nanoparticles are acting as a nucleating agent during the crystallisation process, providing higher crystalline order and increasing the number of spherulites (Vasanthan et al., 2011; Wang et al., 2013a). A representation of this heterogeneous nucleation and spherulitic growth is shown in Figure 5.11. The experimental data was limited between 10 and 75% to maintain linearity in the Avrami relationship. This limitation is often exercised in the literature to account for deviations caused by voids in the crystal mass (Chong, 2001; Vasanthan et al., 2011).

Table 5.7: Avrami exponent and rate constant values.

Sample	Avrami exponent, *n*	Avrami constant, *k*
0% Fe_3O_4 (Sample G)	1.8	0.5
1% Fe_3O_4 (Sample H)	3.2	143.5

Since chitosan is low in concentration, it does not affect the nucleation dramatically in this particular case. However it has been proven in past studies that it can accelerate the crystallisation process of PCL at concentration of 10 – 20%, although this would be impractical in the scope of electrospinning due to the impact of viscosity (Garcia Cruz, Gomez Ribelles & Salmeron Sanchez, 2008).

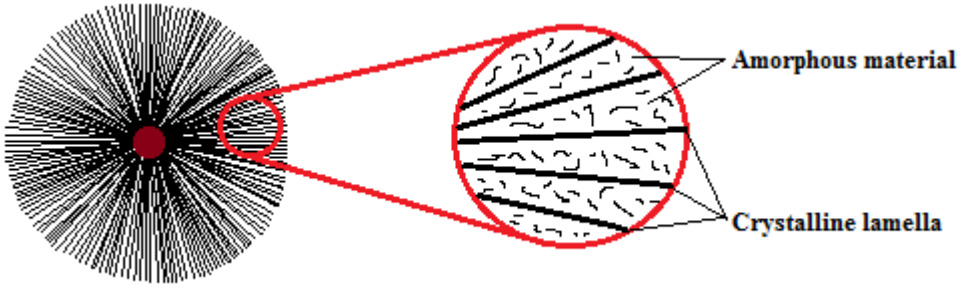

Figure 5.11: Representation of the spherulitic growth from Fe_3O_4 nucleation sites.

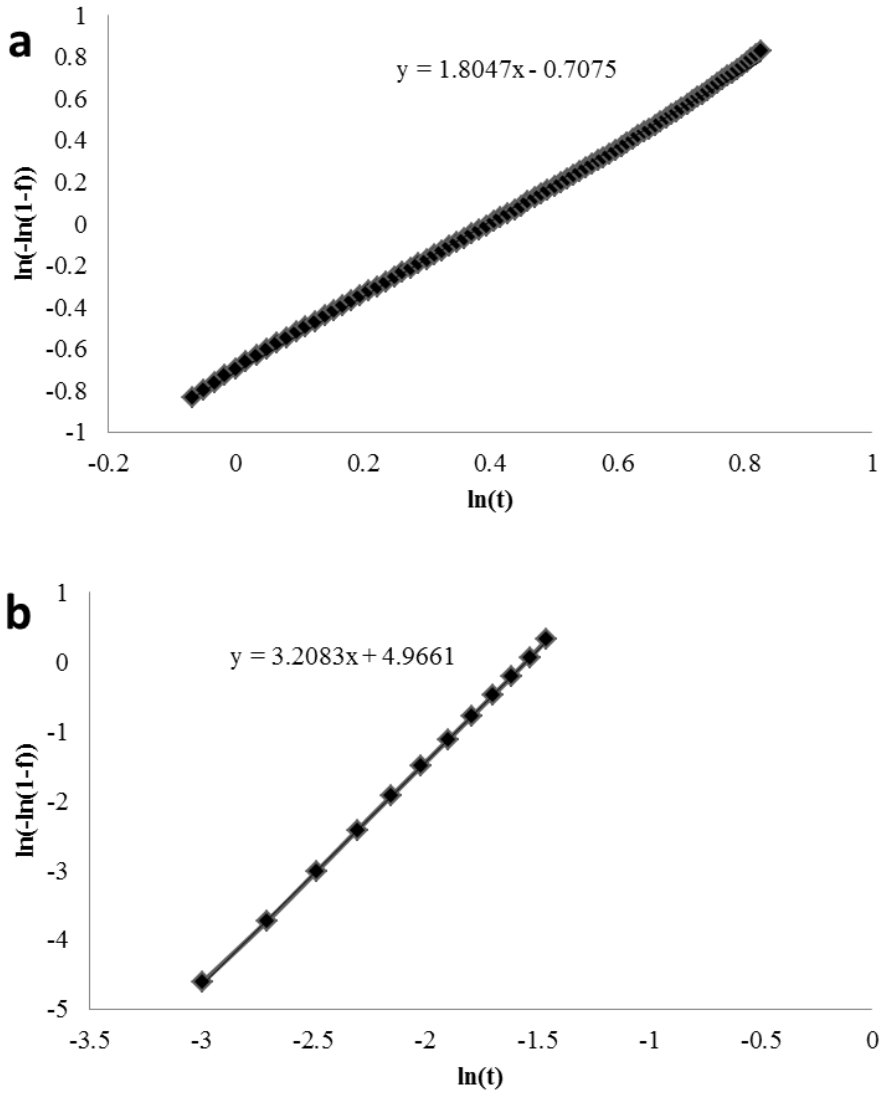

Figure 5.12: Avrami plots of ln[–ln(1–f)] vs. ln(t) for (a) Sample G, and (b) Sample H.

5.5 Discussion

The two key stimuli-responsive properties of the produced samples are pH-response via chitosan, and magnetic-response from the presence of superparamagnetic nanoparticles. As mentioned in Chapter 2, the pH-responsive nature of chitosan arises from the isoelectric point of pH 7.4, where the molecule exhibits no charge. In media that are above the isoelectric point of chitosan, free amino groups are present that promote wound healing through the activation of macrophages and cytokines (Baldrick, 2010). Furthermore, chitosan has been proven to be a suitable bio-adhesive material for the delivery of hydrophilic drugs. Pure chitosan has issues with prolonged drug release due to hydrophilicity. However this can be overcome by blending with a hydrophobic, biodegradable, and biocompatible polymer like PCL to prolong the release (Perugini et al., 2003).

As it was discovered through thermal characterisation, the nanoparticles provided an indication of the crystalline behaviour of the nanocomposites in addition to its superparamagnetic nature. The spherulitic formation from the nucleating nanoparticles leads to an increase in crystallinity, density, and tensile strength. The increased density comes from the increased packing of the molecules, which also increases the hardness, brittleness, and abrasion resistance (Charles E. Carraher, 2006). The increased thermal stability of the sample allows the use of the material in applications where heat may be generated. This can come from the process of Néel relaxation (oscillating external magnetic field stimuli), which will cause the nanoparticles to generate localised heat within the sample while also becoming magnetised (Davidson, 2012). The use of this stimulus is common in applications such as: magnetic separation in biological media, therapeutic drug delivery, radio frequency methods for tumour catabolism, and magnetic resonance applications (Pankhurst et al., 2003). Chitosan-based magnetic composites have also proven to be effective in bone regeneration via cell adhesion and proliferation, which would also be easily implemented with the chitosan/PCL/Fe_3O_4 nanostructure (Wei et al., 2011).

5.6 Summary

The electrospinning of a chitosan-based, stimuli-responsive nanofibre was successfully manufactured, and was studied using relevant characterisation techniques. The effect of Fe_3O_4 nanoparticles on the characteristics on the nanofibres was analysed using these techniques. The key design parameters and characteristics are summarised below.

- Chitosan was successfully electro-spun in a blended nanocomposite with PCL (with and without Fe_3O_4 nanoparticles), utilising the properties of PCL and Fe_3O_4 to alter the physical properties of the solution such as: surface tension, conductivity, and viscosity.

- The presence of the Fe_3O_4 nanoparticles within the sample was confirmed using EDS, and the nanofibre diameter was measured to range from 36 – 262 nm by SEM. The superparamagnetic nature of the nanoparticles was measured by SQUID. It was confirmed the nanoparticles had zero coercivity (and thus superparamagnetic) using hysteresis testing. The nanoparticles were measured to be 5 – 8 nm by TEM.

- The effect of the nanoparticles on the nanofibre diameter was analysed through SEM initially. A more consistent normal distribution was measured for the blended polymer sample containing the nanoparticles.

- Furthermore, DSC analysis proved that the nanoparticles had a direct effect on the crystallisation process. They promoted three-dimension spherulitic growth by acting as nucleation sites, with an increase in the crystallisation temperature from 37ºC to 45ºC, and crystallisation time.

CHAPTER 6

CONCLUSIONS AND RECOMMENDATIONS

6.1 Conclusions

Through the understanding of the contributing factors of polymer electrospinning, stimuli-responsive nanostructures based on PNIPAM and chitosan were successfully produced. These contributing factors included: solution viscosity and conductivity, polymer concentration, the applied voltage, flow rate, and distance to the collector. The effect of magnetic nanoparticles on each of the nanostructures was also made apparent through thermal and magnetic analysis. The nanoparticles had a positive interaction of the electrospinning process, resulting in a more uniform distribution of the size of the nanofibres.

6.1.1 The thermo-responsive nanostructure

A thermo-responsive coaxial nanofibre-based structure was produced from PNIPAM, PCL, and Fe_3O_4 nanoparticles. The electrospinning process was optimised at 25 kV, with a collector distance of 12 cm. The average nanofibre diameter was measured at 247 nm for the optimised coaxial nanofibres. The presence of the PCL and low concentration of nanoparticles appeared to have little effect on the LCST of the system, measuring the transition at just above 32ºC. The magnetic presence provided by the nanoparticles was also low, suggesting that the relative thickness of the PNIPAM shell material was minimal. The temperature and magnetic response of this nanostructure would be invaluable in applications involving triggered release such as drug delivery. Similarly, tissue engineering could benefit from this type of material through target cell proliferation.

6.1.2. The pH-responsive nanostructure

Chitosan provided a pH-based stimulus in a polymer blended nanostructure with PCL and Fe_3O_4 nanoparticles. The electrospinning parameters were optimised at 25 kV, with a collector distance of 10 cm. The average nanofibre diameter and

crystalline properties were affected by the presence of the nanoparticles. The average diameter was increased from 99.8 nm to 109.7 nm in a nanostructure that contained 1% Fe_3O_4 nanoparticles, 1% chitosan, and 8% PCL. From thermal analysis, it was confirmed that the nanoparticles act as nucleation sites within the nanostructure, promoting three-dimensional spherulitic growth. The pH and magnetic response from this nanostructure will be attractive for applications such as tissue engineering, drug delivery, and magnetic separation in biological media.

6.2 Recommendations

The recommendations for future work are outline below:

- The magnetic strength of the PNIPAM/PCL coaxial nanocomposites can be improved through further experimentation at higher concentrations. This would include rigorous mechanical testing to determine the amount of foreign nanoparticles that can be embedded, without comprising the integrity of the nanofibre.

- The next step for the coaxial release design is to perform trials with drug load release. This should be completed at temperature below and above the LCST of the PNIPAM material to observe the difference in release times. Trials involving cell proliferation are also of interest, utilising the effective magnetic stimulus.

- The next step for the chitosan/PCL blend nanocomposites is also to begin trial applications. The most interesting applications that could benefit from the properties of the prepared material are: tissue engineering via polymer scaffolds, drug delivery, and magnetically-controlled cell proliferation.

REFERENCES

Angammana, C. J., & Jayaram, S. H. (2011). Analysis of the Effects of Solution Conductivity on Electrospinning Process and Fiber Morphology. *IEEE Transaction on Industry Applications, 47***,** 1109-1117.

Baldrick, P. (2010). The safety of chitosan as a pharmaceutical excipient. *Regul Toxicol Pharmacol, 56***,** 290-9.

Bcc. 2013a. *Global Markets and Technologies for Nanofibers* [Online]. Wellesley, Massachusetts, USA: BCC Research. Available: http://www.bccresearch.com/market-research/nanotechnology/nanofibers-market-nan043c.html [Accessed 18th December 2013].

Bcc. 2013b. *Nanomagnetics: Materials, Devices and Markets* [Online]. Wellesley, Massachusetts, USA: BCC Research. Available: http://www.bccresearch.com/market-research/nanotechnology/nanomagnetics-materials-devices-market-nan033b.html [Accessed 18th December 2013].

Burke, N. a. D., & Stöver, H. D. H. (2002). Magnetic Nanocomposites: Preparation and Characterization of Polymer-Coated Iron Nanoparticles. *Chemistry of Materials, 14***,** 4752-4761.

Chang, Y.-C., Chang, S.-W., & Chen, D.-H. (2006). Magnetic chitosan nanoparticles: Studies on chitosan binding and adsorption of Co(II) ions. *Reactive and Functional Polymers, 66***,** 335-341.

Chao, T. Y., & Cheng, Y. T. Synthesis and Characterization of Cu/CoFe(2)O(4) Magnetic Nanocomposites for RFIC Application. *In:* I. Institute of Electrical and Electronics Engineers, ed. IEEE-NANO 2006, 2006 Ohio, USA. Nanotechnology, 810-813.

Charles E. Carraher, J. 2006. Seymour/Carraher's Polymer Chemistry. *In:* C. E. Carraher (ed.) 7th ed. Boca Raton, Florida, U.S.A: CRC Press: Taylor & Francis Group.

Chaw, C. S., Chooi, K. W., Liu, X. M., Tan, C. W., Wang, L., & Yang, Y. Y. (2004). Thermally responsive core-shell nanoparticles self-assembled from cholesteryl end-capped and grafted polyacrylamides:; drug incorporation and in vitro release. *Biomaterials, 25***,** 4297-308.

Chen, B., Xu, F. J., Fang, N., Neoh, K. G., Kang, E. T., Chen, W. N., & Chan, V. (2008). Engineering cell de-adhesion dynamics on thermoresponsive poly(N-isopropylacrylamide). *Acta Biomater, 4***,** 218-29.

Chen, M., Dong, M., Havelund, R., Regina, V. R., Meyer, R. L., Besenbacher, F., & Kingshott, P. (2010). Thermo-Responsive Core−Sheath Electrospun Nanofibers from Poly (N-isopropylacrylamide)/Polycaprolactone Blends. *Chemistry of Materials, 22***,** 4214-4221.

Chen, Y. H., Chung, Y. C., Wang, I. J., & Young, T. H. (2012). Control of cell attachment on pH-responsive chitosan surface by precise adjustment of medium pH. *Biomaterials, 33***,** 1336-42.

Chen, Y. S., Tsou, P. C., Lo, J. M., Tsai, H. C., Wang, Y. Z., & Hsiue, G. H. (2013). Poly(N-isopropylacrylamide) hydrogels with interpenetrating multiwalled carbon nanotubes for cell sheet engineering. *Biomaterials, 34***,** 7328-34.

Chong, C. L. (2001). Crystallization of Palm Oil Products. In N. Widlak, R. Hartel, & S. Narine (Eds.), *Crystallization and Solidification Properties of Lipids* (pp. 110-119). United States of America: AOCS Press.

Chowdhury, M., & Stylios, G. (2010). Effect of Experimental Parameters on the Morphology of Electrospun Nylon 6 fibres. *International Journal of Basic & Applied Sciences, 10***,** 70-78.

Chuang, W.-J., & Chiu, W.-Y. (2012). Thermo-responsive nanofibers prepared from poly(N-isopropylacrylamide-co-N-methylol acrylamide). *Polymer, 53***,** 2829-2838.

Davidson, A. M. 2012. *Magnetic Induction Heating of Superparamagnetic Nanoparticles for Applications in the Energy Industry.* Master of Science in Engineering, The University of Texas.

Deitzel, J. M., Kosik, W., Mcknight, S. H., Beck Tan, N. C., Desimone, J. M., & Crette, S. (2002). Electrospinning of polymer nanofibres with specific surface chemistry. *Polymer, 43***,** 1025-1029.

Depan, D., Kumar, A. P., & Singh, R. P. (2009). Cell proliferation and controlled drug release studies of nanohybrids based on chitosan-g-lactic acid and montmorillonite. *Acta Biomaterialia, 5***,** 93-100.

Duan, B., Dong, C., Yuan, X., & Yao, K. (2004). Electrospinning of chitosan solutions in acetic acid with poly(ethylene oxide). *Journal of Biomaterials Science, Polymer Edition, 15***,** 797-811.

Duarte, A. R. C., Mano, J. F., & Reis, R. L. (2010). Novel 3D scaffolds of chitosan–PLLA blends for tissue engineering applications: Preparation and characterization. *The Journal of Supercritical Fluids, 54***,** 282-289.

Ehrenfreund-Kleinman, T., Golenser, J., & Domb, A. J. (2006). Polysaccharide Scaffolds for Tissue Engineering. In P. X. Ma, & J. Elisseeff (Eds.), *Scaffolding in Tissue Engineering* (pp. 27-44). Boca Raton, FL: CRC Press, Taylor & Francis Group LLC.

Gan, Y. C., Yuan, J. F., Liu, X. J., Pan, W., & Gao, Q. Y. (2011). ABC triblock copolymers with pH-responsive LCST for controlled drug delivery. *Journal of Bioactive and Compatible Polymers, 26***,** 173-190.

Garcia Cruz, D. M., Gomez Ribelles, J. L., & Salmeron Sanchez, M. (2008). Blending polysaccharides with biodegradable polymers. I. Properties of chitosan/polycaprolactone blends. *J Biomed Mater Res B Appl Biomater, 85***,** 303-13.

Geng, X., Kwon, O. H., & Jang, J. (2005). Electrospinning of chitosan dissolved in concentrated acetic acid solution. *Biomaterials, 26***,** 5427-32.

Graziano, G. (2000). On the temperature-induced coil to glouble transition of poly-*N*-isopropylacrylamide in dilute aqueous solutions. *International Journal of Biomedical Macromolecules, 27***,** 89-97.

Homayoni, H., Ravandi, S. a. H., & Valizadeh, M. (2009). Electrospinning of chitosan nanofibers: Processing optimization. *Carbohydrate Polymers, 77***,** 656-661.

Huang, H.-Y., Shieh, Y.-T., Shih, C.-M., & Twu, Y.-K. (2010). Magnetic chitosan/iron (II, III) oxide nanoparticles prepared by spray-drying. *Carbohydrate Polymers, 81***,** 906-910.

Invista. 2012. *Tetrahydofuran (THF) Properties, Uses, Storage, and Handling* [Online]. Invista. Available: http://terathane.invista.com/doc/files/780/thfpush.pdf].

Islam, A., & Yasin, T. (2012). Controlled delivery of drug from pH sensitive chitosan/poly (vinyl alcohol) blend. *Carbohydrate Polymers, 88***,** 1055-1060.

Iwasaki, Y., Sakiyama, M., Fujii, S., & Yusa, S. (2013). Surface modification of mammalian cells with stimuli-responsive polymers. *Chem Commun (Camb), 49***,** 7824-6.

Kannarkat, J. T., Battogtokh, J., Philip, J., Wilson, O. C., & Mehl, P. M. (2010). Embedding of magnetic nanoparticles in polycaprolactone nanofiber scaffolds to facilitate bone healing and regeneration. *Journal of Applied Physics, 107***,** 09B307-09B307-3.

Karande, T. S., & Agrawal, C. M. (2008). Functions and Requirements of Synthetic Scaffolds in Tissue Engineering. In C. T. Laurencin, & L. S. Nair (Eds.), *Nanotechnology and Tissue Engineering: The Scaffold* (pp. 53-86). Boca Raton, FL: CRC Press, Taylor & Francis Group.

Kenawy, E.-R., Abdel-Hay, F. I., El-Newehy, M. H., & Wnek, G. E. (2009). Processing of polymer nanofibers through electrospinning as drug delivery systems. *Materials Chemistry and Physics, 113***,** 296-302.

Klossner, R. R., Queen, H. A., Coughlin, A. J., & Krause, W. E. (2008). Correlation of Chitosan's Rheological Properties and Its Ability to Electrospin. *Biomacromolecules, 9***,** 2947-2953.

Kohori, F., Sakai, K., Aoyagi, T., Yokoyama, M., Sakurai, Y., & Okano, T. (1998). Preparation and characterization of thermally responsive block copolymer micelles comprising poly(*N*-isopropylacrylamide-*b*-DL-lactide). *Journal of Controlled Release, 55***,** 87-98.

Kumbar, S. G., Nukavarapu, S. P., James, R., Hogan, M. V., & Laurencin, C. T. (2008). Recent Patents on Electrospun Biomedical Nanostructures: An Overview. *Recent Patents on Biomedical Engineering, 1***,** 68-78.

Kurtoğlu, E., Bilgin, A., Şeşen, M., Mısırlıoğlu, B., Yıldız, M., Acar, H. F. Y., & Koşar, A. (2012). Ferrofluid actuation with varying magnetic fields for micropumping applications. *Microfluidics and Nanofluidics, 13***,** 683-694.

Lee, K. Y., Jeong, L., Kang, Y. O., Lee, S. J., & Park, W. H. (2009). Electrospinning of polysaccharides for regenerative medicine. *Adv Drug Deliv Rev, 61***,** 1020-1032.

Lewkowitz-Shpuntoff, H. M., Wen, M. C., Singh, A., Brenner, N., Gambino, R., Pernodet, N., Isseroff, R., Rafailovich, M., & Sokolov, J. (2009). The effect of organo clay and adsorbed FeO(3) nanoparticles on cells cultured on Ethylene Vinyl Acetate substrates and fibers. *Biomaterials, 30***,** 8-18.

Li, Z., & Wang, C. (2013). Effects of Working Parameters on Electrospinning. *One-Dimensional Nanostructures Electrospinning Technique and Unique Nanofibers* (pp. 15-28). Springer Heidelberg New York Dordrecht London: Springer.

Liao, S., Murugan, R., Chan, C. K., & Ramakrishna, S. (2008). Processing nanoengineered scaffolds through electrospinning and mineralization suitable for biomimetic bone tissue engineering. *J Mech Behav Biomed Mater, 1***,** 252-260.

Liu, J., Guo, S., Han, L., Ren, W., Liu, Y., & Wang, E. (2012). Multiple pH-responsive graphene composites by non-covalent modification with chitosan. *Talanta, 101***,** 151-6.

Liu, X.-M., Pramoda, K. P., Yang, Y.-Y., Chow, S. Y., & He, C. (2004). Cholesteryl-grafted functional amphiphilic poly(N-isopropylacrylamide-co-N-hydroxylmethylacrylamide): synthesis, temperature-sensitivity, self-assembly and encapsulation of a hydrophobic agent. *Biomaterials, 25***,** 2619-2628.

Liu, Y., Ma, G., Fang, D., Xu, J., Zhang, H., & Nie, J. (2011). Effects of solution properties and electric field on the electrospinning of hyaluronic acid. *Carbohydrate Polymers, 83***,** 1011-1015.

Lue, S. J., Chen, C.-H., Shih, C.-M., Tsai, M.-C., Kuo, C.-Y., & Lai, J.-Y. (2011). Grafting of poly(N-isopropylacrylamide-co-acrylic acid) on micro-porous polycarbonate films: Regulating lower critical solution temperatures for drug controlled release. *Journal of Membrane Science, 379***,** 330-340.

Mack, J. J., Cox, B. N., Lee, M., Dunn, J. C. Y., & Wu, B. W. (2007). Magnetically actuable polymer nanocomposites for bioengineering applications. *Journal of Materials Science, 42***,** 6139-6147.

Mi. 2014. *Methanol Drum Transport, Handling, and Storage* [Online]. Methanol Institute. Available: http://www.methanol.org/getattachment/health-and-safety/technical-bulletins/methanoldrumtransport.pdf.aspx [Accessed 10th April 2014].

Mukherjee, P., & Atala, A. (2006). Biomaterials for Genitourinary Tissue Engineering. In P. X. Ma, & J. Elisseeff (Eds.), *Scaffolding in Tissue Engineering* (pp. 355-369). Boca Raton, FL: CRC Press, Taylor & Francis Group LLC.

Nathani, H., Gubbala, S., & Misra, R. D. K. (2004). Magnetic behavior of nickel ferrite–polyethylene nanocomposites synthesized by mechanical milling process. *Materials Science and Engineering: B, 111***,** 95-100.

Nitanan, T., Opanasopit, P., Akkaramongkolporn, P., Rojanarata, T., Ngawhirunpat, T., & Supaphol, P. (2011). Effects of processing parameters on morphology of electrospun polystyrene nanofibers. *Korean Journal of Chemical Engineering, 29***,** 173-181.

Nukavarapu, S. P., Kumbar, S. G., Merrell, J. G., & Laurencin, C. T. (2008). Electrospun Polymeric Nanofiber Scaffolds for Tissue Regeneration. In C. T. Laurencin, & L. S. Nair (Eds.), *Nanotechnology and Tissue Engineering: The Scaffold* (pp. 199-219). Boca Raton, FL: CRC Press, Taylor & Francis Group.

Ohkawa, K., Cha, D., Kim, H., Nishida, A., & Yamamoto, H. (2004). Electrospinning of Chitosan. *Macromolecular Rapid Communications, 25***,** 1600-1605.

Okuzaki, H., Kobayashi, K., & Yan, H. (2009). Non-woven fabric of poly(N-isopropylacrylamide) nanofibers fabricated by electrospinning. *Synthetic Metals, 159***,** 2273-2276.

Palchesko, R. N., Sun, Y., Zhang, L., Szymanski, J. M., Jallerat, Q., & Feinberg, A. W. (2013). Nanofiber Biomaterials. In R. Vajtai (ed.) (pp. 977-1010). Springer-Verlag Berlin Heidelberg.

Pankhurst, Q. A., Connolly, J., Jones, S. K., & Dobson, J. (2003). Applications of magnetic nanoparticles in biomedicine. *Journal of Physics D: Applied Physics, 36***,** 167-181.

Park, B. W., Yoon, D. Y., & Kim, D. S. (2010). Recent progress in bio-sensing techniques with encapsulated enzymes. *Biosens Bioelectron, 26***,** 1-10.

Perugini, P., Genta, I., Conti, B., Modena, T., & Pavanetto, F. (2003). Periodontal delivery of ipriflavone: new chitosan/PLGA film delivery system for a lipophilic drug. *International Journal of Pharmaceutics, 252***,** 1-9.

Pinol, R., Jia, L., Gubellini, F., Levy, D., Albouy, P.-A., Keller, P., Cao, A., & Li, M.-H. (2007). Self-Assembly of PEG-*b*-Liquid Crystal Polymer: The Role of Smectic Order in the Formation of Nanofibers. *Macromolecules, 40***,** 5625-5627.

Pradhan, P., Giri, J., Banerjee, R., Bellare, J., & Bahadur, D. (2007). Cellular interactions of lauric acid and dextran-coated magnetite nanoparticles. *Journal of Magnetism and Magnetic Materials, 311***,** 282-287.

Provenzano, V., Levin, I., Shull, R. D., Bennett, L. H., Li, J., & Royburd, A. L. Magnetic properties of Self-assembled CoFe(2)O(4)-PbTiO(3) Multiferroic Nanostructures. *In:* I. Institute of Electrical and Electronics Engineers, ed. INTERMAG 2006, 8-12 May 2006 2006 San Diego, CA. Magnetics Conference, 743.

Rockwood, D. N. 2007. *Characterization of electrospun polymer fibers for applications in cardiac tissue engineering and regenerative medicine.* Doctor of Philosophy, University of Delaware.

Rockwood, D. N., Chase, D. B., Akins, R. E., & Rabolt, J. F. (2008). Characterization of electrospun poly(N-isopropyl acrylamide) fibers. *Polymer, 49***,** 4025-4032.

Rodoplu, D., & Mutlu, M. (2012). Effects of Electrospinning Setup and Process Parameters on Nanofiber Morphology Intended for the Modification of Quartz Crystal Microbalance Surfaces. *Journal of Engineered Fibers and Fabrics, 7***,** 118-123.

Sarasam, A., & Madihally, S. V. (2005). Characterization of chitosan-polycaprolactone blends for tissue engineering applications. *Biomaterials, 26***,** 5500-8.

Sarasam, A. R., Samli, A. I., Hess, L., Ihnat, M. A., & Madihally, S. V. (2007). Blending chitosan with polycaprolactone: porous scaffolds and toxicity. *Macromol Biosci, 7***,** 1160-7.

Satcher, M. R. 2006. *De-bottlenecking the electrospinning process using superparamagnetic particles.* Master of Science (Textile Engineering), North Carolina State University.

Shalumon, K. T., Anulekha, K. H., Girish, C. M., Prasanth, R., Nair, S. V., & Jayakumar, R. (2010). Single step electrospinning of chitosan/poly(caprolactone) nanofibers using formic acid/acetone solvent mixture. *Carbohydrate Polymers, 80***,** 413-419.

Shell. 2010. *Datasheet Acetone* [Online]. Shell Chemicals. Available: http://s04.static-shell.com/content/dam/shell/static/chemicals/downloads/products-services/datasheet-acetone.pdf [Accessed 10th April 2014].

Song, F., Wang, X. L., & Wang, Y. Z. (2011). Poly (N-isopropylacrylamide)/poly (ethylene oxide) blend nanofibrous scaffolds: thermo-responsive carrier for controlled drug release. *Colloids Surf B Biointerfaces, 88***,** 749-54.

Sousa, R. G., Magalhaes, W. F., & Freitas, R. F. S. (1998). Glass transition and thermal stability of poly(N-isopropylacrylamide) gels and some of their copolymers with acrylamide. *Polymer Degradation and Stability, 61***,** 275-281.

Sugiura, S., Imano, W., Takagi, T., Sakai, K., & Kanamori, T. (2009). Thermoresponsive protein adsorption of poly(N-isopropylacrylamide)-modified streptavidin on polydimethylsiloxane microchannel surfaces. *Biosens Bioelectron, 24***,** 1135-40.

Suzuki, H., & Kumagai, A. (2003). A disposable biosensor employing a glucose-sensitive biochemomechanical gel. *Biosensors and Bioelectronics, 18***,** 1289-1297.

Tan, E. P. S., & Lim, C. T. (2008). Structure and Mechanical Properties of Electrospun Nanofibres and Nanocomposites. In C. T. Laurencin, & L. S. Nair (Eds.), *Nanotechnology and Tissue Engineering: The Scaffold* (pp. 221-242). Boca Raton, FL: CRC Press, Taylor & Francis Group.

Tateishi, T., Chen, G., & Ushida, T. (2002). Biodegradable porous scaffolds for tissue engineering. *The Japanese Society of Artificial Organs, 5***,** 77-83.

Tauer, K., Gau, D., Schulze, S., Völkel, A., & Dimova, R. (2009). Thermal property changes of poly(N-isopropylacrylamide) microgel particles and block copolymers. *Colloid and Polymer Science, 287***,** 299-312.

Temperature Sensitivityhermann, A., Mruk, R., Roskamp, R. F., Scherer, M., Ma, L., & Zentel, R. (2013). Poly(N-isopropylacrylamide)-Modified Styrene-Butadiene Rubber as Thermoresponsive Material. *Macromolecular Chemistry and Physics***,** n/a-n/a.

Uyar, T., Balan, A., Toppare, L., & Besenbacher, F. (2009). Electrospinning of cyclodextrin functionalized poly(methyl methacrylate) (PMMA) nanofibers. *Polymer, 50***,** 475-480.

Van Der Schueren, L., Steyaert, I., De Schoenmaker, B., & De Clerck, K. (2012). Polycaprolactone/chitosan blend nanofibres electrospun from an acetic acid/formic acid solvent system. *Carbohydrate Polymers, 88***,** 1221-1226.

Vasanthan, N., Ly, H., & Ghosh, S. (2011). Impact of nanoclay on isothermal cold crystallization kinetics and polymorphism of poly(L-lactic acid) nanocomposites. *J Phys Chem B, 115***,** 9556-63.

Vrieze, S., Westbroek, P., Camp, T., & Langenhove, L. (2007). Electrospinning of chitosan nanofibrous structures: feasibility study. *Journal of Materials Science, 42***,** 8029-8034.

Wang, G.-S., Wang, L., Wei, Z.-Y., Sang, L., Dong, X.-F., Qi, M., Chen, G.-Y., Chang, Y., & Zhang, W.-X. (2013a). Synthesis and characterization of poly(ε-caprolactone)/Fe3o4 nanocomposites by in situ polymerization. *Chinese Journal of Polymer Science, 31***,** 1011-1021.

Wang, J., Sutti, A., Wang, X., & Lin, T. (2011). Fast responsive and morphologically robust thermo-responsive hydrogel nanofibres from poly(N-isopropylacrylamide) and POSS crosslinker. *Soft Matter, 7***,** 4364.

Wang, M., Singh, H., Hatton, T. A., & Rutledge, G. C. (2004). Field-responsive superparamagnetic composite nanofibers by electrospinning. *Polymer, 45***,** 5505-5514.

Wang, P., Liu, J., & Zhang, T. (2013b). In Vitro Biocompatibility of Electrospun Chitosan/Collagen Scaffold. *Journal of Nanomaterials, 2013***,** 1-8.

Wei, H., Cheng, S.-X., Zhang, X.-Z., & Zhuo, R.-X. (2009). Thermo-sensitive polymeric micelles based on poly(N-isopropylacrylamide) as drug carriers. *Progress in Polymer Science, 34***,** 893-910.

Wei, Y., Zhang, X., Song, Y., Han, B., Hu, X., Wang, X., Lin, Y., & Deng, X. (2011). Magnetic biodegradable Fe3O4/CS/PVA nanofibrous membranes for bone regeneration. *Biomed Mater, 6***,** 055008.

Wieghaus, K. A., & Botchwey, E. A. (2008). Nanotechnolgies for Cardiovasculat Tissue Engineering. In C. T. Laurencin, & L. S. Nair (Eds.), *Nanotechnology and Tissue Engineering: The Scaffold* (pp. 311-328). Boca Raton, FL: CRC Press, Taylor & Francis Group.

Yamaji, T., Saito, T., Hayamizu, K., Yanagisawa, M., & Yamamoto, O. 2013. *Spectral Database for Organic Compounds SDBS* [Online]. Japan: National Institute of Advanced Industrial Science and Technology (AIST). Available: http://sdbs.db.aist.go.jp [Accessed 8th April 2011].

Yarin, A. L., Koombhongse, S., & Reneker, D. H. (2001). Taylor cone and jetting from liquid droplets in electrospinning of nanofibers. *Journal of Applied Physics, 90***,** 4836.

You, Y. Z., Zhou, Q. H., Manickam, D. S., Wan, L., Mao, G. Z., & Oupicky, D. (2007). Dually responsive multiblock copolymers via RAFT polymerization: Synthesis of temperature- and redox-responsive copolymers of PNIPAM and PDMAEMA. *Macromolecules, 40***,** 8617-8624.

Zhou, Y., Briand, V. A., Sharma, N., Ahn, S.-K., & Kasi, R. M. (2009). Polymers Comprising Cholesterol: Synthesis, Self-Assembly, and Applications. *Materials, 2***,** 636-660.

APPENDIX A: Polymerisation measurements of PNIPAM

1. ^{1}H NMR measurement of PNIPAM after polymerisation (in $CDCl_3$)

From Figure 1, the vinyl peak was assigned according to the ^{1}H NMR of the NIPAM monomer mentioned in Chapter 4. As NIPAM undergoes polymerisation, this peak is reduced due to the breaking of this bond to form the polymer chain. The calculated conversion is a rough estimate, since the reference peak in this case was the THF solvent. The THF was selected as the reference because the end-capped phenyl group was not easily identified in the deuterated chloroform solvent.

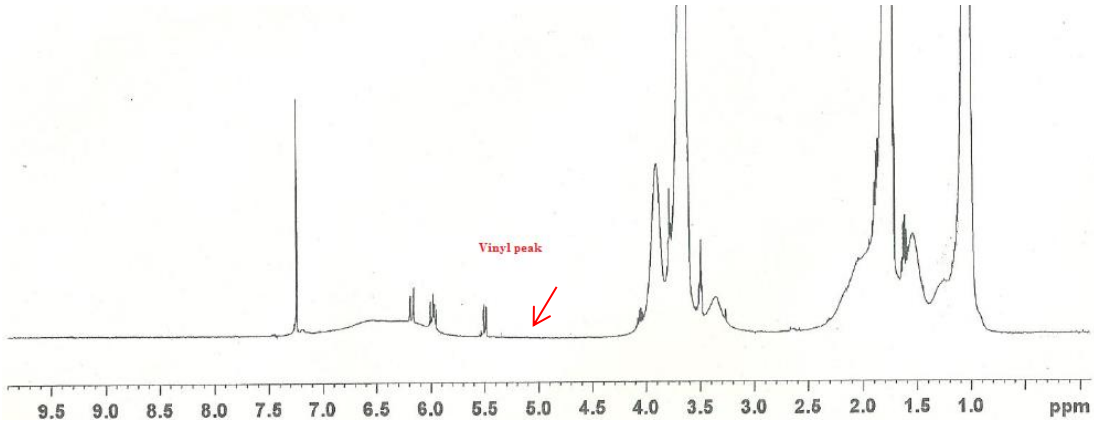

Figure 1: Proton NMR of the impure PNIPAM product, vinyl peak representative of unreacted monomer.

2. Calculation of the degree of polymerisation of PNIPAM from UV-vis spectroscopy

$$X = \frac{0.2676}{59.8344} = 4.47 \times 10^{-3}$$

$$DP = \frac{1}{X} = \frac{1}{4.47 \times 10^{-3}} = 223.68$$

$$M_n(\text{PNIPAM}) = M_n(\text{NIPAM}) \times 223.68 = \mathbf{25312\ g/mol}$$

$$\varepsilon_{MTPA} = 1.546 \times 10^{4} \frac{L}{\text{mol. cm}} = 59.8344 \frac{L}{\text{g. cm}}$$

$$\varepsilon_{PNIPAM} = 0.2676 \frac{L}{\text{g. cm}}$$

Where, DP is the degree of polymerisation, and X is the ratio of the molar absorptivities between the polymer and chain transfer agent.

APPENDIX B: SQUID methodology

Experimental for field-cooled and zero-field-cooled

1. Sample preparation

   A 4 mm square sample was cut with a clean, surgical knife. The end of a straw was cut to make a 'hold' around the sample piece, and was squashed to encase the sample. The sample is then placed in a full length straw (down to approximately the centre). The straw is then placed into the long metal holder (which is to be placed into the machine), and put a plug in the opposite end. The cavity is then opened on top of the magnetometer, and the straw is inserted. The lid is then pushed down so it sits well, and the cap is put back on top of the machine.

2. Setting up the sequence

   A sequence was prepared to complete both a FC and ZFC test on the sample. The sample will be cooled to 10 K at 0 and 200 oersteds for ZFC and FC, respectively.

```
Sequence script
     Set field: 0 Oe          [ZFC]
     Set temp.: 10 K
     Magnet reset
     Set field: 200 Oe
     10K → 50K (5K incremental readings)
     50K → 100K (10K incremental readings)
     100K → 300K (20K incremental readings)
     300K → 310K (10K incremental readings)
     Set field: 10 000 Oe
     Set field: 200 Oe        [FC]
     Set temp.: 10 K
     Magnet reset
     Set field: 200 Oe
     10K → 50K (5K incremental readings)
     50K → 100K (10K incremental readings)
     100K → 300K (20K incremental readings)
     300K → 310K (10K incremental readings)
     Set field: 0 Oe
     Set temp.: 5K
```

Experimental for hysteresis testing

1. Setting up the sequence

   For the hysteresis loop testing, a temperature of 300 K was maintained. Instead of alternating the temperature, the external field is changed over a wide range. For the sequence script, the number of data points need to be specified for each field parameter. The higher gradient sections of the hysteresis loop require more data points to accurately track. In order to roughly determine where these points are, a coarse hysteresis test is performed with wide parameters and measurement steps. The magnetic field is spanned from 2000 Oe to -2000 Oe. At ±1500 Oe, the sequence is split so that the magnet may be reset (quenched). This ensures a true hysteresis reading of the sample, and not that of the magnet. The value of ±1500 Oe is the threshold for quenching the magnet, and thus it is not quenched in excess of these parameters.

   ```
   Sequence script
        ΔH = +50 kOe → -50 kOe
        50K → 20K (10K step)
        20K → 10K (1K step)
        10K → 2K (500 step)
        2K → 1.5K (250 step)
        Magnet reset
        1.5K → -1.5K (200 step)
        Magnet reset
        -1.5K → -2K (250 step)
        -2K → -10K (500 step)
        -10K → -20K (1K step)
        -20K → -50K (10K step)
   ```

   The above is then repeated in reverse, back up to 50 kOe.

   Notes:

   - A slight decline at high field values shows signs of diamagnetism. This is caused by the straw encasing, and the substrate within the sample (moreso the substrate). This is basically background interference.

APPENDIX C: Additional PNIPAM SEM imagery

1. PNIPAM 10% in methanol, at L = 8 cm

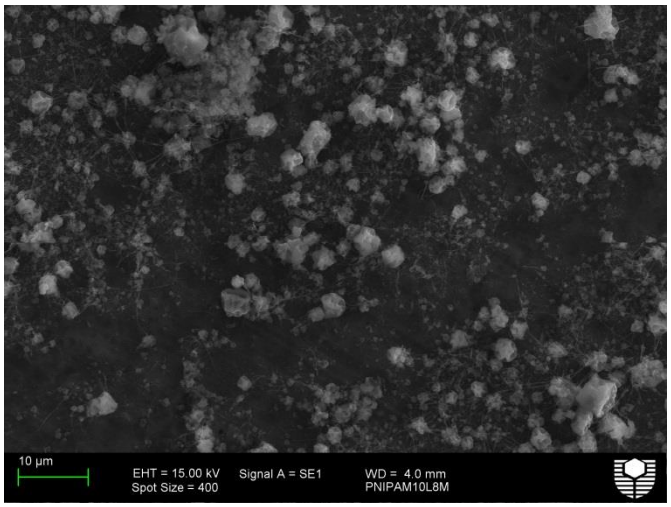

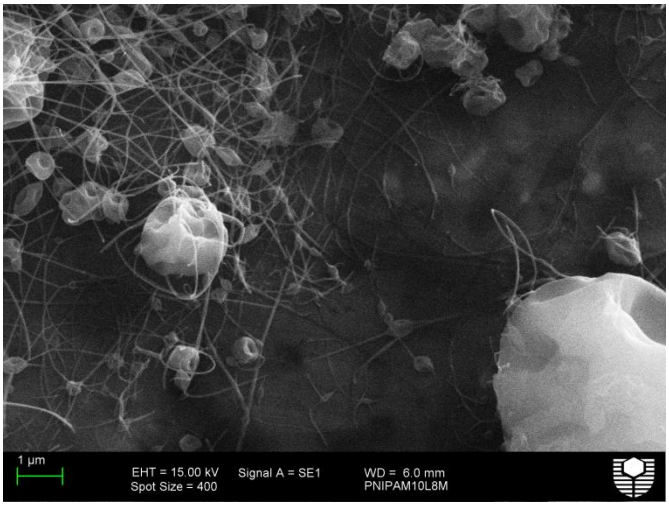

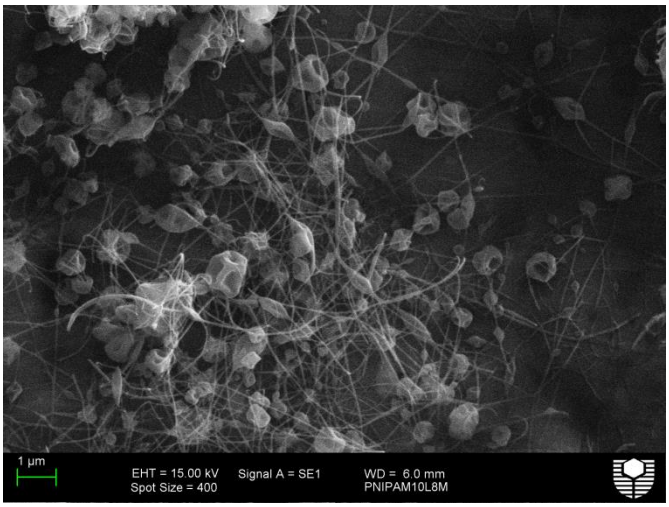

2. PNIPAM 15% in methanol, at L = 8 cm

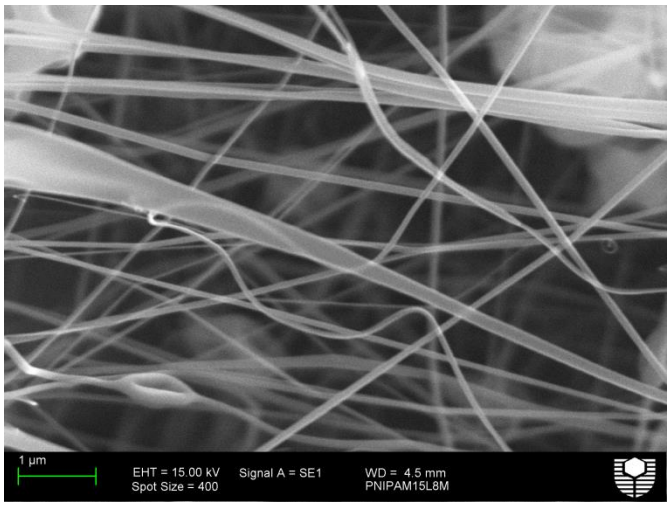

3. PNIPAM 15% in methanol, at L = 12 cm

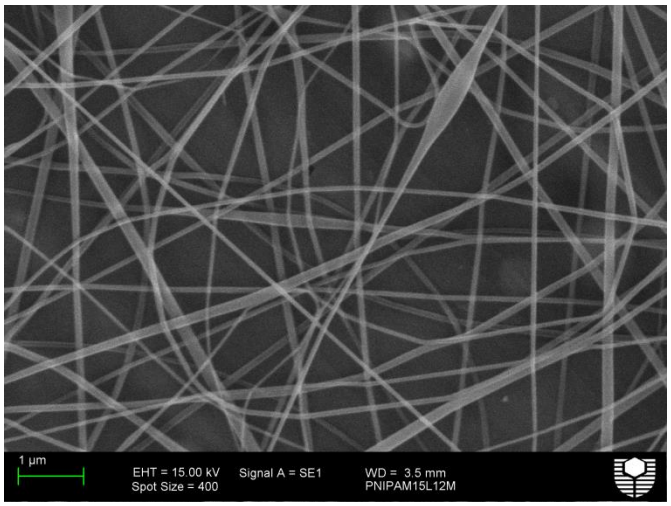

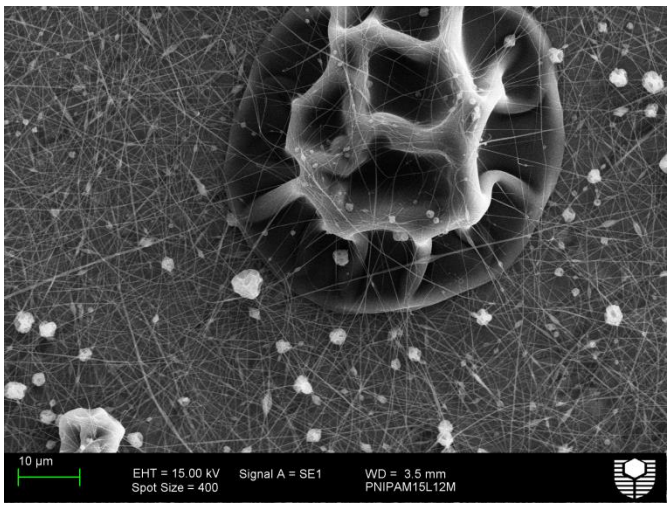

4. PNIPAM 15% in methanol, at L = 16 cm

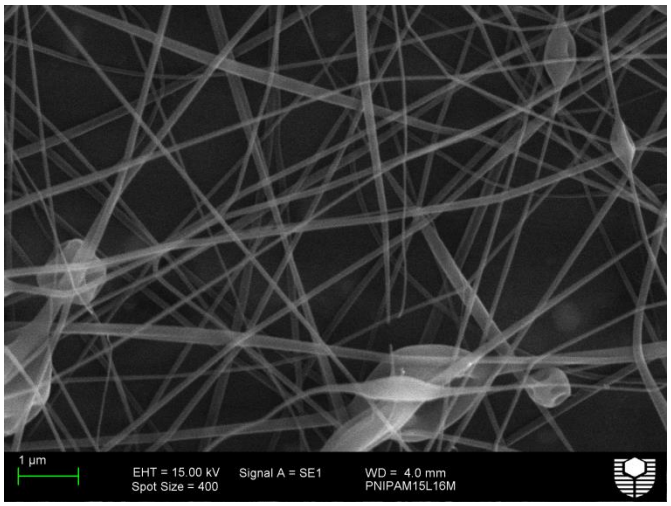

APPENDIX D: Material selection criteria

	Polymer type	Functionality	Melting point	Tensile strength (MPa)	Solubility in H_2O	Optimum solvents	Can it electrospin?	Blended with magnetic NP in the literature?	Cost $AUD/g (SIGMA)
Hyaluronic acid	Glycosamino-glycan	Sodium and potassium salt compounds and possible. Carboxylic acid, acetamide, hydroxyl, and hydroxymethyl groups.	N/A	N/A	Soluble (sodium salt)	Cold water	YES	None found.	68.25
Chitosan	Polysaccharide	Hydroxymethyl and amine group.	> 270°C	50 – 66	Relatively insoluble	A dilute acid	YES	Yes, but was blended with PVA	1.38
Xanthan gum	Polysaccharide	-	N/A	N/A	Soluble	Water	NO	-	0.75
PEG (PEO)	Polyether	Hydroxyl and ether groups	~ 65°C	13 – 22	Soluble	Water, MeOH, benzene, DCM	YES	YES	0.56
PLA	Polyester	Ester group.	150 – 160°C	10 – 60	Insoluble		YES	YES	Variable
PCL	Polyester	Ester group.	60°C	~ 16	Insoluble	THF, chloroform, ethyl acetate, glacial acetic acid	YES	YES “However poorly investigated”	0.58
P(NIPAM)	Unique thermo-responsive polymer	Carbonyl and amide groups	96°C	N/A	Soluble below 32°C	Water, chloroform, acetone, methanol.	YES	None found.	35.70

APPENDIX E: Magnetic nanoparticles calculation

The following calculation was used to determine the necessary volume of Fe_3O_4 solution required to meet a specific mass of solid Fe_3O_4 nanoparticles.

%(Fe_3O_4 needed) = 1%
Volume of solution = 20 mL
Assume a solution density of 1 g/mL.
m(Fe_3O_4 needed) = 0.2 g
Now to determine how much solution this represents:

Concentration of $FeCl_2$ used	= 0.2 M
Concentration of $FeCl_3$ used	= 0.2 M
Volume of $FeCl_2$ used	= 30 mL
Volume of $FeCl_3$ used	= 60 mL
n(Fe_3O_4 needed)	= m / M
	= 0.2 / 231.533
	= 0.000864 mol
n($FeCl_2$ in the solution)	= c * V
	= 0.2 * (30/1000)
	= 0.006 mol
n(Fe_3O_4 produced)	= 0.006 * (1/1)
	= 0.006 mol
m(Fe_3O_4 produced)	= 1.389198 g

Assuming the solution is well mixed (no settling):

m(Fe_3O_4 solution req.)	= 0.2/1.39 * (30mL + 60mL)
	= **13.0 mL**

Calculations are based on the following stoichiometry:

$$Fe^{+2}_{(aq)} + 2Fe^{+3}_{(aq)} + 4H_2O_{(l)} \rightarrow Fe_3O_{4(s)} + 8H^{+}_{(aq)}$$

APPENDIX F: Polymer selection trials – raw data of HA

Based on the material selection table in Appendix D, the three materials selected were chitosan, hyaluronic acid (HA), and PCL (for their stimuli-response and mechanical properties). Hyaluronic acid was the first polymer to be electro-spun, due to the lack of depth in the literature. Due to the high viscosity of HA, a concentration of 1 – 2% was used. The solvents were used based on the limited literature (Liu et al., 2011) to see if the same results could be obtained.

Materials	% w/v	Measured amount
Hyaluronic acid	1	0.5 g
Formic acid	25	12.5 mL
DMF	50	25 mL
Distilled water	25	12.5 mL

The following initial electrospinning parameters were used:

Ambient temperature:	25ºC
Syringe:	5 mL plastic
Pump rate:	0.3 – 1.0 mL/h
Voltage:	10 – 25 kV
Distance:	15 cm

As it can be seen from the figure below, the solution was incredibly viscous. The solution only appeared to electro-spray over range of 10 – 25 kV, with finer droplets at higher voltages.

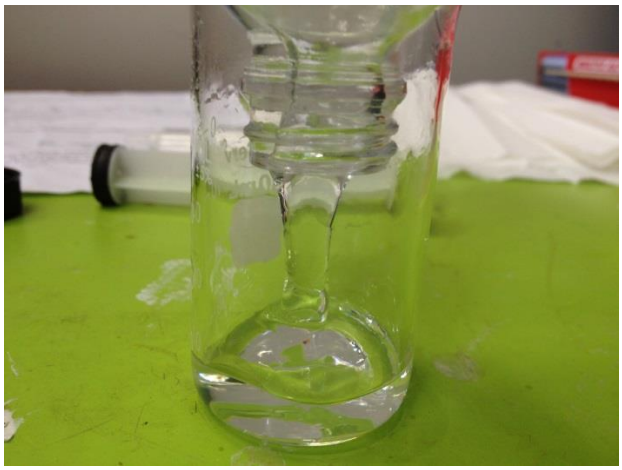

Further testing was completed with a different solvent composition of 3:2 DMF:H_2O. Three samples were prepared as follows:

	HA (mg)	Water (mL)	DMF (mL)	Total solvent (mL)
Sample A (1%)	250	10	15	25
Sample B (1.5%)	375	10	15	25
Sample C (2%)	500	10	15	25

Each of the samples is shown in the following image, with a variance of turbidity evident in Sample B. Solutions were mixed with an ultrasonicator and then placed in the refrigerator for 24 hours to allow dissolution. A distance of 15 cm and a voltage of 22 kV were used, with a flow rate of 1 mL/h. Sample A 'spit' the solution from the needle tip during electrospinning (ranged 8 – 30 kV), with no definite nanofibres produced. A reduction of the flow rate to 0.5 mL/h had no effect. Sample B similarly had drops pulled to the collector, with intermittent spray/spinning observed at 15 kV. Sample C produced an elongated drop from the needle tip. The solution was 'stretching' too much, attributed to the high solution viscosity at 2%. After further inspection at 24 kV and a distance of 10 cm, it was found that the solution was only spraying.

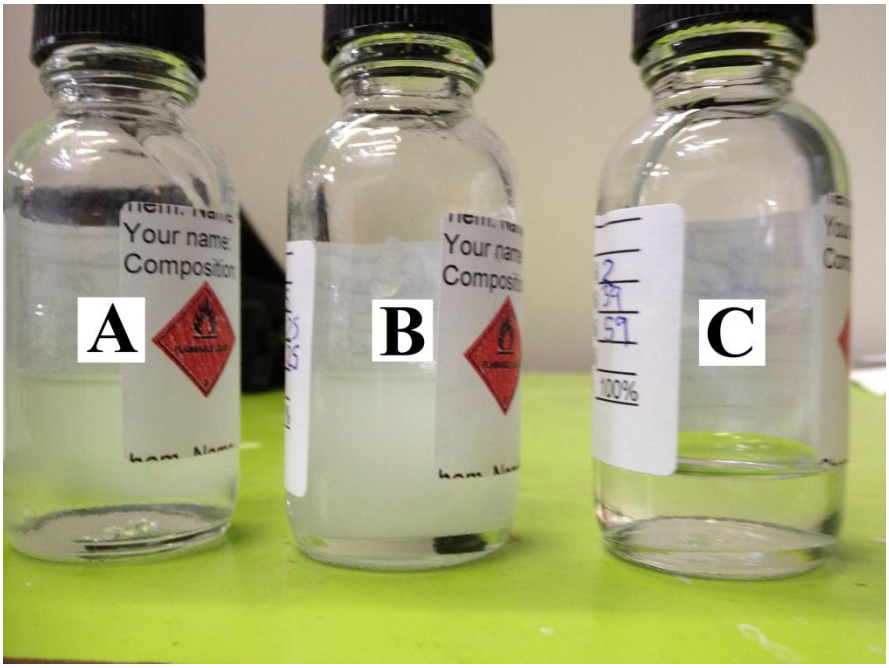

APPENDIX G: PNIPAM co-polymerisation with a ChA-5

After the synthesis of PNIPAM by RAFY polymerisation, co-polymerisation with cholesteryl 6-acryloyloxy hexanoate (ChA-5) was attempted to produce a more functionalised material. The experimental parameters are outlined below:

1. Synthesis

The degree of polymerisation of poly(*N*-isopropylacrylamide) (PNIPAM) to be used is 200. The degree of polymerisation of cholesteryl 6-acryloyloxy hexanoate (ChA-5) will be 10. The solvent for this copolymerisation will be THF. AIBN will be used as an initiator. A mole ratio of 10 : 1 : 0.4 will be used for ChA-5 : PNIPAM : AIBN. Argon gas will be bubbled through the solution for 30 minutes (degassed). NMR is run for the 'before polymerisation' measurement (used to calculate conversion later). Two drops of solution are added to a NMR test tube with $CDCl_3$.

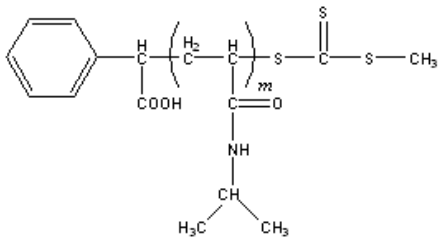

PNIPAM (m = 193.2, ~ 200)
Mol. Wt.: 21862.512 g/mol

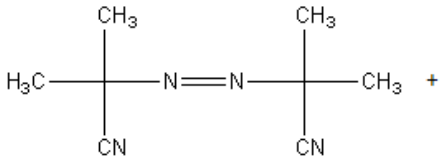

AIBN ($C_8H_{12}N_4$)
Mol. Wt.: 164.21 g/mol

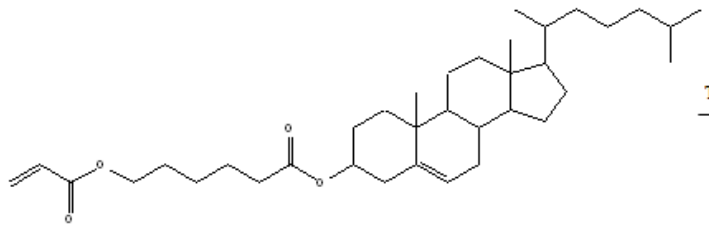

THF 60°C → PNIPAM-*b*-PChA-5

ChA-5 ($C_{36}H_{58}O_4$)
Mol. Wt.: 554.84 g/mol

	M.W.	Mole (mmol)	Weight (g)	Mole ratio
ChA-5	554.84	0.4574	253.79 mg	10
PNIPAM	21862.512	0.0457	1.0 g	1
AIBN	164.21	0.0183	3.004 mg	0.4
THF	0.88 g/mL		11.05 mL (9.83g)	

The flask is put into an oil bath for 16 hours at 60°C for polymerisation. After polymerisation, the flask is allowed to cool and washed with ethyl acetate to remove oil. NMR will then be prepared to observe polymerisation conversion/structure.

2. Purification

A 400 mL solution is prepared of 1:1 di-ethyl ether/*n*-hexane, and placed on a magnetic stirrer. The copolymer solution is added drop-wise to this solution, precipitating the copolymer. The solution was put into a centrifuge, and the solvent was removed through decantation. The centrifuge tubes with the precipitate were covered with a Kimwipe and elastic band for the dry vacuum oven. The dry vacuum oven is run at 60°C, with a cold trap apparatus for approximately 90 minutes. The oven is then allowed to heat the sample for a further 24 hours.

3. Characterisation

- NMR of the purified copolymer is performed with D_2O and $CDCl_3$.
- A LCST measurement is taken of a 1 g/L copolymer solution with purified water. This is run for one hour.
- DLS completed with a concentration of 10 g/L in purified water for the block copolymer.

4. Results

The LCST measurement shows an increase of only 1°C for the block copolymer, compared to the initial PNIPAM LCST measurement. This is attributed to the hydrophobic cholesteryl groups reducing the temperature sensitivity of the PNIPAM homopolymer, as reported in previous studies (Zhou, Briand, Sharma, Ahn & Kasi, 2009). This difference is expected to broaden with increased cholesteryl moiety content.

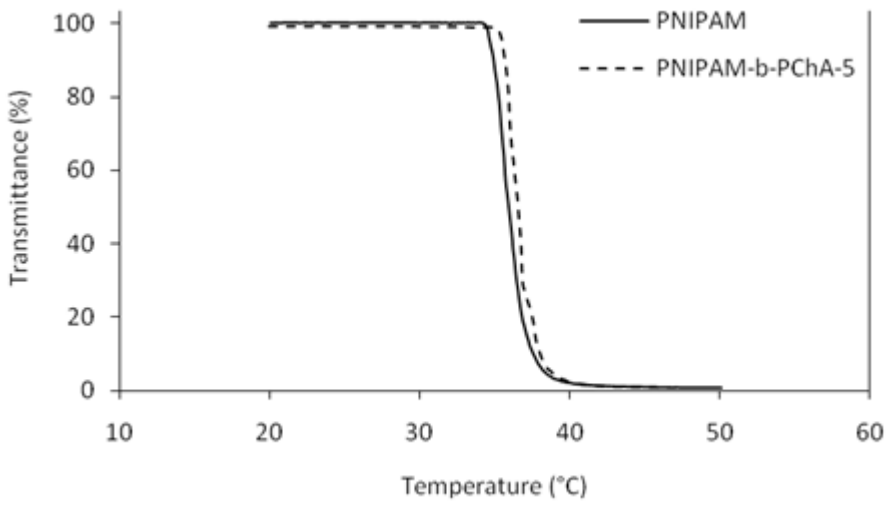

LCST heating measurement for the homopolymer and block copolymer (LCST of 33.5ºC and 34.5ºC respectively).

The DLS data shown below was not characteristic of successful co-polymerisation, and the results were dismissed.

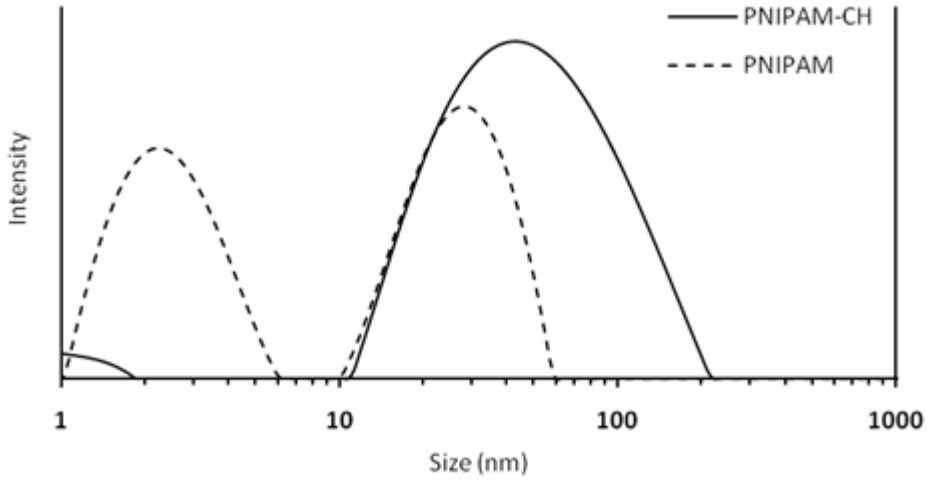

DLS measurement for the homopolymer and block copolymer.

Further variations of this experiment were carried out to determine if co-polymerisation was possible at different reactant ratios. Each of these trials are outlined briefly below:

Synthesis of p(NIPAM)$_{200}$-b-(ChA-5)$_{10}$

- Ratio of ChA-5 : p(NIPAM) was 10 : 1.
- Analysed with: ^{1}H NMR and DLS.
- The DLS data was not characteristic of successful co-polymerisation (**discarded**).

Synthesis of p(NIPAM)$_{200}$-b-(ChA-5)$_{20}$

- Ratio of ChA-5 : p(NIPAM) was 20 : 1.
- Analysed with: ^{1}H NMR.
- The ^{1}H NMR data was not characteristic of successful co-polymerisation (**discarded**).

Synthesis of p(NIPAM)$_{50}$-b-(ChA-5)$_{10}$

- Ratio of ChA-5 : p(NIPAM) was 10 : 1.
- Analysed with: ^{1}H NMR and GPC.
- The GPC data showed a shoulder peak, so unsuccessful co-polymerisation (**discarded**).

Synthesis of p(NIPAM)$_{50}$-b-(ChA-5)$_{10}$ → with 50% less AIBN initiator

- Ratio of ChA-5 : p(NIPAM) was 10 : 1.
- Analysed with: ^{1}H NMR and GPC.
- The GPC data showed a shoulder peak, so unsuccessful co-polymerisation (**discarded**).

Synthesis of p(ChA-5) and determination of polymerisation time

- Ratio of ChA-5 : CPD was 20 : 1.
- Analysed with: ^{1}H NMR and GPC.
- The polymerisation time was successfully determined for large scale synthesis.

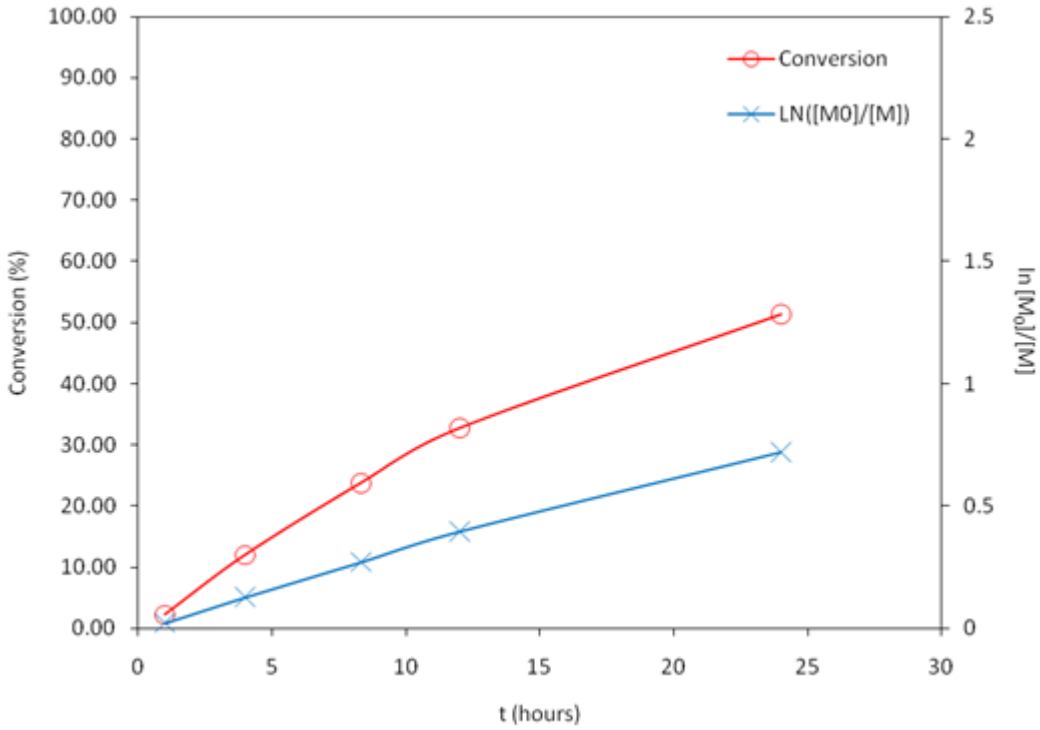

Synthesis of p(ChA-5)$_{20}$

- Ratio of ChA-5 : CPD was 20 : 1.
- Analysed with: ^{1}H NMR, GPC, and dialysis.
- Successful collection of 0.39 grams of p(ChA-5).

Synthesis of p(ChA-5)$_{20}$-b-(NIPAM)$_{200}$

- Ratio of NIPAM : p(ChA-5) was 200 : 1.
- Analysed with: ^{1}H NMR.
- Unsuccessful due to little relative change in the peaks between the two polymers (**discarded**).